Distribution Agreement

In presenting this thesis or dissertation as a partial fulfillment of the requirements for an advanced degree from Emory University, I hereby grant to Emory University and its agents the non-exclusive license to archive, make accessible, and display my thesis or dissertation in whole or in part in all forms of media, now or hereafter known, including display on the world wide web. I understand that I may select some access restrictions as part of the online submission of this thesis or dissertation. I retain all ownership rights to the copyright of the thesis or dissertation. I also retain the right to use in future works (such as articles or books) all or part of this thesis or dissertation.

Signature:	
Kristen Fowler Easley	Date

INTOXICATING INTERACTIONS: THE IMPACTS OF CHRONIC ALCOHOL USE AND SARS-COV-2 INFECTION ON AIRWAY EPITHELIAL CELLS

By

Kristen Fowler Easley Doctor of Philosophy

Graduate Division of Biological and Biomedical Science Biochemistry, Cell, and Developmental Biology

Michael Koval, PhD, Advisor
Paul Dawson, PhD, Committee Member
Andrew Kowalczyk, PhD, Committee Member
Nael McCarty, PhD, Committee Member
John Hepler, PhD, Committee Member
Accepted:
Kimberly Jacob Arriola
Dean of the James T. Laney School of Graduate Studies
Date

INTOXICATING INTERACTIONS: THE IMPACTS OF CHRONIC ALCOHOL USE AND SARS-COV-2 INFECTION ON AIRWAY EPITHELIAL CELLS

By

Kristen Fowler Easley
B.S., Xavier University of Louisiana, 2015
M.S., Tulane University, 2016

Advisor: Dr. Michael Koval, Ph.D.

An abstract of
A dissertation submitted to the Faculty of the
James T. Laney School of Graduate Studies of Emory University
in partial fulfillment of the requirements for the degree of
Doctor of Philosophy
in Graduate Division of Biological and Biomedical Science
Biochemistry, Cell, and Developmental Biology
2023

Abstract

INTOXICATING INTERACTIONS: THE IMPACTS OF CHRONIC ALCOHOL USE AND SARS-COV-2 INFECTION ON AIRWAY EPITHELIAL CELLS

By: Kristen Fowler Easley

The airway epithelial barrier is the first line of defense against environmental and biological insults to the lung. To accurately study how these insults, in addition to airway diseases, affect epithelial cell function, we must develop in vitro cell culture systems that best mimic the in vivo microenvironment. We created a differentiation medium with physiologic glucose levels (150mg/dL) called Emory-ALI (E-ALI) that encouraged differentiation of non-diseased and CF respiratory epithelial cells and allowed for insulin-stimulated glucose uptake and metabolic analysis. We used this improved system to examine whether Alcohol Use Disorder (AUD) was a risk factor for a more severe outcome in response to SARS-CoV-2 infection. We examined early responses to infection using cultured differentiated bronchial epithelial cells derived from brushings obtained from people with AUD or without AUD. We found that AUD cells had a significant decrease in barrier function up to 72 h after infection, while non-AUD cells increased their barrier function. AUD cells secreted more pro-inflammatory cytokines during the 72 h infection time course and displayed increased basolateral secretion compared to non-AUD cells. RNA-seq analysis revealed 164 differentially expressed genes between AUD and non-AUD cells, and suggested that AUD cells adapted an inflammatory, epidermal gene expression profile. To further determine how chronic alcohol use impacts the airway epithelial barrier, I utilized a variety of bronchial epithelial cell sources. I found that ethanol-treated airway cells had a decrease in barrier function during differentiation but had similar barrier function to untreated cells once differentiation into a mucociliary monolayer was complete. Interestingly, differentiation of AUD and non-AUD cells revealed a correlation between patient age and unjamming, a phenomenon where cells undergo aberrant collective cell migration. Together, these data underscore the sensitive yet resilient nature of airway epithelial cells in response to environmental and biological insults and highlight the need to further study the impacts of glucose levels, chronic alcohol use and SARS-CoV-2 infection on the airway epithelium.

INTOXICATING INTERACTIONS: THE IMPACTS OF CHRONIC ALCOHOL USE AND SARS-COV-2 INFECTION ON AIRWAY EPITHELIAL CELLS

By

Kristen Fowler Easley
B.S., Xavier University of Louisiana, 2015
M.S., Tulane University, 2016

Advisor: Dr. Michael Koval, Ph.D.

A dissertation submitted to the Faculty of the James T. Laney School of Graduate Studies of Emory University in partial fulfillment of the requirements for the degree of Doctor of Philosophy in Graduate Division of Biological and Biomedical Science Biochemistry, Cell, and Developmental Biology 2023

Acknowledgements

I would like to start off my acknowledgements by thanking my committee members: Dr. Nael McCarty, Dr. John Hepler, Dr. Paul Dawson, and Dr. Andrew Kowalczyk. Thank you for sticking with me through my (3!) project changes and being a fantastic sounding board for my ideas and my data. You all contributed to different aspects of my projects and enabled me to think differently about my results and data interpretation. I thoroughly enjoyed every single one of my committee meetings and appreciate the support immensely.

The BCDB program is a wonderful program to be a part of, and I met some of the most supportive and wonderful people. To my cohort: Izabela, Sean, Lauren, Emily, Maria, Julia, Cato, Bejan, and Courtney, I couldn't imagine a better group of people to go through Foundations and the program with. To Julia DeAmorim, I wish we didn't wait until 5th year to grow close! I can't imagine cofounding AMSLE with anyone else. Thank you, Colby Schweibenz, Olivia Mistretta and Bhrugu Yagnik for sharing our vision for AMSLE and taking on the good work. I just know we will all make incredible MSLs one day.

To the Easley Lab, thank you for being a home away from my lab home and for opening the lab to an adopted graduate student. You all know how to have a good time in and out of the lab, and I enjoyed every single one of our epic house parties and Halloween parties. I'm looking forward to more in the years to come!

To current Koval Lab members, Yasmin, Anna, Ryan, Prestina, Kahled and Josh, words are not enough to thank you for your support, especially in the last year as I wrapped up my PhD. You are all incredible scientists and friends. To previous lab mates Lauren, Sabrina, and Raven, Skye, Sam, Lionel and Sarah, I remember thinking how lucky I was to join a lab with you all in it. I had no idea how important our friendships would be and that the daily laughs, shenanigans, and

support are what truly got me through graduate school and the pandemic. I'm not sorry that most of the pictures in my phone from 2018-2020 are of us taking selfies or action shots during incubations and our failed western blots.

To my friends and family (there are way too many of you to record here!), I can't thank you all enough for the continued support up to this point in my life. Each one of you has shaped me into the person and scientist I am today, and I am forever grateful. To my sisters, Lauren and Kelly, thank you for keeping me grounded and reminding me of my roots while in graduate school. To my parents, Carla and Rick, thank you for your relentless hard work and sacrifices to make education a top priority in our household. As a first-generation college student, I can't think of anything more selfless. I hope I have made you proud.

To Mike, thank you for taking a chance on me as a new graduate student and for shaping my mind into that of a scientist's. I especially want to thank you for trusting me to work in two cities and two labs. I wouldn't be the scientist, wife and mother I am today without your support, and this is something I will never forget!

And to my main squeezes, Chas, Charlie and Ollie, completing my PhD would have been impossible without you. Chas, what a gift that you know exactly what it takes to get a PhD. Between the ups and downs these past six years, your support and encouragement are what truly kept me going and staying positive. Thank you for being my rock and my comfort at the end of every day. Charlie, thank you for reminding me what matters most: striving every day to be the best mom and person I can be. I love you more than words can say. Ollie butt, thank you for the daily snuggles and love, especially during the pandemic and while writing my dissertation at home.

Table of Contents

Abstract	i\
Acknowledgements	ν
List of Figures	x
List of Tables	xii
Abbreviations	xi\
Chapter 1: Introduction	1
1.1 Lung Anatomy and Physiology	
1.2 The Apical Junctional Complex 1.2.1 Tight Junctions 1.2.2 Adherens Junctions	
1.3 Chronic Alcohol Use and the Lung 1.3.1 Susceptibility to infections 1.3.2 Oxidative Stress 1.3.3 Barrier Dysfunction	10
1.4 Scope of Dissertation	13
References	16
Chapter 2: A medium composition containing normal resting glucose that sudifferentiation of primary human airway cells	32
2.2 Introduction	33
2.3 Material and Methods 2.3.1 Donor consent 2.3.2 Tracheal epithelial cell isolation	36
2.3.3 Bronchial epithelial cell isolation	37
2.3.4 3T3 Fibroblast feeder cell preparation 2.3.5 Airway epithelial cell expansion 2.3.6 Airway epithelial cell differentiation	38
2.3.7 Cell stock cryopreservation and use 2.3.8 nasal epithelial cell isolation and expansion	41
2.3.9 Immunofluorescence and imaging 2.3.10 Transepithelial resistance and electrophysiology 2.3.11 Insulin stimulation and glucose uptake 2.3.12 Statistics	43 44
2.4 Results and Discussion	
2.4.1 Isolation and differentiation of airway epithelial cells 2.4.2 Cells cultured in E-ALI medium show insulin-stimulated glucose uptake 2.4.3 Expansion and maturation of CF nasal epithelial cells using E-ALI	45 47
2.5 Acknowledgements	65
2. C. Author Contributions	C

inflammatory response during SARS-CoV-2 infection	•••••
3.1 Abstract	
3.2 Introduction	
3.3 Material and Methods	
3.3.1 Donor Consent	
3.3.2 Airway epithelial cell culture and infection	
3.3.3 RNA-seq Analysis	
3.3.4 Transepithelial Resistance (TER)	
3.3.5 Immunofluorescence Microscopy	
3.3.6 Cytokine Analysis	
3.4 Results	
3.4.1 RNA-seq reveals differentially expressed genes between non-AUD cells and AUD cell	
3.4.2 SARS-CoV-2 infection impairs barrier function of AUD cells	
3.4.3 Differential secretion of cytokines by infected AUD and non-AUD cells	
3.5 Discussion	
3.6 Acknowledgements	
3.7 Author Contributions	
5.7 Author Contributions	
References	
References	
References Chapter 4: Characterization of alcohol-exposed airway cells	•••••
References Chapter 4: Characterization of alcohol-exposed airway cells	
References Chapter 4: Characterization of alcohol-exposed airway cells 4.1 Abstract	
References	
References Chapter 4: Characterization of alcohol-exposed airway cells 4.1 Abstract 4.2 Introduction 4.3 Material and Methods 4.3.1 Donor Consent 4.3.2 Airway epithelial cell culture and EtOH treatment 4.3.3 Rat airway epithelial cell isolation and culture 4.3.4 Transepithelial Resistance (TER)	
References Chapter 4: Characterization of alcohol-exposed airway cells 4.1 Abstract 4.2 Introduction 4.3 Material and Methods 4.3.1 Donor Consent 4.3.2 Airway epithelial cell culture and EtOH treatment 4.3.3 Rat airway epithelial cell isolation and culture 4.3.4 Transepithelial Resistance (TER) 4.3.5 Immunofluorescence Microscopy 4.3.6 Statistics 4.4 Results	
References	
References	
References	
References	nming
References	nming
References	nming

5.2 Future Directions	165
5.2.1 Implications of hyperglycemia on airway cell function	165
5.2.2 Investigating alcohol-induced modifications to the epigenome and transcriptome	166
5.2.3 Improvements to our in vitro ethanol exposure model	167
5.2.4 Linking aging-related effects to unjamming in airway epithelial cells	168
References	170

List of Figures

Figure 2.2 Airway epithelial cells from different tissue sources propagate with similar doubling times Figure 2.3 Tracheal and bronchial epithelial cells differentiate into mucociliary cultures in E-ALI medium Figure 2.4 Glucose and insulin sensitivity depends on differentiation medium Figure 2.5 Expansion and differentiation of non-CF and CF nasal epithelial cells Figure 2.6 Representative electrophysiological analysis of primary tracheal and nasal airway epithelia expanded using CRC conditions and differentiated in E-ALI Figure 2.7 Representative electrophysiological analysis of primary nasal CF airway epithelia expanded using CRC conditions and differentiated in E-ALI Figure 3.1 Summary of RNA-seq analysis of AUD and non-AUD cells Figure 3.2 AUD cells have impaired barrier function following SARS-CoV-2 infection Figure 3.3 Changes to non-AUD and AUD bronchial cell junctions in response to SARS-CoV-2 infection Figure 3.4 Pro-inflammatory cytokines were preferentially secreted by AUD cells in a polarized manner in response to infection	Figure 2.1	Workflow for isolation of cells from distinct anatomic regions of
Figure 2.3 Tracheal and bronchial epithelial cells differentiate into mucociliary cultures in E-ALI medium Figure 2.4 Glucose and insulin sensitivity depends on differentiation medium Figure 2.5 Expansion and differentiation of non-CF and CF nasal epithelial cells Figure 2.6 Representative electrophysiological analysis of primary tracheal and nasal airway epithelia expanded using CRC conditions and differentiated in E-ALI Figure 2.7 Representative electrophysiological analysis of primary nasal CF airway epithelia expanded using CRC conditions and differentiated in E-ALI Figure 3.1 Summary of RNA-seq analysis of AUD and non-AUD cells Figure 3.2 AUD cells have impaired barrier function following SARS-CoV-2 infection Figure 3.3 Changes to non-AUD and AUD bronchial cell junctions in response to SARS-CoV-2 infection Figure 3.4 Pro-inflammatory cytokines were preferentially secreted by AUD		the airway tree
Figure 2.3 Tracheal and bronchial epithelial cells differentiate into mucociliary cultures in E-ALI medium Figure 2.4 Glucose and insulin sensitivity depends on differentiation medium Figure 2.5 Expansion and differentiation of non-CF and CF nasal epithelial cells Figure 2.6 Representative electrophysiological analysis of primary tracheal and nasal airway epithelia expanded using CRC conditions and differentiated in E-ALI Figure 2.7 Representative electrophysiological analysis of primary nasal CF airway epithelia expanded using CRC conditions and differentiated in E-ALI Figure 3.1 Summary of RNA-seq analysis of AUD and non-AUD cells Figure 3.2 AUD cells have impaired barrier function following SARS-CoV-2 infection Figure 3.3 Changes to non-AUD and AUD bronchial cell junctions in response to SARS-CoV-2 infection Figure 3.4 Pro-inflammatory cytokines were preferentially secreted by AUD	Figure 2.2	Airway epithelial cells from different tissue sources propagate with
cultures in E-ALI medium Figure 2.4 Glucose and insulin sensitivity depends on differentiation medium Figure 2.5 Expansion and differentiation of non-CF and CF nasal epithelial cells Figure 2.6 Representative electrophysiological analysis of primary tracheal and nasal airway epithelia expanded using CRC conditions and differentiated in E-ALI Figure 2.7 Representative electrophysiological analysis of primary nasal CF airway epithelia expanded using CRC conditions and differentiated in E-ALI Figure 3.1 Summary of RNA-seq analysis of AUD and non-AUD cells Figure 3.2 AUD cells have impaired barrier function following SARS-CoV-2 infection Figure 3.3 Changes to non-AUD and AUD bronchial cell junctions in response to SARS-CoV-2 infection Figure 3.4 Pro-inflammatory cytokines were preferentially secreted by AUD		similar doubling times
Figure 2.4 Glucose and insulin sensitivity depends on differentiation medium Figure 2.5 Expansion and differentiation of non-CF and CF nasal epithelial cells Figure 2.6 Representative electrophysiological analysis of primary tracheal and nasal airway epithelia expanded using CRC conditions and differentiated in E-ALI Figure 2.7 Representative electrophysiological analysis of primary nasal CF airway epithelia expanded using CRC conditions and differentiated in E-ALI Figure 3.1 Summary of RNA-seq analysis of AUD and non-AUD cells Figure 3.2 AUD cells have impaired barrier function following SARS-CoV-2 infection Figure 3.3 Changes to non-AUD and AUD bronchial cell junctions in response to SARS-CoV-2 infection Figure 3.4 Pro-inflammatory cytokines were preferentially secreted by AUD	Figure 2.3	Tracheal and bronchial epithelial cells differentiate into mucociliary
Figure 2.5 Expansion and differentiation of non-CF and CF nasal epithelial cells Figure 2.6 Representative electrophysiological analysis of primary tracheal and nasal airway epithelia expanded using CRC conditions and differentiated in E-ALI Figure 2.7 Representative electrophysiological analysis of primary nasal CF airway epithelia expanded using CRC conditions and differentiated in E-ALI Figure 3.1 Summary of RNA-seq analysis of AUD and non-AUD cells Figure 3.2 AUD cells have impaired barrier function following SARS-CoV-2 infection Figure 3.3 Changes to non-AUD and AUD bronchial cell junctions in response to SARS-CoV-2 infection Figure 3.4 Pro-inflammatory cytokines were preferentially secreted by AUD		cultures in E-ALI medium
rigure 2.6 Representative electrophysiological analysis of primary tracheal and nasal airway epithelia expanded using CRC conditions and differentiated in E-ALI Figure 2.7 Representative electrophysiological analysis of primary nasal CF airway epithelia expanded using CRC conditions and differentiated in E-ALI Figure 3.1 Summary of RNA-seq analysis of AUD and non-AUD cells Figure 3.2 AUD cells have impaired barrier function following SARS-CoV-2 infection Figure 3.3 Changes to non-AUD and AUD bronchial cell junctions in response to SARS-CoV-2 infection Figure 3.4 Pro-inflammatory cytokines were preferentially secreted by AUD	Figure 2.4	Glucose and insulin sensitivity depends on differentiation medium
Figure 2.6 Representative electrophysiological analysis of primary tracheal and nasal airway epithelia expanded using CRC conditions and differentiated in E-ALI Figure 2.7 Representative electrophysiological analysis of primary nasal CF airway epithelia expanded using CRC conditions and differentiated in E-ALI Figure 3.1 Summary of RNA-seq analysis of AUD and non-AUD cells Figure 3.2 AUD cells have impaired barrier function following SARS-CoV-2 infection Figure 3.3 Changes to non-AUD and AUD bronchial cell junctions in response to SARS-CoV-2 infection Figure 3.4 Pro-inflammatory cytokines were preferentially secreted by AUD	Figure 2.5	Expansion and differentiation of non-CF and CF nasal epithelial
and nasal airway epithelia expanded using CRC conditions and differentiated in E-ALI Figure 2.7 Representative electrophysiological analysis of primary nasal CF airway epithelia expanded using CRC conditions and differentiated in E-ALI Figure 3.1 Summary of RNA-seq analysis of AUD and non-AUD cells Figure 3.2 AUD cells have impaired barrier function following SARS-CoV-2 infection Figure 3.3 Changes to non-AUD and AUD bronchial cell junctions in response to SARS-CoV-2 infection Figure 3.4 Pro-inflammatory cytokines were preferentially secreted by AUD		cells
Figure 2.7 Representative electrophysiological analysis of primary nasal CF airway epithelia expanded using CRC conditions and differentiated in E-ALI Figure 3.1 Summary of RNA-seq analysis of AUD and non-AUD cells Figure 3.2 AUD cells have impaired barrier function following SARS-CoV-2 infection Figure 3.3 Changes to non-AUD and AUD bronchial cell junctions in response to SARS-CoV-2 infection Figure 3.4 Pro-inflammatory cytokines were preferentially secreted by AUD	Figure 2.6	Representative electrophysiological analysis of primary tracheal
Figure 2.7 Representative electrophysiological analysis of primary nasal CF airway epithelia expanded using CRC conditions and differentiated in E-ALI Figure 3.1 Summary of RNA-seq analysis of AUD and non-AUD cells Figure 3.2 AUD cells have impaired barrier function following SARS-CoV-2 infection Figure 3.3 Changes to non-AUD and AUD bronchial cell junctions in response to SARS-CoV-2 infection Figure 3.4 Pro-inflammatory cytokines were preferentially secreted by AUD		and nasal airway epithelia expanded using CRC conditions and
airway epithelia expanded using CRC conditions and differentiated in E-ALI Figure 3.1 Summary of RNA-seq analysis of AUD and non-AUD cells Figure 3.2 AUD cells have impaired barrier function following SARS-CoV-2 infection Figure 3.3 Changes to non-AUD and AUD bronchial cell junctions in response to SARS-CoV-2 infection Figure 3.4 Pro-inflammatory cytokines were preferentially secreted by AUD		differentiated in E-ALI
in E-ALI Figure 3.1 Summary of RNA-seq analysis of AUD and non-AUD cells Figure 3.2 AUD cells have impaired barrier function following SARS-CoV-2 infection Figure 3.3 Changes to non-AUD and AUD bronchial cell junctions in response to SARS-CoV-2 infection Figure 3.4 Pro-inflammatory cytokines were preferentially secreted by AUD	Figure 2.7	Representative electrophysiological analysis of primary nasal CF
Figure 3.1 Summary of RNA-seq analysis of AUD and non-AUD cells Figure 3.2 AUD cells have impaired barrier function following SARS-CoV-2 infection Figure 3.3 Changes to non-AUD and AUD bronchial cell junctions in response to SARS-CoV-2 infection Figure 3.4 Pro-inflammatory cytokines were preferentially secreted by AUD		airway epithelia expanded using CRC conditions and differentiated
Figure 3.2 AUD cells have impaired barrier function following SARS-CoV-2 infection Figure 3.3 Changes to non-AUD and AUD bronchial cell junctions in response to SARS-CoV-2 infection Figure 3.4 Pro-inflammatory cytokines were preferentially secreted by AUD		in E-ALI
infection Figure 3.3 Changes to non-AUD and AUD bronchial cell junctions in response to SARS-CoV-2 infection Figure 3.4 Pro-inflammatory cytokines were preferentially secreted by AUD	Figure 3.1	Summary of RNA-seq analysis of AUD and non-AUD cells
Figure 3.3 Changes to non-AUD and AUD bronchial cell junctions in response to SARS-CoV-2 infection Figure 3.4 Pro-inflammatory cytokines were preferentially secreted by AUD	Figure 3.2	AUD cells have impaired barrier function following SARS-CoV-2
to SARS-CoV-2 infection Figure 3.4 Pro-inflammatory cytokines were preferentially secreted by AUD		infection
Figure 3.4 Pro-inflammatory cytokines were preferentially secreted by AUD	Figure 3.3	Changes to non-AUD and AUD bronchial cell junctions in response
		to SARS-CoV-2 infection
cells in a polarized manner in response to infection	Figure 3.4	Pro-inflammatory cytokines were preferentially secreted by AUD
		cells in a polarized manner in response to infection

Supplemental Figure 3.1	Distribution of normalized read counts
Supplemental Figure 3.2	Cytokines that were preferentially secreted by AUD cells in
	response to infection
Supplemental Figure 3.3	Cytokines that were equivalently secreted by AUD cells and non-
	AUD cells in response to infection
Supplemental Figure 3.4	Polarized secretion of cytokines by AUD and non-AUD cells in
	response to infection
Supplemental Figure 3.5	Equal apical and basolateral secretion of cytokines by AUD and
	non-AUD cells in response to infection
Figure 4.1	Ethanol treatment in vitro decreases barrier function only during
	differentiation
Figure 4.2	Most AUD cells are unjammed
Figure 4.3	Some AUD patient samples show diminished JAM-A
Figure 4.4	Ethanol treatment in vitro does not decrease JAM-A or ZO-1
	expression and may cause unjamming

List of Tables

Table 2.1	FYRM medium composition
Table 2.2	E-ALI medium composition
Table 3.1	Subject Characteristics
Table 3.2	Differentially expressed genes related to epidermal regulation and
	inflammation identified in the Gene Ontology analysis
Table 3.3	Differentially expressed genes by AUD and non-AUD bronchial
	cells that were identified in both our study and by Bailey et al
Supplemental Table 3.1	List of differentially expressed genes
Supplemental Table 3.2	GO enrichment analysis GO terms with a padj value <0.05
Table 4.1	Unjamming correlates with patient age

Abbreviations

ACE2 Angiotensin Converting Enzyme 2

ADH Alcohol Dehydrogenase

AGS Acetaldehyde Generating System

AJ Adherens Junction

AJC Apical Junctional Complex

ALI Air-Liquid Interface

ATAC-seq Assay for transposase-accessible chromatin with sequencing

AUD Alcohol Use Disorder

ARDS Acute Respiratory Distress Syndrome

BAC Blood Alcohol Concentration

CAPS Conducting Airway Protease Solution

CF Cystic Fibrosis

CFhTE Cystic Fibrosis human Tracheal Epithelial

CFTR Cystic fibrosis Transmembrane Regulator

ChIP Chromatin immunoprecipitation

COPD Chronic Obstructive Pulmonary Disease

CRB Crumbs

E-ALI Emory Air-Liquid Interface

ECM Extracellular Matrix

EGF Epidermal Growth Factor

EMT Epithelial to Mesenchymal Transition

FYRM F+Y Reprogramming Medium

GM-CSF Granulocyte-Macrophage Colony-Stimulating Factor

GO Gene Ontology

GSTA1 Glutathione S-Transferase alpha 1

JAM Junction Adhesion Molecule

KRH Krebs-Ringers HEPES

MCC Mucocilliary Clearance

NhBE Normal human Bronchial Epithelial

NhNE Normal human Nasal Epithelial

NhTE Normal human Tracheal Cells

PBS Phosphate Buffered Saline

PCD Primary Ciliary Dyskinesia

PFA Paraformaldehyde

PKCα Protein Kinase C alpha

PNEC Pulmonary Neuroendocrine Cells

ROCK Rho-associated protein kinase

ROS Reactive Oxygen Species

S1SP Subunit 1 Spike Protein

SARS-CoV-2 Severe Acute Respiratory Syndrome Coronavirus 2

SPRR Small Proline Rich

TER Transepithelial Electrical Resistance

TGF-β1 Transforming Growth Factor Beta-1

TJ Tight Junction

ZO Zonula occludins

Chapter 1: Introduction

1.1 Lung Anatomy and Physiology

The respiratory system is an extremely complex and multi-structured system with two main functions: enabling gas exchange between the bloodstream and inhaled air and maintaining acid-base balance. In order to do this, the respiratory system must also provide a physical barrier to infectious agents and particulate matter. Examining the structure of each part of the respiratory system can elucidate how they support the abovementioned functions (1).

The respiratory system is divided into two zones: the conducting zone (proximal) and the respiratory zone (distal). The main functions of the conducting zone include purifying, warming, humidifying and shunting the inspired and expired air. Air enters through the nose and is filtered as it passes through the nasal cavities. It then enters the pharynx and larynx, conducting tubes that consist of skeletal muscle and cartilage, respectively and epithelia. Air continues through the trachea, which then branches into the primary bronchi and bronchial tree. The trachea and bronchi are also composed of cartilaginous structures to enable air conductance and prevent airway collapse. Mucus membranes are found throughout the conducting zone and trap infectious agents and debris (1).

The respiratory zone starts with non-cartilage containing structures called terminal bronchioles, which lead into an alveolar duct and open into a group of alveoli. A single alveolus is a grape-like structure that is the site of gas exchange (1). Human lungs can contain between 274-790 million alveoli (2). This large number of alveoli and their elastic nature enables maximum surface area for gas exchange (1).

Respiratory epithelium in the conducting zone act as a physical barrier against microbes,

environmental insults and mechanical stress to maintain interstitium sterility. They are thought to have both innate and adaptive immune functions since they detect insults, enable localized attack of microbes and secrete inflammatory signals to immune cells patrolling the respiratory tract (3). The large airways are lined with a pseudostratified layer of epithelial cells that becomes more columnar and cuboidal in the small airways. Both large and small airway epithelium consist of ciliated cells, secretory cells, various columnar cells, neuroendocrine cells and basal cells with different percentages of these cell types depending on the proximodistal site (4). The respiratory zone is lined with small, cuboidal type II alveolar epithelial cells and large, squamous type I alveolar epithelial cells (5). Type II cells secrete surfactant to prevent alveolar collapse, elicit immune responses and can differentiate into type I cells to repair alveoli (6, 7). Type I cells facilitate gas exchange between the bloodstream and atmosphere (5).

1.1.1 The Airway Epithelium

The airway epithelium consists of numerous cells types with unique functions that enable respiratory homeostasis. Classically, cuboidal-shaped basal cells are the progenitor/stem cells of the airway and comprise 6-31% of airway epithelial cells (8). They are the primary cell type to repair the airway after injury and are crucial for maintaining airway homeostasis. Basal cells self-renew and differentiate into cell types such as goblet cells, club cells, ciliated cells, tuft cells, pulmonary neuroendocrine cells (PNECs), and pulmonary ionocytes. Basal cell dysfunction can be detrimental to airway homeostasis and was found to contribute to the pathogenesis of airway diseases such as COPD, asthma, cystic fibrosis (CF) and lung cancer (9-12).

Club cells are dome-shaped, secretory cells that have interesting stem cell-like properties.

They are capable of differentiating into goblet and ciliated cells and dedifferentiating into basal

cells if repopulation is necessary (13). They secrete the protein uteroglobin (SCGB1A1) abundantly into the airway lining fluid, which exhibits anti-inflammatory and immunosuppressive properties likely through cytokine inhibition (14, 15). In addition, club cell dysfunction has been found to contribute to many respiratory conditions such as COPD, pulmonary fibrosis and acute respiratory distress syndrome (16, 17).

Goblet cells are another type of secretory cell that mostly reside in submucosal glands in the airway and are the main producers of mucus. Mucus is composed of numerous proteins and other products, including mucins, electrolytes, fluids and antimicrobials and is vital to clearing pathogens and debris from the airway upon expulsion (18, 19). The mucin glycoproteins MUC5AC and MUC5B have been heavily studied in regards allergic airway, cystic fibrosis and infection susceptibility (20-22). Single cell RNA-seq analysis revealed two district mature goblet cell populations: Goblet-1 cell secrete mucins, and mucosal proteins such as Trefoil factor 2 (Tff2) and Goblet-2 secrete Lipf, a lipase that hydrolyses triglycerides (23).

Ciliated cells are columnar epithelial cells and contain apically localized hair-like structures known as cilia. Ciliated cells comprise 47-73% of cells lining the airway depending on proximodistal site (24). Cilia uniformly beat to clear mucus-trapped bacteria and debris, a process known as mucocilliary clearance (MCC) (4). Genetic mutations that cause dysfunctional or malformed cilia and are known as primary ciliary dyskinesias (PCD) and are characterized by severe respiratory infections and decreased mucocilliary clearance (25). In addition to mutations, numerous airway diseases and activities such as smoking and drinking cause cilia dysfunction (26-29). Receptors found on ciliated cells are used for cell entry for many RNA viruses. For example, SARS-CoV-2 targets angiotensin-converting enzyme 2 (ACE2) and Rhinovirus C targets cadherin related family member 3 (CDHR3) (30).

Pulmonary ionocytes were first discovered in 2018 and likely comprise only 2% of the airway epithelium (23, 31). They highly express CF transmembrane conductance regulator (CFTR), an ion channel that allows passive diffusion of chloride ions and contributes to fluid homeostasis of the airway surface liquid. Cystic Fibrosis is caused by mutations in CFTR and is characterized by viscous mucus production and increased susceptibility to respiratory infections (32). Interestingly, one study found that ionocytes expressed 55% of the detectable *Cftr* transcripts, while ciliated cells expressed 1.5% (23). Pulmonary ionocytes are of particular interest to CF researchers with the goal of finding new therapies to target this debilitating disease.

Pulmonary neuroendocrine cells (PNECs) are unique in the airway epithelium in that they have neurological and immune capabilities (33). They are innervated but comprise only 0.5% of the airway epithelium (33, 34). In addition, they secrete neuropeptides such as bombesin, serotonin, GAPA and CRGP that modulate both a nervous and immune response. For example, serotonin secretion by PNECs contributes to both bronchoconstriction and leukocyte recruitment through cytokine secretion (35, 36). In regard to fetal and neonatal roles for PNECs, they are important for proper lung development, yet contribute to sudden infant death syndrome (SIDS) through hyperplasic mechanisms (37, 38).

Airway cells whose functions are understudied in comparison to the abovementioned cell types include tuft cells, hillock cells and microfold cells. Much is known about tuft cells in regard to other organ systems, but they seem to have chemosensory and immunological functions in the airway (23, 39). Hillock cells form stratified layers in the airway, express keratin 13 and have a high turnover rate (23, 40). Similar to their function in the gut, microfold cells likely have pathogen-clearing and immunological properties (41).

The literature on the cell types that comprise the airway epithelium is vast, and each cell

type has a specific and vital function that contributes to airway and lung homeostasis.

1.2 The Apical Junctional Complex

It is critical for lung epithelial cells to maintain separation between the inhaled air and sterile environment of the lung to maintain homeostasis. They must have tight control over both transcellular and paracellular routes of transport for molecules, ions and fluid. As its name suggests, the apical junctional complex (APC) is located at the apical membrane in epithelial cells at sites of intercellular contact, creating a gate between the apical and basolateral domains. The APC encircles each cell and initiates bicellular and tricellular contacts with adjacent cells, creating a monolayer. The APC is composed of junctional complexes, including tight junctions and adherens junctions that play critical roles in barrier permeability and cellular integrity. In addition, polarity of epithelial cells is established by the APC through organization of the Crumbs (CRB) and partitioning defective complexes (42).

1.2.1 Tight Junctions

Tight junctions (TJs) regulate epithelial barrier permeability to molecules, ions and water. Three classes of membrane proteins found in TJs execute this function: Claudins, MarvelD proteins and Ig-superfamily proteins. Claudins form paracellular ion channels that range in specificity and permeability depending on the claudin isoform. There are twenty-three claudin isoforms, designated as classic or non-classic based on their degree of sequence similarity. Additionally, claudins can be designated as sealing (tighter barrier) or pore forming (leakier barrier) claudins. Claudin isoforms are expressed in a cell-specific and, therefore, tissue-specific manner, allowing for specialized barrier permeability depending on the needs of each organ (43, 44). Ion specificity is further specialized depending on how claudin isoforms are interacting with

one another in the same cell and in the adjacent cell (44).

The MarvelD proteins occludin and tricellulin contribute to TJ assembly and barrier integrity in a bicellular and tricellular manner, respectively (45). Further contributing to barrier integrity are the junctional adhesion molecules (JAMs) that are part of the Ig-superfamily proteins. JAMs expressed in barrier-forming cells control permeability of macromolecules and have been recently linked to cell migration mechanisms (46, 47). All three classes of membrane proteins bind to cytosolic scaffolding proteins such as zonula occludens (ZO) that link tight junctions to the actin cytoskeleton (43, 45, 47).

The major claudin isoforms expressed in bronchial epithelial cells are claudin-1, claudin-3, claudin-4, claudin-5 and claudin-7, which are all sealing claudins (48). Interestingly, many claudin isoforms have non-canonical roles in the cell and can be found at the basolateral membrane (49). For example, claudin-7, when palmitoylated, complexes with EpCAM in glycolipid-enriched membrane domains and promotes cell motility (50). Additionally, claudin-7 was found to interact beta 1 integrin at focal adhesion complexes and is important for cellular adhesion to the ECM (51). The regulation of TJs, while complex, is critical to epithelial cell homeostasis.

1.2.2 Adherens Junctions

Adherens junctions (AJs) work in concert with TJs as part of the AJC to promote integrity and cell-cell adhesion. In epithelial cells, the plasma membrane component of AJs consist of E-cadherin and nectin, which interact with intracellular catenin proteins and afadin, respectively. Catenin family members p120-catenin, β -catenin and α -catenin are regulated by a variety of kinases and have unique roles for stabilizing and maintaining cell-cell contacts. Like TJs, AJs interact with the actin cytoskeleton via α -catenin and afadin and are considered a signaling hub

for a variety of adhesion processes (52, 53).

In addition to it cell adhesion properties, β -catenin enacts transcriptional regulation via the Wnt/ β -catenin signaling pathway (54). Upon Wnt binding to its receptor at the plasma membrane, β -catenin translocates to the nucleus, binds Tcf/Lef transcription factors and regulates proliferation, differentiation, migration, stem-cell renewal and apoptosis (55). Aberrant activation of the Wnt/ β -catenin pathway occurs in a multitude of solid tumors and cancers, likely contributing to tumor invasion and metastasis (56).

1.3 Chronic Alcohol Use and the Lung

In 2019, 14.5 million people had alcohol use disorder (AUD) in the United States (57), and an estimated 283 million people had AUD worldwide (58). Excessive alcohol use affects multiple organs and can lead to chronic health issues such as liver disease, certain cancers, cardiac and vascular diseases, mental health issues and alcoholic lung disease (58, 59).

Chronic alcohol users are 2-4 times more likely to develop acute respiratory distress syndrome (ARDS), which carries a high mortality rate upwards of 35-55% (60, 61). ARDS is a more severe form of acute lung injury, in which airspace inflammation leads to alveolar flooding, inadequate gas exchange and severely low blood oxygen levels (62). In addition to alcohol use, ARDS can result from other comorbidities and insults such as smoking, sepsis, pneumonia, trauma, ventilator-induced lung injury and is associated with smoking (63).

1.3.1 Susceptibility to infections

Chronic alcohol use diminishes pulmonary function and immunity, leading to an increased risk of viral infections and bacterial pneumonia (64). Remarkably, this association was noted as

early as 1795 and was continually recognized into the early 1900's (65-67). In recent times, it was found that chronic alcohol users are more likely to be admitted to the ICU and require a ventilator (68-70). An independent association was found between current or past chronic alcohol use and increased risk of acquiring a pneumococcal infection (68). Further, heavy alcohol use was associated with a more severe outcome (ICU admission or death) from influenza (69).

A thorough examination of alcohol's effects on the innate and adaptive immunity of respiratory system suggests widespread dysfunction. Chronic alcohol use impairs mechanical defenses, such as diaphragm movement and ciliary function in airway cells (64, 71). In addition, it was associated with reduced production of surfactant-associated proteins as well as suppressed alveolar macrophage function and neutrophil function. Alveolar macrophages and neutrophils are two key innate immune cells that use phagocytosis to protect the host against pathogens. As part of the acquired immune system, lymphocyte recruitment was suppressed due to chronic alcohol exposure (64).

SARS-CoV-2, the virus responsible for the COVID-19 pandemic, stands for "severe acute respiratory syndrome coronavirus 2." In regard to the respiratory system, SARS-CoV-2 infects mostly nasal epithelial cells, ciliated cells in the airway and type II alveolar cells, due to their expression of ACE2 and TMPRSS2, the two main receptors used for viral entry. The four main stages of COVID 19 are upper respiratory tract infection, onset of dyspnea and pneumonia, cytokine storm and hyperinflammatory state and death or recovery (72). In late 2020, a group speculated that people with AUD may have a higher risk of developing worse outcomes with COVID-19 (73), highlighting the need to study how chronic alcohol use coupled with SARS-CoV-2 infection affects all organ systems, especially the respiratory system. However, upon further investigation, clinical and epidemiological studies report conflicting data regarding chronic

alcohol consumption and SARS-CoV-2 infection outcomes. Two studies indicate there was no correlation between chronic alcohol consumption and increased risk or severity of COVID-19 (74, 75), while an epidemiological study correlated number of drinks with ARDS following SARS-CoV-2 infection (76).

Recently, two studies investigated a connection between chronic alcohol use and SARS-CoV-2 infection in rodent models. The first study utilized three different alcohol exposure models to mimic sub chronic exposure, non-abstinence (chronic) and abstinence (3-weeks of recovery). They measured gene expression of ACE2 and TMPRSS2 in whole liver, lung, ileum, liver, kidney and brain. There was a two-fold increase in ACE2 gene expression is all three model systems, indicating that the lungs are particularly sensitive to alcohol and potentially require an extended recovery time. In all three groups, TMPRSS2 was not upregulated in the lungs, although there was a trending increase in the sub chronic and non-abstinent groups (77). The second study utilized ethanol-fed transgenic mice expressing the human ACE2 receptor and instilled subunit 1 of the SARS-CoV-2 spike protein (S1SP) intratracheally. Ethanol-fed mice instilled with S1SP showed an increase in white blood cell count and cytokine production in bronchoalveolar lavage (BAL) fluid compared to control-fed mice. Additionally, lung tissue from ethanol-fed mice had an increase in ACE2 expression compared to control-fed mice (78).

The authors of the study and others hypothesize that an increase in ACE2 receptor protein could lead to a more severe infection and outcomes. To date, numerous studies highlight this correlation (79). Lung tissues from patients who died from COVID-19 show increased levels of ACE2 expression compared to patients who died from other causes (80); in the lungs, males have a 3x increase expression of ACE2, and males have a significantly higher fatality rate for COVID-19 (81, 82); in nasal and bronchial epithelium, ACE2 expression is lower in children compared to

adults, which may explain why children have less severe respiratory symptoms following SARS-CoV-2 infection (83, 84). Despite these correlations, it is still unknown how infection, comorbidities and ACE2 shedding alter ACE2 expression and how these parameters play a role in disease severity.

1.3.2 Oxidative Stress

The lung specializes in the uptake of oxygen and the release of carbon dioxide, and therefore, heavily relies on combating oxidative stress caused by reactive oxygen species (ROS). ROS are produced in the healthy lung and released as cellular respiration products and by immune cells as part of their bactericidal properties (85). Enzymes such as peroxidases, catalases and superoxide dismutases, and antioxidants, such as glutathione, Vitamin C, Vitamin E and ubiquinol work together to prevent ROS-induced oxidative damage to the lung (86, 87). In the alcoholic lung, the epithelial lining fluid was found to have an 80% decrease in glutathione levels (400uM to 50uM) as well as increased oxidation of glutathione into the glutathione disulfide form (88-90). Oxidative stress and depletion of glutathione can be partially explained by the metabolism of ethanol to acetaldehyde since acetaldehyde is known to reduce available glutathione levels. (89, 91). In an alcoholic rat model, alveolar type II cells were found to have depleted glutathione levels, mitochondrial-generated ROS and diminished surfactant synthesis, which led to increased apoptosis of these critical cells (91, 92). However, dietary procysteine, a precursor to glutathione, restored both cytosolic and mitochondrial glutathione levels, reduced mitochondrial ROS, recovered surfactant production and reduced apoptosis of rat alveolar type II cells from the alcoholic rat model (92, 93).

Alveolar macrophages rely on the glutathione found in the epithelial lining fluid to combat

ROS production (91). Alveolar macrophages from AUD subjects also show depleted levels of available glutathione and increased levels of NADPH oxidases, rendering cellular functions such as phagocytosis and clearance of pathogens dysfunctional (94, 95). In an alcohol fed rat model however, zinc supplementation prevented ethanol-induced dysfunction of alveolar macrophages and improved bacterial clearance in the lungs (96). Identifying pathways to combat oxidative stress in the alcoholic lung is crucial to create prophylactic therapies for patients struggling with chronic alcohol use (97).

It was discovered that following oxidative stress due to chronic alcohol use, there was an increase in transforming growth factor beta-1 (TGF- β 1). TGF- β 1 can act in both an autocrine and paracrine fashion by injury-induced separation from its latency complex and causes cell death and barrier dysfunction of alveolar cells (98). Further, an increase in TGF- β 1 due to chronic alcohol consumption primes the lung for ARDS due to sepsis or lung injury (99).

1.3.3 Barrier Dysfunction

The association between chronic alcohol use and ARDS encouraged further investigation into the alveolar epithelial cell barrier and the junctions that regulate it. As stated above, ARDS is characterized by flooding of the alveoli and points to a disruption in fluid dynamics as highlighted by increased protein found in BAL fluid in alcoholic patients. In vitro and in vivo models of chronic alcohol use and lung injury reveal TJ-related decreases in barrier function, which is not surprising since TJs promote barrier function (100, 101). Notably, claudin-3, claudin-7, claudin-18, occludin, and ZO-1 decreased in response to chronic alcohol exposure. Interestingly, claudin-5 expression was upregulated in response to chronic alcohol, and is associated with decreased barrier function, TJ strand breaks, intracellular claudin staining and spike-like protrusions at TJs

(TJ spikes). (101-104). This increased presence of claudin-5 at TJs caused more claudin-18:claudin-5 interactions and less claudin-18:ZO-1 interactions to occur, elucidating a mechanism for how hetero-claudin interactions influence barrier function (105). While increased claudin-5 correlated with the presence of TJ spikes, the TJ spikes are likely not influencing barrier function, but rather have an unknown regulatory function (104).

Less is known about the impact of chronic alcohol exposure on the airway and its effects on airway epithelial cells. However, it is clear that acute, mild exposure to alcohol has drastically different effects compared to chronic exposure. Acute exposure may enhance MCC, cause bronchodilation and mitigate detrimental inflammatory responses in asthma and COPD patients. Chronic exposure, however, impairs MCC and contributes to worsening asthma and COPD (106).

In vitro models of acute ethanol exposure using bronchial epithelial cell lines suggest that ethanol exposure alters TJ protein expression and barrier function. Bronchial epithelial cells exposed to ethanol for 48 hours displayed a dose-dependent increase in barrier permeability, and this was associated with decreased localization of claudin-1, claudin-5 and claudin-7 to TJs through protein kinase C alpha (PKCα) activation (107).

The cytokine TGF-β1 is upregulated in chronic ethanol exposure and contributes to barrier dysfunction in alveolar cells. This is also the case for bronchial epithelial cells acutely exposed to 60mM ethanol *in vitro*. However, the addition of the cytokine GM-CSF mitigated these effects in both bronchial and alveolar cells and suggests that the relative balance of GM-CSF and TGF-β1 regulates barrier function. Remarkably, a higher GM-CSF:TGF-β1 ratio correlated with increased survival of critically ill patients with ventilatory associated pneumonia suggesting this balance is important for overcoming acute lung injury (108) . Given the drastic differences between acute and chronic alcohol exposure on the airway, it is critical that chronic alcohol exposure models are

developed in order to study the effects of chronic alcohol use on barrier function.

1.4 Scope of Dissertation

To properly study diseases of the airway, we must develop *in vitro* cell culture systems that best mimic the *in vivo* environment. Primary airway cells cultured at air-liquid interface (ALI) on Transwell permeable supports remain one of the most thoroughly used and tested model systems, especially for studying airway cell barrier function. The culture medium must support airway cell differentiation and function for 2 weeks at minimum, encourage barrier formation, and consist of the nutrients and growth factors found in the *in vivo* microenvironment at physiologic concentrations. In addition to supporting the differentiation of normal/healthy airway cells, the system must support differentiation of diseased cells. This can be tested using various confirmational assays such as qRT-PCR, western blot and immunofluorescence of common airway cell markers, and functional assays such as transepithelial electrical resistance, dye flux and Ussing chamber analysis.

In Chapter 2, I along with Koval lab members and Emory collaborators tested if a medium composition with human physiologic glucose levels (150mg/dL) can support primary nasal, tracheal and bronchial cell differentiation from healthy and cystic fibrosis donors. Most airway cell culture mediums are derived from DMEM and other base mediums with glucose concentrations ranging from 300- 450mg/dL, which supports the culture of most primary rodent cells and immortalized cell lines from multiple species. These high glucose mediums can be problematic because it is unclear how a hyperglycemic environment affects airway cell differentiation and function, and metabolic studies will be difficult to perform. This new physiologic glucose medium formulation is called Emory-ALI (E-ALI) medium, and it encouraged

differentiation of basal cells into ciliated cells, mucus-producing cells, ionocytes and club cells. Bronchial epithelial cells expanded and differentiated in E-ALI medium showed insulin-stimulated glucose uptake and increased barrier function, which were both inhibited by high glucose concentrations. This medium also supported primary CF nasal epithelia as demonstrated by immunofluorescence of airway cell markers and electrophysiological analysis of ENaC and CFTR currents. These data indicate that high glucose levels impact the airway cell barrier and further highlight the need for physiological glucose levels when subjecting primary human airway cells to metabolic analysis.

In Chapter 3, I, along with Koval lab members and collaborators from Emory and the University of Georgia determine if chronic alcohol use in combination with SARs-CoV-2 infection negatively impacts airway cell function. We differentiated bronchial brushings from patients with alcohol use disorder (AUD) and non-alcohol users (non-AUD) in E-ALI media and infected with SARs-CoV-2 for 72 hours. We found that the barrier function of AUD cells did not recover after 72 hours, while the barrier function of non-AUD cells recovered above baseline. SARs-CoV-2 infection of both AUD and non-AUD cells displayed a decrease in β catenin expression as measured by fluorescence intensity. Both apical and basolateral media was collected at 6, 24, 48, and 72 hpi and subjected to multiplex cytokine analysis. Multiplex analysis of cytokine secretion by SARS-CoV-2 infected cells revealed that many pro-inflammatory cytokines, including IL-1β and IFNy, showed higher levels of secretion by AUD cells during the 72h period post-infection as compared to non-AUD cells. Bulk RNA sequencing analysis revealed 117 upregulated differentially expressed (DE) genes and 47 downregulated DE genes in AUD cells compared to non-AUD cells. Of note, ACE2 and two TMPRESS isoforms were upregulated while GSTA1, WNT3a and MUC5B were downregulated. GO enrichment analysis indicated that AUD cells

adapted an inflammatory, epidermal profile with keratinocyte differentiation, epidermis development and inflammatory response as top GO terms. Taken together our data suggests that AUD may prime airway cells for a worse outcome in SARs-CoV-2 infection and further establishes AUD as a risk factor for COVID-19.

In Chapter 4, I summarize my unpublished work on teasing apart ethanol's effects on bronchial cell barrier function. To do this, I utilized human airway cells, rat airway cells and an in vitro system of ethanol exposure. I treated healthy human bronchial epithelial cells with 10mM, 60mM and 100mM ethanol and found that ethanol caused a decrease in transepithelial electrical resistance (TER) during differentiation but has similar barrier function to untreated cells once differentiation into a mucociliary monolayer was complete. Additionally, primary airway epithelial cells isolated from healthy (non-AUD) and alcoholic (AUD) patients had a similar result and most samples from chronic alcohol users remained migratory and in an "unjammed" state, since areas of stretched cells and swirls of cells were present after differentiation. Rat tracheal cells were more susceptible to in vitro ethanol exposure since barrier function was significantly lower than untreated cells once differentiation was complete. The protein junctional adhesion molecule A (JAM-A) regulates barrier function and epithelial cell migration and may play a role in causing the sustained unjammed phenotype, although in vitro exposure did not decrease JAM-A expression. I also discovered that unjamming may be an age-dependent phenotype, though further analysis must be done to determine this.

My dissertation research features a body of work focused on utilizing a physiologically improved *in vitro* model system to study the impacts of alcohol use disorder on airway cell morphology, migration and function and its implications in COVID-19 disease progression. The findings from this body of work suggest AUD negatively impacts airway cells at epigenetic, RNA

and protein levels revealing widespread changes in cell profile and function. The implications and	
future directions of this work are discussed in Chapter 5 .	
References	

- 1. Betts JG, Young KA, Wise JA, Johnson E, Poe B, Kruse DH, et al. Anatomy and Physiology. Houston, Texas: OpenStax; 2013.
- 2. Ochs M, Nyengaard JR, Jung A, Knudsen L, Voigt M, Wahlers T, Richter J, Gundersen HJ. The number of alveoli in the human lung. Am J Respir Crit Care Med. 2004.
- 3. Larsen SB, Cowley CJ, Fuchs E. Epithelial cells: liaisons of immunity. Curr Opin Immunol. 2020.
- 4. Crystal RG, Randell SH, Engelhardt JF, Voynow J, Sunday ME. Airway epithelial cells: current concepts and challenges. Proc Am Thorac Soc. 2008.
- Crapo JD, Barry BE, Gehr P, Bachofen M, Weibel ER. Cell Number and Cell Characteristics of the Normal Human Lung. American Review of Respiratory Disease 1982;126:332–7.
- 6. Evans MJ, Cabral LJ, Stephens RJ, Freeman G. Transformation of alveolar Type 2 cells to Type 1 cells following exposure to NO2. Exp Mol Pathol 1975;22:142–50.
- 7. Fehrenbach H. Alveolar epithelial type II cell: defender of the alveolus revisited. Respir Res 2001;2:33.
- 8. Boers JE, Ambergen AW, Thunnissen FBJM. Number and proliferation of basal and parabasal cells in normal human airway epithelium.
- 9. Shaykhiev R, Crystal RG. Early events in the pathogenesis of chronic obstructive pulmonary disease: smoking-induced reprogramming of airway epithelial basal progenitor cells. *Ann. Am. Thorac. Soc.* 2014;11:S252–S258.
- 10. Heijink IH, Kuchibhotla VNS, Roffel MP, Maes T, Knight DA, Sayers I, Nawijn MC. Epithelial cell dysfunction, a major driver of asthma development. Allergy. 2020 Aug;75(8):1902-1917. doi: 10.1111/all.14421. Epub 2020 Jun 16. PMID: 32460363;

- PMCID: PMC7496351.
- 11. Voynow JA, Fischer BM, Roberts BC, Proia AD. Basal-like cells constitute the proliferating cell population in cystic fibrosis airways. Am J Respir Crit Care Med. 2005 Oct 15;172(8):1013-8. doi: 10.1164/rccm.200410-1398OC. Epub 2005 Jul 14. PMID: 16020799.
- 12. Fukui T, et al. Lung adenocarcinoma subtypes based on expression of human airway basal cell genes. *Eur. Respir. J.* 2013;42:1332–1344. doi: 10.1183/09031936.00144012.
- 13. Hong KU, Reynolds SD, Giangreco A, Hurley CM, Stripp BR. Clara cell secretory proteinexpressing cells of the airway neuropitelial body microenvironment include a labelretaining subset and are critical for epithelial renewal after progenitor cell depletion.
- 14. Broeckaert F, Bernard A. Clara cell secretory protein (CC16): characteristics and perspectives as lung peripheral biomarker. *Clin. Exp. Allergy*. 2000;30:469–475. doi: 10.1046/j.1365-2222.2000.00760.x
- 15. Dierynck I, Bernard A, Roels H, De, Ley M. Potent inhibition of both human interferongamma production and biologic activity by the Clara cell protein CC16. *Am. J. Respir. Cell Mol. Biol.* 1995;12:205–210. doi: 10.1165/ajrcmb.12.2.7865218.
- 16. Rokicki W, Rokicki M, Wojtacha J, Dżeljijli A. The role and importance of club cells (Clara cells) in the pathogenesis of some respiratory diseases. *Kardiochirurgia i torakochirurgia Pol. = Pol. J. Cardio-Thorac. Surg.* 2016;13:26–30. doi: 10.5114/kitp.2016.58961.
- 17. Zuo WL, et al. Dysregulation of club cell biology in idiopathic pulmonary fibrosis. *PLoS ONE*. 2020;15:e0237529. doi: 10.1371/journal.pone.0237529.
- 18. Whitsett JA. Airway epithelial differentiation and mucociliary clearance. Ann. Am. Thorac.

- Soc. 2018;15:S143–S148. doi: 10.1513/AnnalsATS.201802-128AW.
- Ma J, Rubin BK, Voynow JA. Mucins, Mucus, and Goblet Cells. Chest. 2018
 Jul;154(1):169-176. doi: 10.1016/j.chest.2017.11.008. Epub 2017 Nov 21. PMID: 29170036.
- 20. Evans CM, et al. The polymeric mucin Muc5ac is required for allergic airway hyperreactivity. *Nat. Commun.* 2015;6:6281. doi: 10.1038/ncomms7281.
- 21. Roy MG, et al. Muc5b is required for airway defence. *Nature*. 2014;505:412–416. doi: 10.1038/nature12807.
- 22. Niv Y, Ho SB, Rokkas T. Mucin Secretion in Cystic Fibrosis: A Systematic Review. Dig Dis. 2021;39(4):375-381. doi: 10.1159/000512268. Epub 2020 Oct 13. PMID: 33049746.
- 23. Montoro DT, Haber AL, Biton M, Vinarsky V, Lin B, Birket SE, Yuan F, Chen S, Leung HM, Villoria J, Rogel N, Burgin G, Tsankov AM, Waghray A, Slyper M, Waldman J, Nguyen L, Dionne D, Rozenblatt-Rosen O, Tata PR, Mou H, Shivaraju M, Bihler H, Mense M, Tearney GJ, Rowe SM, Engelhardt JF, Regev A, Rajagopal J. A revised airway epithelial hierarchy includes CFTR-expressing ionocytes. Nature. 2018 Aug;560(7718):319-324. doi: 10.1038/s41586-018-0393-7. Epub 2018 Aug 1. PMID: 30069044; PMCID: PMC6295155.
- 24. Raman T, O'Connor TP, Hackett NR, Wang W, Harvey BG, et al. Quality control in microarray assessment of gene expression in human airway epithelium. *BMC Genomics*. 2009;10:493.
- 25. Horani A, Ferkol TW. Understanding Primary Ciliary Dyskinesia and Other Ciliopathies. J Pediatr. 2021 Mar;230:15-22.e1. doi: 10.1016/j.jpeds.2020.11.040. Epub 2020 Nov 23. PMID: 33242470; PMCID: PMC8690631.

- 26. Tamashiro E, et al. Cigarette smoke exposure impairs respiratory epithelial ciliogenesis. *Am. J. Rhinol. Allergy.* 2009;23:117–122. doi: 10.2500/ajra.2009.23.3280.
- 27. Ghosh M, et al. Exhaustion of airway basal progenitor cells in early and established chronic obstructive pulmonary disease. *Am. J. Respir. Crit. Care Med.* 2018;197:885–896. doi: 10.1164/rccm.201704-0667OC.
- 28. Tilley AE, Walters MS, Shaykhiev R, Crystal RG. Cilia dysfunction in lung disease. Annu Rev Physiol. 2015;77:379-406. doi: 10.1146/annurev-physiol-021014-071931. Epub 2014 Oct 29. PMID: 25386990; PMCID: PMC4465242.
- 29. Simet SM, Pavlik JA, Sisson JH. Dietary antioxidants prevent alcohol-induced ciliary dysfunction. Alcohol. 2013a; 47:629–635. [PubMed: 24169090]
- 30. Griggs TF, Bochkov YA, Basnet S, Pasic TR, Brockman-Schneider RA, Palmenberg AC, Gern JE. Rhinovirus C targets ciliated airway epithelial cells. Respir Res. 2017 May 4;18(1):84. doi: 10.1186/s12931-017-0567-0. PMID: 28472984; PMCID: PMC5418766.
- 31. Plasschaert LW, et al. A single-cell atlas of the airway epithelium reveals the CFTR-rich pulmonary ionocyte. *Nature*. 2018;560:377–381. doi: 10.1038/s41586-018-0394-6.
- 32. Miah KM, Hyde SC, Gill DR. Emerging gene therapies for cystic fibrosis. *Expert Rev. Respir. Med.* 2019;13:709–725. doi: 10.1080/17476348.2019.1634547.
- 33. Branchfield K, et al. Pulmonary neuroendocrine cells function as airway sensors to control lung immune response. *Science*. 2016;351:707–710. doi: 10.1126/science.aad7969.
- 34. Boers JE, Brok JLD, Koudstaal J, Arends JW, Thunnissen FB. Number and proliferation of neuroendocrine cells in normal human airway epithelium. *Am. J. Respir. Crit. Care Med.* 1996;154:758–763. doi: 10.1164/ajrccm.154.3.8810616.
- 35. Jankala EO, Virtama P. On the bronchoconstrictor effect of serotonin. Bronchographic

- studies on rabbits and guinea-pigs. *J. Physiol.* 1961;159:381–383. doi: 10.1113/jphysiol.1961.sp006815.
- 36. Herr N, Bode C, Duerschmied D. The effects of serotonin in immune cells. *Front. Cardiovas. Med.* 2017;4:48–48.. doi: 10.3389/fcvm.2017.00048
- 37. Cutz E, Perrin DG, Pan J, Haas EA, Krous HF. Pulmonary neuroendocrine cells and neuroepithelial bodies in sudden infant death syndrome: potential markers of airway chemoreceptor dysfunction.
- 38. Cutz E, Pan J, Yeger H, Domnik NJ, Fisher JT. Recent advances and contraversies on the role of pulmonary neuroepithelial bodies as airway sensors. *Semin. Cell Dev. Biol.* 2013;24:40–50. doi: 10.1016/j.semcdb.2012.09.003.
- 39. Sharma P, et al. Bitter taste receptor agonists mitigate features of allergic asthma in mice. *Sci. Rep.* 2017;7:46166. doi: 10.1038/srep46166.
- 40. Deprez, M et al. A single-cell atlas of the human healthy airways. *Am. J. Respir. Crit. Care Med.* **202**, 1636–1645 (2020).
- 41. Kim D-Y, et al. The airway antigen sampling system: respiratory M cells as an alternative gateway for inhaled antigens. *J. Immunol.* 2011;186:4253–4262. doi: 10.4049/jimmunol.0903794.
- 42. Wang Q, Margolis B. Apical junctional complexes and cell polarity. Kidney Int. 2007 Dec;72(12):1448-58. doi: 10.1038/sj.ki.5002579. Epub 2007 Oct 3. PMID: 17914350.
- 43. Krause G, Winkler L, Mueller SL, Haseloff RF, Piontek J, Blasig IE. Structure and function of claudins. Biochim Biophys Acta. 2008 Mar;1778(3):631-45. doi: 10.1016/j.bbamem.2007.10.018. Epub 2007 Oct 25. PMID: 18036336.
- 44. Overgaard CE, Daugherty BL, Mitchell LA, Koval M. Claudins: control of barrier function

- and regulation in response to oxidant stress. Antioxid Redox Signal. 2011 Sep 1;15(5):1179-93. doi: 10.1089/ars.2011.3893. Epub 2011 May 9. PMID: 21275791; PMCID: PMC3144428.
- 45. Raleigh DR, Marchiando AM, Zhang Y, Shen L, Sasaki H, Wang Y, Long M, Turner JR. Tight junction-associated MARVEL proteins marveld3, tricellulin, and occludin have distinct but overlapping functions. Mol Biol Cell. 2010 Apr 1;21(7):1200-13. doi: 10.1091/mbc.e09-08-0734. Epub 2010 Feb 17. PMID: 20164257; PMCID: PMC2847524.
- 46. Hartmann C, Schwietzer YA, Otani T, Furuse M, Ebnet K. Physiological functions of junctional adhesion molecules (JAMs) in tight junctions. Biochim Biophys Acta Biomembr. 2020 Sep 1;1862(9):183299. doi: 10.1016/j.bbamem.2020.183299. Epub 2020 Apr 2. PMID: 32247783.
- 47. Wang J, Liu H. The Roles of Junctional Adhesion Molecules (JAMs) in Cell Migration. Front Cell Dev Biol. 2022 Mar 9;10:843671. doi: 10.3389/fcell.2022.843671. PMID: 35356274; PMCID: PMC8959349.
- 48. Molina SA, Stauffer B, Moriarty HK, Kim AH, McCarty NA, Koval M. Junctional abnormalities in human airway epithelial cells expressing F508del CFTR. Am J Physiol Lung Cell Mol Physiol. 2015 Sep 1;309(5):L475-87. doi: 10.1152/ajplung.00060.2015. Epub 2015 Jun 26. PMID: 26115671; PMCID: PMC4556929.
- 49. Hagen SJ. Non-canonical functions of claudin proteins: Beyond the regulation of cell-cell adhesions. Tissue Barriers. 2017 Apr 3;5(2):e1327839. doi: 10.1080/21688370.2017.1327839. Epub 2017 May 19. PMID: 28548895; PMCID: PMC5501131.
- 50. Heiler S, Mu W, Zöller M, Thuma F. The importance of claudin-7 palmitoylation on

- membrane subdomain localization and metastasis-promoting activities. Cell Commun Signal. 2015 Jun 9;13:29. doi: 10.1186/s12964-015-0105-y. PMID: 26054340; PMCID: PMC4459675.
- 51. Lu Z, Kim DH, Fan J, Lu Q, Verbanac K, Ding L, Renegar R, Chen YH. A non-tight junction function of claudin-7-Interaction with integrin signaling in suppressing lung cancer cell proliferation and detachment. Mol Cancer. 2015 Jun 17;14:120. doi: 10.1186/s12943-015-0387-0. PMID: 26081244; PMCID: PMC4470020.
- 52. Niessen CM, Gottardi CJ. Molecular components of the adherens junction. Biochim Biophys Acta. 2008 Mar;1778(3):562-71. doi: 10.1016/j.bbamem.2007.12.015. Epub 2008 Jan 14. PMID: 18206110; PMCID: PMC2276178.
- 53. Hartsock A, Nelson WJ. Adherens and tight junctions: structure, function and connections to the actin cytoskeleton. Biochim Biophys Acta. 2008 Mar;1778(3):660-9. doi: 10.1016/j.bbamem.2007.07.012. Epub 2007 Jul 27. PMID: 17854762; PMCID: PMC2682436.
- 54. Buechel D, Sugiyama N, Rubinstein N, Saxena M, Kalathur RKR, Lüönd F, Vafaizadeh V, Valenta T, Hausmann G, Cantù C, Basler K, Christofori G. Parsing β-catenin's cell adhesion and Wnt signaling functions in malignant mammary tumor progression. Proc Natl Acad Sci U S A. 2021 Aug 24;118(34):e2020227118. doi: 10.1073/pnas.2020227118. PMID: 34408016; PMCID: PMC8403962.
- 55. Pai SG, Carneiro BA, Mota JM, Costa R, Leite CA, Barroso-Sousa R, Kaplan JB, Chae YK, Giles FJ. Wnt/beta-catenin pathway: modulating anticancer immune response. J Hematol Oncol. 2017 May 5;10(1):101. doi: 10.1186/s13045-017-0471-6. PMID: 28476164; PMCID: PMC5420131.

- 56. Zhang Y, Wang X. Targeting the Wnt/β-catenin signaling pathway in cancer. J Hematol Oncol. 2020 Dec 4;13(1):165. doi: 10.1186/s13045-020-00990-3. PMID: 33276800; PMCID: PMC7716495.
- 57. SAMHSA, Center for Behavioral Health Statistics and Quality. 2019 National Survey on Drug Use and Health. Table 5.4A Alcohol Use Disorder in Past Year among Persons Aged 12 or Older, by Age Group and Demographic Characteristics: Numbers in Thousands. 2018 and 2019.
- 58. World Health Organization 2018 Alcohol pdf Global status report on alcohol and health 2018.
- 59. Kershaw CD, Guidot DM. Alcoholic lung disease. Alcohol Res Health. 2008
- 60. Moss, M., Bucher, B., Moore, F. A., Moore, E. E. & Parsons, P. E. The role of chronic alcohol abuse in the development of acute respiratory distress syndrome in adults. JAMA. 1996.
- 61. Moss, M. *et al.* Chronic alcohol abuse is associated with an increased incidence of acute respiratory distress syndrome and severity of multiple organ dysfunction in patients with septic shock. Crit Care Med. 2003.
- 62. Petty, T. L. & Ashbaugh, D. G. The adult respiratory distress syndrome. Clinical features, factors influencing prognosis and principles of management. Chest. 1971.
- 63. Matthay MA, Zemans RL, Zimmerman GA, Arabi YM, Beitler JR, Mercat A, et al. Acute respiratory distress syndrome. Nat Rev Dis Primers 2019;5:18.
- 64. Zhang P, Bagby GJ, Happel KI, Summer WR, Nelson S. Pulmonary host defenses and alcohol. Front Biosci. 2002;7:d1314–30.
- 65. Rush B.: An inquiry into the effects of ardent spirits upon the human body and mind. Q J

- Stud Alcohol 4, 321-943)
- 66. Olser W: The Principles and Practice of Medicine. New York, Appleton (1905)
- 67. Capps J. A., G. H. Coleman: Influence of alcohol on prognosis of pneumonia in Cook County Hospital. JAMA 80, 750-752 (1923)
- 68. de Roux, A. *et al.* Impact of alcohol abuse in the etiology and severity of community-acquired pneumonia. Chest. 2006.
- 69. Greenbaum, A. *et al.* Heavy alcohol use as a risk factor for severe outcomes among adults hospitalized with laboratory-confirmed influenza, 2005-2012. Infection. 2014.
- 70. Saitz, R., Ghali, W. A. & Moskowitz, M. A. The impact of alcohol-related diagnoses on pneumonia outcomes. Arch Intern Med. 1997.
- 71. Wyatt, T. A. *et al.* Alcohol potentiates RSV-mediated injury to ciliated airway epithelium. Alcohol. 2019.
- 72. Stasi C, Fallani S, Voller F, Silvestri C. Treatment for COVID-19: An overview. Eur J Pharmacol. 2020 Dec 15;889:173644. doi: 10.1016/j.ejphar.2020.173644. Epub 2020 Oct 11. PMID: 33053381; PMCID: PMC7548059.
- 73. Bailey KL, Samuelson DR, Wyatt TA. Alcohol use disorder: A pre-existing condition for COVID-19? Alcohol. 2021.
- 74. Dai, M., Tao, L., Chen, Z., Tian, Z., Guo, X., Allen-Gipson, D.S. et al. (2020) Influence of cigarettes and alcohol on the severity and death of COVID-19: a multicenter retrospective study in Wuhan, China. *Frontiers in Physiology*, **11**, 588553.
- 75. Zhong, R., Chen, L., Zhang, Q., Li, B., Qiu, Y., Wang, W. et al. (2021) Which factors, smoking, drinking alcohol, betel quid chewing, or underlying diseases, are more likely to influence the severity of COVID-19? *Frontiers in Physiology*, **11**, 623498.

- 76. Lassen MCH, Skaarup KG, Sengeløv M, Iversen K, Ulrik CS, Jensen JUS, Biering-Sørensen T. Alcohol Consumption and the Risk of Acute Respiratory Distress Syndrome in COVID-19. Ann Am Thorac Soc. 2021 Jun;18(6):1074-1076. doi: 10.1513/AnnalsATS.202008-988RL. PMID: 33315543; PMCID: PMC8456730.
- 77. Friske MM, Giannone F, Senger M, Seitz R, Hansson AC, Spanagel R. Chronic alcohol intake regulates expression of SARS-CoV2 infection-relevant genes in an organ-specific manner. Alcohol Clin Exp Res. 2023 Jan;47(1):76-86. doi: 10.1111/acer.14981. Epub 2023 Feb 12. PMID: 36774629.
- 78. Solopov PA, Colunga Biancatelli RML, Catravas JD. Alcohol Increases Lung Angiotensin-Converting Enzyme 2 Expression and Exacerbates Severe Acute Respiratory Syndrome Coronavirus 2 Spike Protein Subunit 1-Induced Acute Lung Injury in K18-hACE2 Transgenic Mice. Am J Pathol. 2022 Jul;192(7):990-1000. doi: 10.1016/j.ajpath.2022.03.012. Epub 2022 Apr 25. PMID: 35483427; PMCID: PMC9040477.
- 79. Beyerstedt S, Casaro EB, Rangel ÉB. COVID-19: angiotensin-converting enzyme 2 (ACE2) expression and tissue susceptibility to SARS-CoV-2 infection. Eur J Clin Microbiol Infect Dis. 2021 May;40(5):905-919. doi: 10.1007/s10096-020-04138-6. Epub 2021 Jan 3. PMID: 33389262; PMCID: PMC7778857.
- 80. Gheware A, Ray A, Rana D, Bajpai P, Nambirajan A, Arulselvi S, Mathur P, Trikha A, Arava S, Das P, Mridha AR, Singh G, Soneja M, Nischal N, Lalwani S, Wig N, Sarkar C, Jain D. ACE2 protein expression in lung tissues of severe COVID-19 infection. Sci Rep. 2022 Mar 8;12(1):4058. doi: 10.1038/s41598-022-07918-6. PMID: 35260724; PMCID: PMC8902283.

- 81. Docherty AB, Harrison EM, Green CA, Hardwick HE, Pius R, Norman L, Holden KA, Read JM, Dondelinger F, Carson G, Merson L, Lee J, Plotkin D, Sigfrid L, Halpin S, Jackson C, Gamble C, Horby PW, Nguyen-Van-Tam JS, Ho A, Russell CD, Dunning J, Openshaw PJ, Baillie JK, Semple MG. Features of 20133 UK patients in hospital with COVID-19 using the ISARIC WHO Clinical Characterisation Protocol: prospective observational cohort study.
- 82. Zhao Y, Zhao Z, Wang Y, Zhou Y, Ma Y, Zuo W. Single-cell RNA expression profiling of ACE2, the receptor of SARS-CoV-2. *American Journal of Respiratory and Critical Care Medicine*. 2020;202:756–759.
- 83. Bunyavanich S, Do A, Vicencio A. Nasal gene expression of angiotensin-converting enzyme 2 in children and adults. *JAMA*. 2020;323:2427–2429. doi: 10.1001/jama.2020.8707.
- 84. Saheb Sharif-Askari N, Saheb Sharif-Askari F, Alabed M, Temsah M-H, al Heialy S, Hamid Q, Halwani R. Airways expression of SARS-CoV-2 receptor, ACE2, and TMPRSS2 is lower in children than adults and increases with smoking and COPD. *Molecular Therapy. Methods & Clinical Development*. 2020;18:1–6. doi: 10.1016/j.omtm.2020.05.013.
- 85. Rosanna DP, Salvatore C. Reactive oxygen species, inflammation, and lung diseases. Curr Pharm Des. 2012;18(26):3889-900. doi: 10.2174/138161212802083716. PMID: 22632750.
- 86. Thorpe GW, Fong CS, Alic N, Higgins VJ, Dawes IW. Cells have distinct mechanisms to maintain protection against different reactive oxygen species: oxidative-stress-response genes. Proc Natl Acad Sci U S A. 2004 Apr 27;101(17):6564-9.

- doi:10.1073/pnas.0305888101. Epub 2004 Apr 15. PMID: 15087496; PMCID: PMC404085.
- 87. Jean JC. Liu Y. Brown LA. Marc RE. Klings E. Joyce-Brady M. Gamma-glutamyl transferase deficiency results in lung oxidant stress in normoxia. *Am J Physiol Lung Cell Mol Physiol*. 2002;283:L766–L776.
- 88. Yeh MY, Burnham EL, Moss M, Brown LAS. Chronic alcoholism alters systemic and pulmonary glutathione redox status. *American Journal of Respiratory and Critical Care Medicine*. 2007;176(3):270–276.
- 89. Moss M, Guidot DM, Wong-Lambertina M, Ten Hoor T, Perez RL, Brown LA. The effects of chronic alcohol abuse on pulmonary glutathione homeostasis. Am J Respir Crit Care Med. 2000 Feb;161(2 Pt 1):414-9. doi: 10.1164/ajrccm.161.2.9905002. PMID: 10673179.
- 90. Johnson LN, Koval M. Cross-talk between pulmonary injury, oxidant stress, and gap junctional communication. Antioxid Redox Signal. 2009 Feb;11(2):355-67. doi: 10.1089/ars.2008.2183. PMID: 18816185; PMCID: PMC2933150.
- 91. Brown LAS, Harris FL, Ping XD, Gauthier TW. Chronic ethanol ingestion and the risk of acute lung injury: a role for glutathione availability? *Alcohol.* 2004;33(3):191–197.
- 92. Guidot DM, Brown LA. Mitochondrial glutathione replacement restores surfactant synthesis and secretion in alveolar epithelial cells of ethanol-fed rats. Alcohol Clin Exp Res. 2000 Jul;24(7):1070-6. PMID: 10924012.
- 93. Brown LA. Harris FL. Guidot DM. Chronic ethanol ingestion potentiates TNF-alphamediated oxidative stress and apoptosis in rat type II cells. *Am J Physiol Lung Cell Mol Physiol*. 2001;281:L377–L386.

- 94. Brown LAS, Ping XD, Harris FL, Gauthier TW. Glutathione availability modulates alveolar macrophage function in the chronic ethanol-fed rat. *American Journal of Physiology*—*Lung Cellular and Molecular Physiology*. 2007;292(4):L824–L832
- 95. Yeligar SM, Harris FL, Hart CM, Brown LAS. Ethanol induces oxidative stress in alveolar macrophages via upregulation of NADPH oxidases. *Journal of Immunology*. 2012;188(8):3648–3657
- 96. Mehta AJ, Joshi PC, Fan X, Brown LA, Ritzenthaler JD, Roman J, Guidot DM. Zinc supplementation restores PU.1 and Nrf2 nuclear binding in alveolar macrophages and improves redox balance and bacterial clearance in the lungs of alcohol-fed rats. Alcohol Clin Exp Res. 2011 Aug;35(8):1519-28. doi: 10.1111/j.1530-0277.2011.01488.x. Epub 2011 Mar 29. PMID: 21447000; PMCID: PMC3128659.
- 97. Liang Y, Yeligar SM, Brown LA. Chronic-alcohol-abuse-induced oxidative stress in the development of acute respiratory distress syndrome. ScientificWorldJournal. 2012;2012:740308. doi: 10.1100/2012/740308. Epub 2012 Dec 27. PMID: 23346021; PMCID: PMC3543796.
- 98. Bechara RI, Pelaez A, Palacio A, Joshi PC, Hart CM, Brown LA, Raynor R, Guidot DM. Angiotensin II mediates glutathione depletion, transforming growth factor-beta1 expression, and epithelial barrier dysfunction in the alcoholic rat lung. Am J Physiol Lung Cell Mol Physiol. 2005 Sep;289(3):L363-70. doi: 10.1152/ajplung.00141.2005. Epub 2005 May 20. PMID: 15908476.
- 99. Pittet JF, Griffiths MJ, Geiser T, Kaminski N, Dalton SL, Huang X, Brown LA, Gotwals PJ, Koteliansky VE, Matthay MA, Sheppard D. TGF-beta is a critical mediator of acute

- lung injury. J Clin Invest. 2001 Jun;107(12):1537-44. doi: 10.1172/JCI11963. PMID: 11413161; PMCID: PMC200192.
- 100. Guidot DM, Modelska K, Lois M, Jain L, Moss IM, Pittet JF, Brown LA. Ethanol ingestion via glutathione depletion impairs alveolar epithelial barrier function in rats. Am
 J Physiol Lung Cell Mol Physiol. 2000 Jul;279(1):L127-35. doi: 10.1152/ajplung.2000.279.1.L127. PMID: 10893211.
- 101. Fernandez AL, Koval M, Fan X, Guidot DM. Chronic alcohol ingestion alters claudin expression in the alveolar epithelium of rats. Alcohol. 2007 Aug;41(5):371-9. doi: 10.1016/j.alcohol.2007.04.010. PMID: 17889313; PMCID: PMC2048749.
- 102. Overgaard CE, Mitchell LA, Koval M. Roles for claudins in alveolar epithelial barrier function. Ann N Y Acad Sci. 2012 Jun;1257(1):167-74. doi: 10.1111/j.1749-6632.2012.06545.x. PMID: 22671603; PMCID: PMC3375852.
- 103. Wang F, Daugherty B, Keise LL, Wei Z, Foley JP, Savani RC, Koval M. Heterogeneity of claudin expression by alveolar epithelial cells. Am J Respir Cell Mol Biol. 2003 Jul;29(1):62-70. doi: 10.1165/rcmb.2002-0180OC. Epub 2003 Jan 23. PMID: 12600828.
- 104. Lynn KS, Easley KF, Martinez FJ, Reed RC, Schlingmann B, Koval M. Asymmetric distribution of dynamin-2 and β-catenin relative to tight junction spikes in alveolar epithelial cells. Tissue Barriers. 2021 Jul 3;9(3):1929786. doi: 10.1080/21688370.2021.1929786. Epub 2021 Jun 10. PMID: 34107845; PMCID: PMC8489912.
- 105. Schlingmann B, Overgaard CE, Molina SA, Lynn KS, Mitchell LA, Dorsainvil White S, Mattheyses AL, Guidot DM, Capaldo CT, Koval M. Regulation of claudin/zonula

- occludens-1 complexes by hetero-claudin interactions. Nat Commun. 2016 Jul 25;7:12276. doi: 10.1038/ncomms12276. PMID: 27452368; PMCID: PMC4962485.
- 106. Sisson JH. Alcohol and airways function in health and disease. Alcohol. 2007 Aug;41(5):293-307. doi: 10.1016/j.alcohol.2007.06.003. Epub 2007 Aug 30. PMID: 17764883; PMCID: PMC2081157.
- 107. Simet SM, Wyatt TA, DeVasure J, Yanov D, Allen-Gipson D, Sisson JH. Alcohol increases the permeability of airway epithelial tight junctions in Beas-2B and NHBE cells. Alcohol Clin Exp Res. 2012 Mar;36(3):432-42. doi: 10.1111/j.1530-0277.2011.01640.x. Epub 2011 Sep 26. PMID: 21950588; PMCID: PMC3251733.
- 108. Overgaard CE, Schlingmann B, Dorsainvil White S, Ward C, Fan X, Swarnakar S, Brown LA, Guidot DM, Koval M. The relative balance of GM-CSF and TGF-β1 regulates lung epithelial barrier function. Am J Physiol Lung Cell Mol Physiol. 2015 Jun 15;308(12):L1212-23. doi: 10.1152/ajplung.00042.2014. Epub 2015 Apr 17. PMID: 25888574; PMCID: PMC4499033.

Chapter 2: A medium composition containing normal resting glucose that supports differentiation of primary human airway cells

Rachel Morgan*, Candela Manfredi*, Kristen F. Easley*, Lionel D. Watkins,

William R. Hunt, Steven L. Goudy, Eric J. Sorscher, Michael Koval,

Samuel A. Molina

This work is published in Scientific Reports 12, 1540 (2022). https://doi.org/10.1038/s41598-

022-05446-x

*authors contributed equally

2.1 Abstract

Primary cells isolated from the human respiratory tract are the state-of-the-art for in vitro airway epithelial cell research. Airway cell isolates require media that support expansion of cells in a basal state to maintain the capacity for differentiation as well as proper cellular function. By contrast, airway cell differentiation at an air—liquid interface (ALI) requires a distinct medium formulation that typically contains high levels of glucose. Here, we expanded and differentiated human basal cells isolated from the nasal and conducting airway to a mature mucociliary epithelial cell layer at ALI using a medium formulation containing normal resting glucose levels. Of note, bronchial epithelial cells expanded and differentiated in normal resting glucose medium showed insulin-stimulated glucose uptake which was inhibited by high glucose concentrations. Normal glucose containing ALI also enabled differentiation of nasal and tracheal cells that showed comparable electrophysiological profiles when assessed for cystic fibrosis transmembrane conductance regulator (CFTR) function and that remained responsive for up to 7 weeks in culture. These data demonstrate that normal glucose containing medium supports differentiation of primary

nasal and lung epithelial cells at ALI, is well suited for metabolic studies, and avoids pitfalls associated with exposure to high glucose.

2.2 Introduction

When isolated, human airway epithelial cells are a mixture reflecting their site of origin, including the nasal, conducting and terminal airway (1,2). Nasal and conducting airways show many similarities in morphology and cell type including non-ciliated, ciliated, secretory and multipotent basal progenitor cells. A full complement of mature, location-appropriate and niche appropriate cell types are required to accurately study the airway within a native physiological context. Each cell type contributes to the overall physiology particular to their location in the airway (3). Basal cells are largely responsible for the maintenance of a differentiated epithelium, acting as the common airway progenitor cell (4). Ciliated cells move mucus unidirectionally out of the airways (5). Goblet cells and cells originating from the epithelial lined ducts of submucosal glands secrete heavily glycosylated, mucus-forming proteins (6,7). Solitary chemosensory cells sense xenobiotics and other stimuli that induce calcium-mediated intercellular signaling to nearby cells (8). Single cell RNAseq analysis has revealed heterogeneity among different cell types and rare subpopulations, such as ionocytes that express high levels of CFTR (9,10,11). Each cell type is influenced by environmental niche factors which contribute to collective cellular homeostasis and disease dynamics in tissues (12,13).

Cultured human primary cells have proven to be a valuable model to study airway cell differentiation and disease states including cystic fibrosis (14,15,16,17,18,19,20,21), asthma (22,23), chronic obstructive pulmonary disease (COPD) (24) and COVID-19 (25,26,27). To mimic the native cell environment, cell culture media contain key factors found in tissue fluids in vivo

required to support proper cell differentiation (4,28,29). Culture media resembling human plasma has supported the premise that nutrient sources in vitro can negatively impact cellular homeostasis which influences assays widely used in research such as cell-based drug screens (30). Early passage primary cells grown in traditional epithelial growth medium often do not fully differentiate after expansion which limits their utility as a model to study native tissue physiology. This is even more of a concern when considering human cell samples obtained from non-invasive epithelial sampling techniques, such as nasal or conducting airway brushings, which are valuable for rare disease research but limited by the absolute number of cells that are collected (17,31,32). Basal cells derived from human induced pluripotent stem cells (iPSCs) represent another potential source of differentiable cells (33). Methods to expand small samples into a large bank of cells with the capacity to be well-differentiated allows better access to primary respiratory epithelial cells for human disease research.

Expanding primary cells while maintaining their capacity to differentiate requires methods that rely on chemical inhibition or stalling of differentiation while still enabling basal progenitor cells to propagate. In addition to retaining multipotency in the expanding pool of basal progenitor cells, expansion methods prolong the differentiation potential of the resulting expanded cells. The cells are then able to undergo more population doublings than using traditional expansion methods, while retaining their ability to differentiate into a properly differentiated cell layer in vitro.

Chief among these is the conditional reprogramming culture (CRC) method where primary epithelial cells are co-cultured with irradiated (non-proliferating) fibroblasts in medium containing the rho-associated protein kinase (ROCK) inhibitor Y-27632 (28,34,35). These conditions preserve the basal cell phenotype, prevent differentiation and are fully reversible (36,37). Epithelial cells expanded using CRC conditions retain their ability to differentiate for at least twice

as long as compared to cells grown in traditional epithelial growth medium (36).

Another approach, the Dual SMAD inhibitor method, has also proven effective and involves culturing basal cells in the presence of inhibitors that target TGFβ (usually SB431542) and BMP4 signaling (dorsomorphin, LDN193189 or recombinant Noggin) (29,38,39). Note that the CRC and Dual SMAD basal cell expansion methods are not completely equivalent. For instance, recent evidence suggests that the CRC method better preserves some aspects of airway cell differentiation potential including ciliation and CFTR channel function (40).

Traditional culture techniques rely on expansion media with formulations that are rich in sugars, serum proteins, and supplements that exceed levels found in healthy human serum. This results in medium that fosters cell viability but causes cell overgrowth due to an overreliance in anerobic glycolytic energy metabolism over aerobic oxidative phosphorylation (41,42). Given accumulating evidence that the metabolic microenvironment can have a significant impact on airway epithelial cell function (14,18,20,43,44,45), it is important to consider medium composition as a variable that can influence behavior of cells in vitro (46). Of note, several media commonly used to support airway epithelial cell differentiation have high glucose concentrations, including LHC Basal:DMEM-H 50:50 (47) and Pneumocult-ALI (48) both of which contain ~ 300 mg/dL glucose.

Here we describe a method that can be used to propagate and differentiate basal cells from the upper and conducting airways in medium containing normal resting glucose concentrations. The ALI medium formulation described here supports the ability of airway cells to respond to insulin by stimulating glucose uptake, suggesting that these cultures are well suited for use in studying the impact of energy metabolism on airway cell function.

2.3 Material and Methods

2.3.1 Donor consent

Research involving human research participants was performed in accordance with the Declaration of Helsinki guidelines and samples were de-identified to meet HIPAA requirements. Nasal curettage, tracheal, bronchial, and whole lung tissues were acquired through informed consent via an Emory University IRB approved protocol (protocol #00005792) administered by the Cystic Fibrosis Biospecimen Repository (CFBR). Additional lung tissues were obtained through standardized UNOS consenting procedures for tissue donation for research in conjunction with an IRB-approved waiver from Emory University.

2.3.2 Tracheal epithelial cell isolation

To prepare tracheal epithelial cells, intact human donor tracheal tissue was cut into segments consisting of two to three cartilage rings starting at the carina of the main tracheal bifurcation proceeding distally. The trachealis muscle was removed to simplify the isolation procedure as the muscle tends to disintegrate during enzymatic digestion and increases copurifying tissue debris. All tracheal segments were placed into a 250 mL sterile plastic bottle and washed in Hanks Balanced Salt Solution (HBSS; Sigma-Aldrich #55021C-1000ML) at least 5 times. Then, the convex outer side of the tracheal segments were cleaned using tweezers and a scalpel to remove excess connective tissue and prevent accumulation of tissue debris.

Epithelial cells were removed from the underlying extracellular matrix by first incubating at 4 °C for least 12–16 h under gentle agitation in 50–150 mL of Conducting Airway Protease Solution (CAPS) consisting of Ham's F-12 medium (Hyclone #SH30026.FS) supplemented with 1.0% w/v Protease XIV (Sigma-Aldrich #P5147), 0.1% w/v DNAse I (Sigma-Aldrich #DN25),

0.2% Primocin (Invivotech #amt-pm-1), and 0.1% Plasmocin treatment agent (Invivotech #ant-mpt). To loosen and remove intact epithelial cell sheets from the concave inner side of the trachea, the digestion solution containing the tracheal segments was lightly vortexed.

The cell solution was separated from the tissue segments by first decanting into a new conical tube, then scraping the concave side with a scalpel to remove any remaining epithelia. The tracheal segments were washed with HBSS and the solution collected into 50 mL centrifuge tubes. All solutions containing cells were centrifuged at 350 × g for 10 min at RT, resuspended in a total of 20 mL normal glucose DMEM (Sigma-Aldrich # D6046 or Hyclone #SH30021.FS), centrifuged again at 350 × g for 10 min at RT, then resuspended in calcium/magnesium-free PBS supplemented with 1 mM EDTA (PBS/EDTA). Cells in solution were triturated to break apart cell clumps, passed through a 100-micron filter (Corning #352360), followed by a 70-micron filter (Corning #431751). The resulting P0 cells were then either cryopreserved at 1 million cells/mL, cultured for differentiation, or cultured for expansion.

2.3.3 Bronchial epithelial cell isolation

Intact human donor bronchial tissue caudal from the tracheal bifurcation to airways 10 mm in diameter were used to isolate pure bronchial epithelial cells. These tissue segments were generally lined with soft cartilage rings. Bronchial tissue segments were isolated from whole lungs or lobes of intact lungs by carefully removing the surrounding terminal airway tissue working from the tracheal bifurcation towards the caudal end of the bronchi. Isolated bronchial tissue segments were washed at least 5 times in HBSS to remove any accumulated mucus and to loosen any remaining connective tissue. Airways beyond bronchi generally include bronchioles that are not heavily collagenous and are smaller than 3 mm in diameter. These airways take time and effort

when isolating to avoid cross contamination with pulmonary arteries and smaller vessels. For bronchi, tissue segments were cleaned of connective tissue, cut longitudinally to expose the epithelium, and then processed to isolate P0 cells as described for tracheal cell isolation. As needed, terminal airway lobe tissue was set aside in normal glucose DMEM for primary fibroblast isolation by established methods (58).

2.3.4 3T3 Fibroblast feeder cell preparation

Fibroblast feeder layers required for expansion of primary human basal airway epithelial cells were prepared using the 3T3-J2 fibroblast cell line (ATCC #SCRC-1010) (4,36,59,60). 3T3 cells were expanded in DMEM containing high glucose (450 mg/dL) (Sigma-Aldrich #D6429 or Hyclone #SH30243.01) supplemented with 10% FBS (ThermoFisher #26170043), 0.2% Primocin (Invivotech #amt-pm-1) and 0.1% Plasmocin prophylactic agent (Invivotech #ant-mpp) to obtain ten 150 mm culture dishes at 80% confluence. For irradiation, ten 150 mm culture dishes of 3T3 cells were trypsinized, centrifuged at 500 × g, resuspended in 30 mL 3T3 expansion culture medium and x-ray irradiated with a dose of 3000 cGy. The irradiated cells were collected by centrifugation and resuspended in 30 mL 3T3 cell freezing medium consisting of 90% FBS and 10% DMSO (Sigma-Aldrich #D2438) (3 ml freezing medium/150 mm dish of 3T3 cells) and stored in liquid nitrogen. When human feeder cells were needed, MRC-5 cells (ATCC #CCL-171) were expanded, irradiated, stored and used in a comparable manner.

2.3.5 Airway epithelial cell expansion

One day prior to seeding plates with primary epithelial cells, irradiated 3T3 fibroblast feeder layers were plated on plasticware coated with Type IV Collagen (Sigma-Aldrich

#C7521) in F + Y Reprogramming Medium (FYRM). FYRM consists of a mixture of DMEM 1.0 g/L glucose w/L-glutamine and w/ sodium pyruvate (Corning 10–014-CV) + Ham's F-12 medium (Cytiva #SH30026.01; 1.8 g/L glucose) supplemented with 5% FBS, Insulin (5 µg/mL), Epidermal Growth Factor (10 ng/mL), Hydrocortisone (480 ng/mL), Adenine (24 µg/mL), Y-27632 (10 µM), Cholera Toxin (8.33 ng/mL), and antibiotics (Table 1), which was stored in foilwrapped glass bottles in the dark at 4 °C for up to four weeks. One vial of 3T3 feeder cells was used for one T75 flask, three T25 flasks, or divided evenly in a 6-well tissue culture dish. Epithelial cell plating density is a key parameter in cell expansion; epithelial cells should be seeded at 1.3×10^5 cells/well of a 6 well plate, 3.3×10^5 cells/T25 flask, or 10^6 cells/T75 flask. FYRM is changed every other day until the cells reach ~ 70% confluence. To remove epithelial cells cultured on 3T3 feeder layers, the 3T3 cells were first detached by washing with PBS/EDTA followed by a 5 min incubation in EDTA/PBS at RT, then light tapping. Rosettes of epithelial cells were detached using Accutase (Sigma-Aldrich #A6964) at room temperature for a maximum of 10 min and then reseeded for further expansion (one well to a T25 flask, one T25 to one T75 flask, or one T75 to three T75 flasks), plated for differentiation, or cryopreserved.

2.3.6 Airway epithelial cell differentiation

E-ALI is based on a 50:50 mixture of DMEM containing 100 mg/dL glucose, w/o L-glutamine and w/sodium pyruvate (Sigma-Aldrich #D5546) and LHC Basal Medium (ThermoFisher #12,677–019) containing the additives summarized in Table 2. This recipe results in medium containing a final glucose concentration of 150 mg/dL. In each case, stock solutions are added to the medium prior to filtering (typically 1 ml of 1000 × stock/L medium). Most biologics were dissolved and aliquoted according to manufacturer's instructions as 1000 × stock

solutions stored frozen at -80 °C. Individual 1000 × stock solutions included 1000 × CaCl₂·2H₂O (1 M in H₂O), 1000 × ZnSO₄·7H₂O (2 mM in H₂O), 1000 × Fe/Mg (1.51 mM FeSO₄·7H₂O, 300 mM MgCl₂·6H₂O, 195 mM MgSO₄·7H₂O, 60 mM HCl in H₂O). To make the 1000 × trace element stocks, first 1,000,000 × stocks were made in H₂O for each component individually: Na₂SeO₃ (30 mM); MnCl₂·4H₂O (1 mM); Na₂SiO₃·9H₂O (500 mM); (NH₄)₆Mo₇O₂₄·4H₂O 1 mM; NH₄VO₃ (5 mM); NiSO₄·6H₂O (1 mM) and SnCl₂·2H₂O (0.5 mM). These individual stocks were diluted 1:1000 in H₂O and HCl was added to 12 μM to produce the 1000 × trace elements stock. For anti-infectives, 1000 × stocks were made as follows, A: 154 mg Ceftazidime was added to 2 mL Gentamycin sulfate solution. B: 50 mg Cilistatin/Imipenem was added to 2 mL H₂O. C: 88 mg Piperacillin and 12 mg Tazobactam were added to 2 mL DMSO. D: 100 mg Azithromycin and 10 mg Voriconazole were added to 2 mL DMSO. E-ALI is stored in foil-wrapped glass bottles in the dark at 4 °C for up to four weeks. Given the light sensitivity of E-ALI, medium changes are done in a biological safety cabinet with the fluorescent light turned off.

To produce differentiated cultures, P0 or expanded epithelial cells were resuspended in 20 mL E-ALI medium and counted. Cells were plated into 0.50 mL of E-ALI onto Type IV collagen coated Transwells at a density of 10⁵ cells/6.5 mm well (Costar #3470) or $3.5 \times 10^5/12$ mm well (Costar #3460), with the bottom chamber containing 0.75 ml E-ALI. After 48 h, the basolateral medium was replaced with fresh E-ALI and the apical medium was removed to bring the cells to ALI. Once at ALI, medium was changed every 2–3 days, where the apical surface was washed once with E-ALI that was immediately removed and the basolateral medium was replaced. Benchmarks for differentiation included formation of a high resistance monolayer (> 500 Ohm x cm²) and initiation of cilia growth (day 7). Monolayers were usually fully differentiated 14–21 days after transition to ALI.

For some experiments, 2% Ultroser G medium containing normal resting glucose was made using 50:50 mixture of DMEM containing 100 mg/dL glucose, w/o L-glutamine and w/ sodium pyruvate (Sigma-Aldrich #D5546) and Ham's F-12 medium (Hyclone #SH30026.FS; 180 mg/dL glucose).

2.3.7 Cell stock cryopreservation and use

Epithelial cells were cryopreserved by diluting them into epithelial cell freezing medium (60% FYRM, 30% FBS, and 10% DMSO) at 1 million cells/mL using a Corning CoolCell according to the manufacturer's directions. Frozen cell stocks were then transferred to liquid nitrogen for long-term storage. For cell thawing, each frozen vial was separately removed and immediately placed in a 37 °C water bath then left undisturbed until a small sliver of ice remained in the vial. The vials were then removed from the water bath, cleaned with 70% ethanol solution, and transferred to a biosafety cabinet for handling. Each vial was plated into either a single well of a 6-well dish or a T25, either of which was coated with Type IV collagen and containing 3T3 feeder cells, fully supplemented with room-temperature FYRM, avoiding centrifugation.

2.3.8 nasal epithelial cell isolation and expansion

Twenty-four hours prior to nasal cell collection, irradiated 3T3 fibroblast feeder cells were plated into 6-well cell culture dishes in Collection Medium consisting of DMEM containing 100 mg/dL glucose, w/o L-glutamine and w/ sodium pyruvate (Sigma-Aldrich #D5546) supplemented with 10% FBS (R&D Systems #S11150), 0.2% Primocin, and 0.1% Plasmocin treatment agent (Invivotech #ant-mpt), stored at 4 °C for up to two weeks. Nasal cell curettage was performed by a trained otorhinolaryngologist. A curettage was used to gently

scrape each inferior nasal turbinate on both sides of the nose. Two separate scrapings were performed for each nostril to increase the number of isolated epithelial cells. Each curettage was placed into a 15 mL conical tube containing 3 mL Collection Medium. Nasal scrapes were then transported on ice for processing. The cells were dislodged from the curette by brief vortex. Nasal curettage samples from a single donor were then combined, centrifuged at 350 g for 5 min at RT, resuspended in PBS/EDTA, dissociated for 5 min at RT prior to straining through a 100 µM filter mesh and then centrifuged at 350 g for 10 min at RT. The dissociated cells were then resuspended in FYRM and placed onto irradiated 3T3 feeder cells at a density of one combined donor sample per well of a six-well culture plate that was precoated with Type IV collagen. After the initial two days of culture, the medium was changed with fresh FYRM daily until 60% confluence was reached. The cells were isolated as described above and then re-seeded in a T25 tissue culture flask containing irradiated 3T3 feeder cells in FYRM. At each passage, a portion of the cells were frozen in epithelial cell freezing medium (60% FYRM, 30% FBS, 10% DMSO) as illustrated in Fig. 5. Nasal epithelial cell differentiation was done using E-ALI as described above.

2.3.9 Immunofluorescence and imaging

Antibodies used for immunofluorescence included: mouse monoclonal antibody (mAb) anti-acetylated tubulin at 1:100 (Sigma-Aldrich clone 6-11-B1; #T7451); mouse monoclonal antibody anti-Mucin 5AC at 1:500 (Abcam clone 2-11M1; #ab24071); rabbit polyclonal antibody anti-ZO-1 at 1:250 (ThermoFisher; #40-2300); mouse anti ZO-1 at 1:100 (ThermoFisher #33-9100), rabbit monoclonal antibody anti-Cytokeratin 5 at 1:250 (Abcam clone EP1601Y; #ab52635); rat monoclonal anti-Uteroglobin/SCGB1A1 at 1:50 (R&D Systems; MAB4218) and mouse monoclonal anti-FOXI1 clone OTI1D4 at 1:100 (Origene; TA800144). Cells were fixed in

4% paraformaldehyde in Dulbecco's PBS containing Ca²⁺ Mg²⁺ (DPBS) for 10 min at RT, washed three times with DPBS, incubated with 1:1 MeOH:acetone for 2 min at RT, washed three times with DPBS, washed once with DPBS containing 0.5% Triton-X 100, blocked with DPBS supplemented with 2% (wt/vol) BSA and 5% (wt/vol) goat serum for 1 h at RT, and then incubated with primary cell phenotype marker antibodies overnight in DPBS containing 2% BSA and 5% goat serum at 4 °C with mixing. The next day, cells were incubated with primary ZO1 antibody for 1 h at RT. Fluorescent secondary antibodies used were Cy2 Goat anti-mouse AffiniPure IgG (1:500; Jackson Immuno #115–165-166), Cy3 goat anti-rabbit AffiniPure IgG (1:500; Jackson Immuno #111–225-144), AlexaFluor568 goat anti-mouse IgG (1:1500; Invitrogen A-11031), AlexaFluor488 goat anti-rabbit IgG (1:1500; Invitrogen A-11034), or AlexaFluor488 donkey antirat IgG (1:500; Jackson Immuno #712-545-150). Secondary antibodies were diluted in DPBS supplemented with 2% BSA and 5% goat serum and incubated with cells for 1 h at RT. Cells were mounted in ProLong Gold Antifade Reagent with DAPI (Invitrogen; #P36931). Images were collected using a Zeiss FV1000 confocal microscope in the Emory University Integrated Cellular Imaging Microscopy Core.

2.3.10 Transepithelial resistance and electrophysiology

To measure confluence and tight junction formation, transepithelial resistance (TER) was measured using an EVOM voltmeter, as previously described [61]. CFTR currents of cells on Transwells in physiologic Krebs-Ringers HEPES (KRH) buffer (1 g/l D-glucose, 50 mM HEPES, 137 mM NaCl, 4.7 mM KCl, 1.85 mM CaCl₂, and 1.3 mM MgSO₄ at pH 7.4) were measured as previously described [61] with an Ussing chamber system (VCC MC-8 Multichannel Voltage/Current Clamp controller and analyzed using Acquire & Analyze software (Physiological

Instruments)). Ion channel inhibitors and activators used for Ussing chamber analysis included amiloride (100 μ M), forskolin (5 μ M), 3-isobutyl-1-methylxanthine (IBMX; 100 μ M), Vx-770 (5 μ M), Vx-809 (3 μ M), and CFTR inh172 (10 μ M) and curcumin (40 μ M).

2.3.11 Insulin stimulation and glucose uptake

Medium glucose was measured using a colorimetric glucose quantification kit (Cayman Chemical; #10009582) and medium insulin was measured using by ELISA (Alpco Diagnostics; #80-INSHU-CH01). Uptake of 2-deoxy-D-[³H] glucose was measured as previously described [20], with modifications. In brief, cells on Transwell permeable supports were washed with KRH and then incubated for 90 min at 37 °C in KRH. The cells were washed and incubated for 30 min at 37 °C with apically added KRH containing 0.5 μCi 2-deoxy-D-[³H]glucose (NEN Radiochemicals, PerkinElmer #NET328250UC) and 2-deoxy-D-glucose (Sigma-Aldrich #D6134) adjusted to 5.6 mM total final concentration in either the presence or absence of 500 nM (2.9 μg/ml) recombinant human insulin with zinc (Gibco #12585014). The cells were washed with cold KRH, Transwell filters were removed and placed in a scintillation vial containing 200 μL 0.1 M NaOH to lyse the cells. Scintillation fluid was added and the samples were measured for ³H using a Beckman-Coulter LS6500 scintillation counter.

2.3.12 Statistics

All statistics were calculated using GraphPad Prism v6 for Windows with methods indicated in each figure legend. Cell doubling rate was calculated as (log(total cells)-log(number seeded cells)/log(2))/(time in culture).

2.4 Results and Discussion

2.4.1 Isolation and differentiation of airway epithelial cells

Figure 1 illustrates the workflow of tissue harvest, primary cell isolation, basal cell selection and propagation and differentiation to produce airway cell models to study in vitro. The overall health of the donor tissue directly affects the quality of the resulting isolated cell culture. In our experience, the number of viable epithelial cells able to be isolated is mainly affected by the condition of the tissue when received and the time since resection. Culture of airway epithelial cells consists of two phases: 1) propagation of basal epithelial cells followed by 2) preparation of differentiated cultures using an air-liquid interface (ALI).

Initially, P0 cells were cultured using the CRC method which is submersion culture in medium based on a mixture of DMEM and F12, resulting in normal resting glucose levels (150 mg/dL; 8.3 mM), and including biologic co-factors, the ROCK inhibitor Y-27638 and cholera toxin (FYRM; Table 1). The cells are seeded on collagen coated dishes and co-cultured with 3T3 fibroblasts that were irradiated to inhibit their propagation (Fig. 2A). When ~ 40% or more P0 cells attached to collagen coated dishes seeded with irradiated 3T3 cells, this was an indication that tissue processing was successful. Generally, cells exhibited a 5-day lag period before beginning to proliferate (Fig. 2B). Following the lag period, growth rates of cells isolated from anatomically different areas of the airway were similar (Fig. 2B) with a population doubling rate of roughly one per day (Fig. 2C).

Once the cells were isolated and propagated, frozen cell stocks were made at each passage creating a bank of cells with consistent properties that can be used for experimentation (Fig. 2A). Generally, we avoid cryobanking after P3 to ensure that the basal cells maintain their capacity to differentiate. For freshly isolated P0 cells, freeze densities of two million cells per vial allow for

at least 500,000 cells per thaw to attach. For P1-P3, freeze densities of one million cells per vial are recommended to facilitate rapid growth from banked vials.

Culture of airway basal cells at ALI is a well-established method to promote their differentiation, however most media used for this purpose contain high glucose concentrations (~300 mg/dL; 16.7 mM) (47,48), which reflects a hyperglycemic state (14,44). Given this, we developed a modified ALI medium, E-ALI, based on a widely used medium formulation (47). As shown in Table 2, E-ALI contains normal resting glucose levels (150 mg/dL; 8.3 mM). Otherwise, E-ALI is comparable to other ALI medium formulations (47,48), except that it has less insulin (5 μg/ml) and is enriched for the following components: CaCl₂ (1 mM), heparin (2 μg/ml), L-glutamine (2.5 mM), hydrocortisone 960 mg/ml, O-phosphorylethanolamine (0.5 μg/ml), bovine pituitary extract (20 μg/ml) and Mg²⁺ (0.5 μM).

We validated the ability of E-ALI to support the growth and differentiation of freshly isolated P0 normal human tracheal epithelial cells (NhTE cells) plated on collagen-coated Transwell permeable supports as assessed by immunofluorescence microscopy using KRT5 as a marker for basal cells (Fig. 2D-E), acetylated-tubulin as a marker for ciliated epithelia (Fig. 2D), and Muc5AC as a marker for mucus producing cells (Fig. 2E). Cultures routinely contained all three different cell types, indicating that they were well differentiated.

Comparable results were obtained using normal human bronchial epithelial cells (NhBE cells), which are delineated by apical junctions as marked by the tight junction protein ZO-1 (Fig. 3A-F) and also show ciliated cells (Fig. 3A,C), mucus producing cells (Fig. 3B,D), ionocytes (Fig. 3E) and club cells (Fig. 3F). After 14 days of culture in E-ALI, NhBE monolayers had significantly more ciliated cells than NhTE monolayers ($32.7 \pm 8.9\%$, n = 3 replicates, 14 fields; $23.2 \pm 9.0\%$, n = 3 replicates, 18 fields) (Fig. 3G). The number of basal cells were comparable for

NhBE and NhTE monolayers $(38.8 \pm 7.2\%, n = 2 \text{ replicates}, 7 \text{ fields}; 41.9 \pm 5.4\%, n = 2 \text{ replicates}, 8 \text{ fields})$. Muc5AC positive cells were also comparable for NhBE and NhTE monolayers $(3.9 \pm 1.9\%, n = 3 \text{ replicates}, 18 \text{ fields}; 5.3 \pm 2.9\%, n = 3 \text{ replicates}, 14 \text{ fields})$. NhBE monolayers also contained low levels of club cells $(2.0 \pm 1.1\%, n = 2 \text{ replicates}, 12 \text{ fields})$ and ionocytes $(0.1 \pm 0.1\%, n = 2 \text{ replicates}, 13 \text{ fields})$. Altogether, we accounted for $77.5 \pm 11.7\%$ of the total cells in NhBE monolayers grown using E-ALI. Other cell types likely to be present include suprabasal cells which express KRT4, KRT8 and KRT13 [49,50], however, suprabasal and other cell populations defined by multiple markers are difficult to detect strictly by immunofluorescence profiling.

Consistent with formation of tight junctions, NhBE and NhTE cells cultured in E-ALI showed high transepithelial resistance (TER) (Fig. 3H), where the barrier formed by NhTE cells after 14 days in E-ALI was slightly, but significantly tighter than NhBE cells ($\sim 1340~\rm vs \sim 1160~\rm Ohm~x~cm^2$). Taken together, these data indicate that the E-ALI formulation containing normal resting glucose supported airway epithelial cell function as determined by apical junction assembly and differentiation of tracheal and bronchial epithelial cells.

2.4.2 Cells cultured in E-ALI medium show insulin-stimulated glucose uptake

To measure the effect of extracellular glucose and medium composition on insulin and glucose clearance, we examined NhBE cells cultured in either E-ALI or 2% Ultroser G containing normal (150 mg/dL) or high (300 mg/dL) glucose (Fig. 4). It is worth noting that E-ALI containing 300 mg/dL glucose is comparable to the glucose content of LHC Basal:DMEM-H 50:50 (47) and Pneumocult-ALI (48). Insulin clearance was not sensitive to medium formulation, where all of the cell culture models tested cleared the majority of insulin within the first 24 h after feeding, causing

it to plateau at a low level ($\sim 0.4 \,\mu g/mL$; Fig. 4A).

Medium glucose content showed a fast decline within the first 24 h where each culture grown used approximately 50% of the available glucose (Fig. 4B). Glucose clearance was significantly more rapid for cells in high glucose E-ALI as compared with cells in high glucose 2% Ultroser G medium. After 72 h, nearly 125 mg/dL glucose remained in cultures fed with high glucose media, consistent with saturation of uptake. By contrast, cells in normal resting glucose cleared nearly all glucose from the medium after 72 h.

We then determined the impact of medium formulation and glucose content on insulin stimulated glucose uptake, as measured using [³H]-2-deoxy-glucose. Since E-ALI used to culture airway cells contains insulin (5 µg/ml; 0.87 µM), cells were first pre-incubated for 90 min with insulin-free KRH prior to challenge with [³H]-2-deoxy-glucose in the presence or absence of 500 nM (2.9 µg/ml) recombinant human insulin. Of all the conditions tested, only E-ALI medium containing normal resting glucose showed a significant, two-fold increase in glucose uptake in response to added insulin (Fig. 4C). By contrast, cells cultured E-ALI containing high glucose showed elevated glucose uptake that was insulin insensitive and significantly higher than the levels of glucose uptake by cells in E-ALI at normal resting glucose in the absence of insulin. This was not due to an effect of high glucose on insulin signaling, since cells cultured in E-ALI showed an increase in transepithelial resistance (TER) in response to insulin, regardless of glucose concentration and consistent with our previous results (20).

Airway cells express multiple glucose transporters, including the insulin regulated Glut4 transporter (20). Our data suggest that cells chronically cultured in the presence of high glucose are likely to upregulate constitutive glucose transporters, which would overshadow the impact of insulin stimulated activation of Glut4 mediated by trafficking from secretory vesicles to the plasma

membrane (20,44). Regardless of mechanism, it is important to note that the glucose concentrations used here represent two extremes as opposed to the physiological glucose levels cells will be exposed to in vivo which significantly vary in response to meals and systemic insulin levels (51). Our data suggest that a culture system based on exposing cells to E-ALI containing varying levels of glucose could provide the basis for an in vitro model that mimics in vivo exposure.

Moreover, cells cultured in 2% Ultroser G did not show insulin stimulated glucose uptake or changes in TER (Fig. 4C,D). Considering that constitutive insulin uptake was comparable for cells cultured in E-ALI and 2% Ultroser G, the differences in insulin stimulated glucose uptake and barrier function were not likely to be due to a difference in insulin binding capacity. Instead, the results in Fig. 4C,D and more likely reflect a difference in the capacity for glucose uptake (Fig. 4B) and/or signaling downstream from insulin receptors. For instance, we have observed that the ability of insulin to promote barrier function requires akt signaling, a pathway that is active in primary human airway cells (20). Taken together, these results underscore the importance of medium formulation, especially in studies of airway cell metabolism, and are consistent with the deleterious effects of hyperglycemia on the airway epithelium (14,44,52) as well as cell homeostasis in general (53).

2.4.3 Expansion and maturation of CF nasal epithelial cells using E-ALI

Nasal cells have proven to be a useful model system that reflects several characteristics of the conducting airway (16,54). Unlike primary tracheal and bronchial cells, primary human nasal epithelial (hNE) cells often originate from small samples that require expansion on an appreciable scale for subsequent analysis. We thus evaluated the ability of E-ALI to support differentiation of

hNE cells including CFhNE cells harboring both rare and common disease-causing CFTR alleles, as well as cells from non-CF subjects (NhNE cells). Nasal cell isolates (Fig. 5A) initially were expanded using CRC conditions (Fig. 5B) and then differentiated using the protocol illustrated in Fig. 2A. Regardless of genotype, hNE cells showed comparable doubling rates of ~ 0.7–0.9 per day during CRC expansion (Fig. 5C). Ciliated cells were readily detected 21 days after initiating culture in E-ALI by scanning EM (Fig. 5D,E) and by confocal immunofluorescence microscopy (Fig. 5F-H). Taken together these data show that expansion of nasal epithelial cells using the CRC method effectively supported their ability to differentiate in E-ALI.

We further characterized the cell electrophysiology of P0 NhTE cells maintained in E-ALI medium. After 16 weeks at ALI (Fig. 6A) NhTE cells demonstrated measurable ENaC and CFTR currents based on amiloride inhibition and forskolin stimulation, respectively. CFTR currents were also modestly enhanced by Vx-770 (ivacaftor) and curcumin and were inhibited by Inh-172. NhTE cells from the same culture preparation extended to 21 weeks ALI had a comparable electrophysiological profile (Fig. 6B). Primary NhNE cells expanded with the CRC method, then differentiated with E-ALI for either 2 weeks (Fig. 6C) or 7 weeks (Fig. 6D) also showed ENaC and CFTR currents with electrophysiological characteristics comparable to those of NhTE cells. These data demonstrate the utility of E-ALI in supporting long-term cultures that maintained ion channel function.

We then examined primary CFhNE cells with a G551D/F508del genotype that were isolated, expanded, and differentiated in E-ALI. Differentiated G551D/F508del CFhNE cells produced mature cells capable of eliciting small, but detectable, CFTR currents when treated with forskolin that were modestly enhanced with Vx-770 and Vx-809 (lumacaftor) and inhibited with Inh-172 (Figs. 7A-B) (55,56). Similarly, CFhNE cells with a W1282X/F508del genotype

exhibited a small CFTR current in response to forskolin and Vx-770 and were also responsive to curcumin which has shown efficacy in CFTR mutants encoding a premature stop codon (Figs. 7C-D) (57). Therefore, E-ALI medium is compatible with CRC expansion and subsequent studying of primary nasal epithelial cells.

Taken together, these data validate E-ALI as a method to differentiate human airway epithelial cells in medium containing normal resting glucose levels. We also confirmed that expanded nasal epithelial cell isolates have preserved their ability to differentiate and express functional CFTR. E-ALI medium provides a new method amenable to investigation of nasal, tracheal, and bronchial airway epithelia for a variety of applications including ciliation and developmental studies, host pathogen interactions, and drug screening. The ability to differentiate cells in normal resting glucose is expected to facilitate the analysis of airway cell functions that are particularly sensitive to cell metabolism.

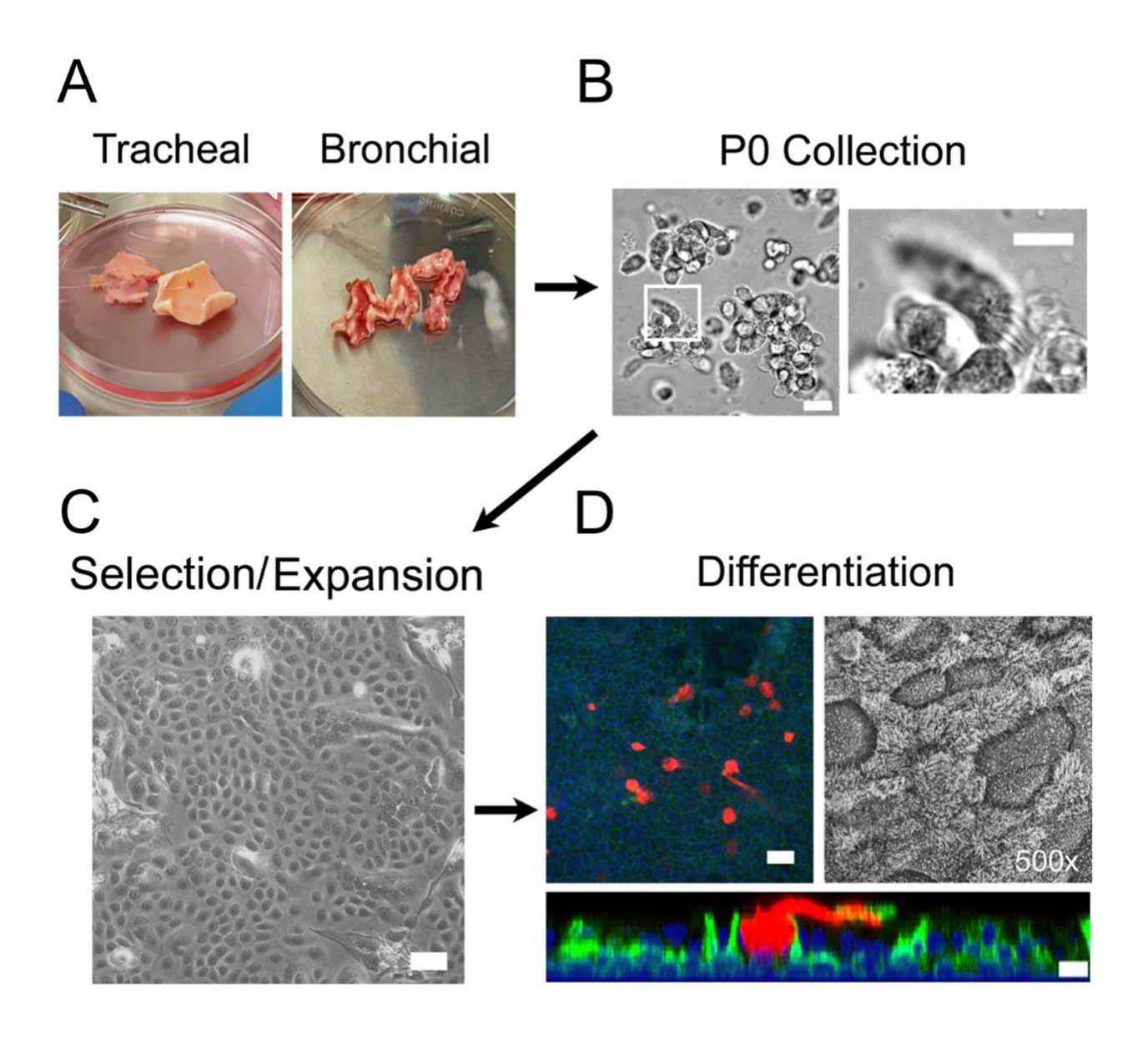


Figure 2.1 Workflow for isolation of cells from distinct anatomic regions of the airway tree.

(A) Examples of healthy tracheal and bronchial tissue isolates are shown based on donor tissue color, shape, and rigidity as markers for tissue health. (B) Freshly isolated primary (passage 0; P0) cells isolated from nasal or lung tissue contain a mixture of cells, including ciliated (inset) and non-ciliated cells. Bars, 20 μm (left) and 10 μm (right). (C) Basal nasal or airway epithelial cells are selected and expanded using CRC conditions, as imaged by phase contrast microscopy. Bar, 10 μm. (D) Basal airway or nasal cells cultured in E-ALI containing normal glucose properly

differentiate as determined by immunofluorescence confocal microscopy using markers for mucus secretion (Muc5AC, red), basal cells (KRT5, green), nuclei (blue, DAPI) and by scanning electron microscopy. Bars, $20~\mu m$ (top and middle) and $10~\mu m$ (bottom).

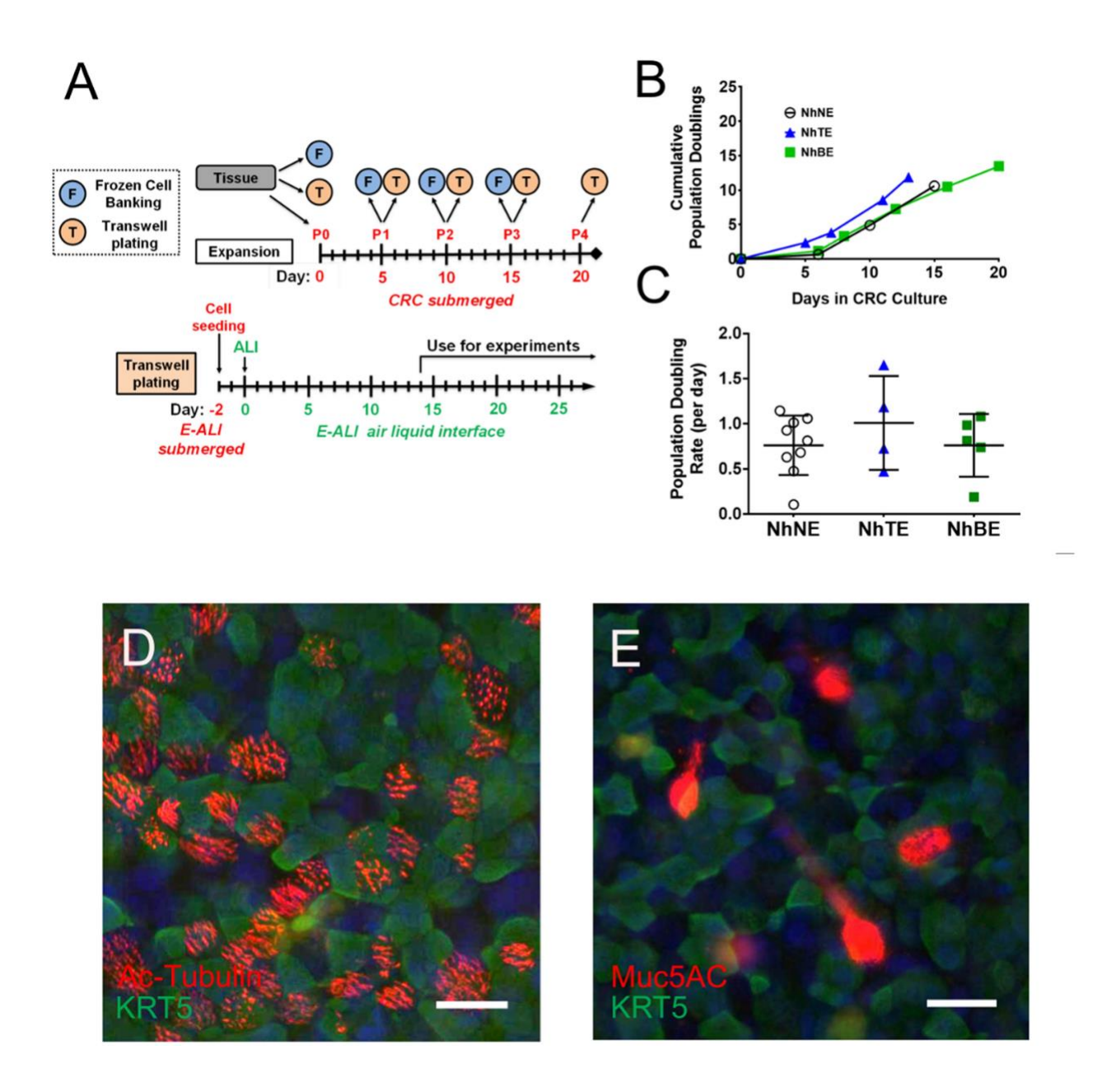


Figure 2.2 Airway epithelial cells from different tissue sources propagate with similar doubling times.

(A) Timeline for processing of cells isolated from lung tissue samples showing frozen cell banking (F), plating for differentiation on Transwell permeable supports (T) or plating for expansion under CRC conditions. Cells from P0 through P3 are banked. Cells beyond P4 are not typically used to generate differentiated cultures for experimental analysis. Detail related to culture on Transwells

(T) is shown below, indicating the shift from submerged to air–liquid interface (ALI). Cells are cultured at least 14 days at ALI prior to use in experiments. (B) Representative NhNE, NhTE, and NhBE displayed a lag phase of growth between Day 0 and Day 5 in CRC conditions before replicating at a linear rate. (C) Regardless of anatomical origin or the initial lag phase, airway epithelial cells showed comparable doubling rates under CRC conditions. n=2-3 wells from n=2 (NhTE, NhBE) or 4 (NhNE) biological replicates plotted as mean \pm SD. (D, E) Immunofluorescence analysis of differentiated tracheal epithelial cells (NhTE) at Day 14 in E-ALI. Ciliated cells were identified by immunostaining for acetylated tubulin (Ac-Tubulin, red) and basal cells by cytokeratin 5 (KRT5, green). Nuclei were labeled with DAPI (blue). (D). Mucus producing cells were identified by Muc5AC expression (red) (E). Bar, 20 μ m.

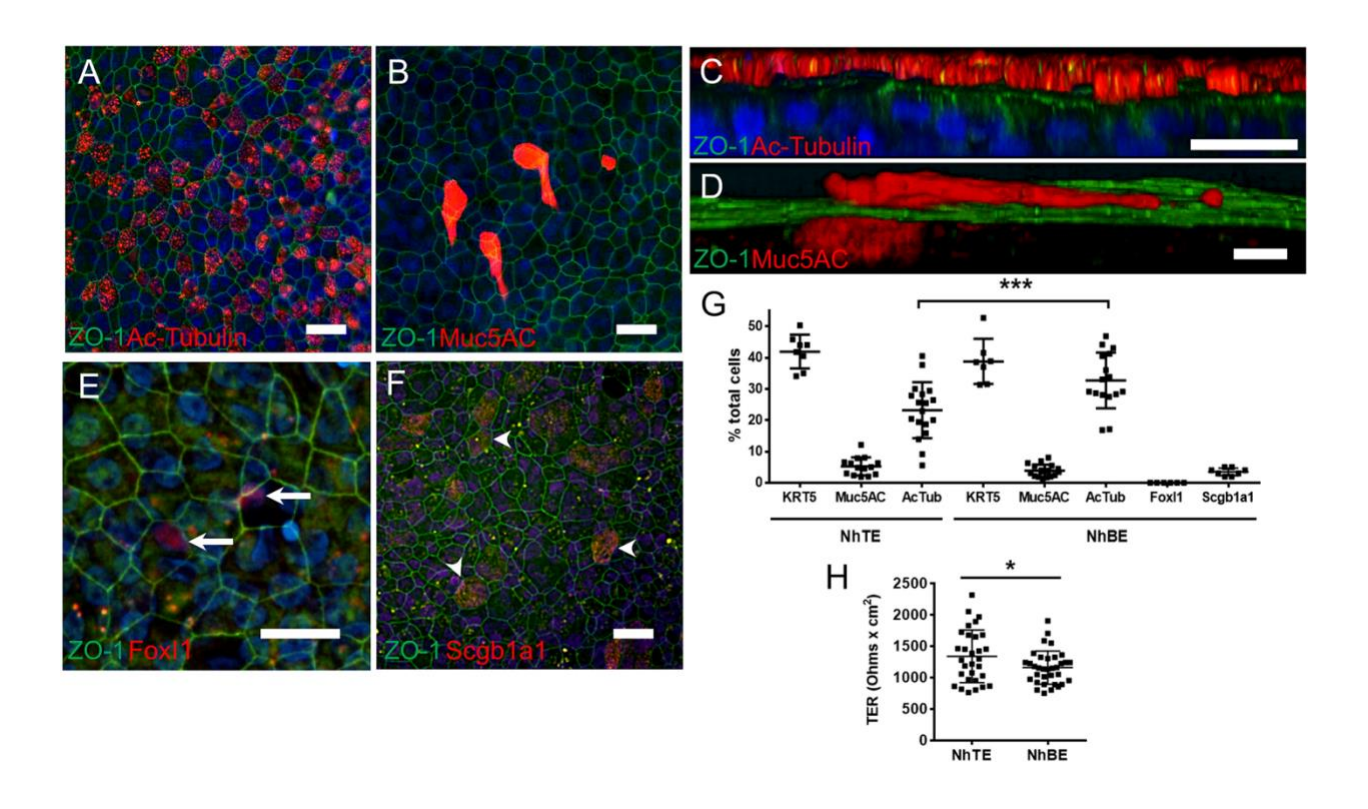


Figure 2.3 Tracheal and bronchial epithelial cells differentiate into mucociliary cultures in E-ALI medium.

(A–F) The E-ALI formulation enabled formation of well-differentiated cultured bronchial epithelial cell (NhBE) monolayers in vitro as observed by the presence of tight junctions (green, zonula occludins-1, ZO-1). Cell differentiation was demonstrated by immunofluorescence microscopy measuring acetylated tubulin (red, Ac-Tubulin; A, C), mucin (red, Muc5AC; B, D), an ionocyte marker (red, FoxI1; E) and a club cell marker (red, Scgb1a1; F). Nuclei were labeled with DAPI (blue). Bar, 20 μ m. (G) Quantitation of NhTE and NhBE phenotype in cells cultured for 14 days in E-ALI. Data are from n = 2 – 9 fields from n = 2 (KRT5, FoxI1, Scgb1a) or 3 (Muc5AC, AcTub) biological replicates. ***P<0.0001 by one-way ANOVA. (H) Transepithelial electrical resistance (TER) of NhTE cells was slightly higher than NhBE cells n = 3—21 wells from 4 biological replicates; *P = 0.042, by t test.

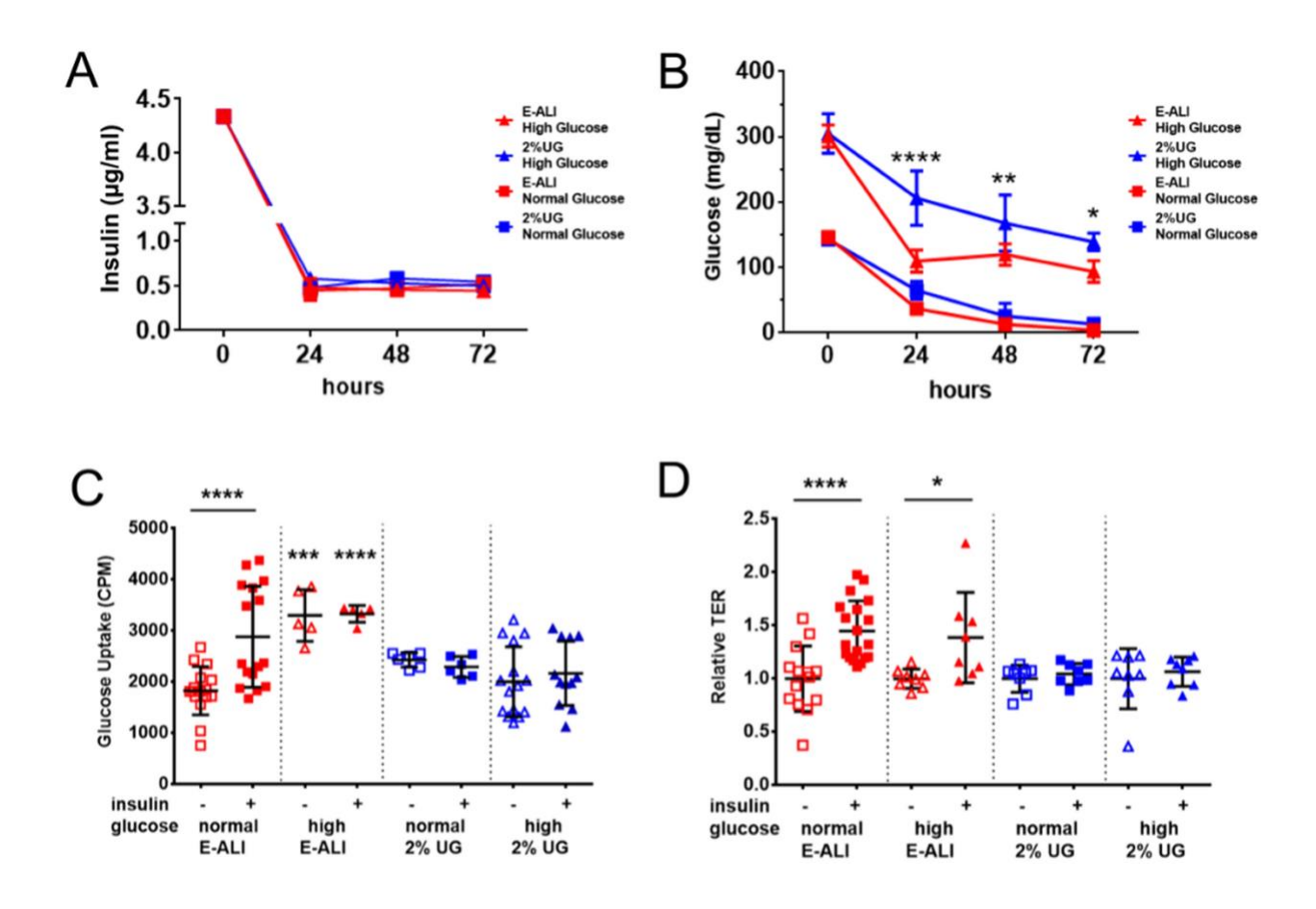


Figure 2.4 Glucose and insulin sensitivity depends on differentiation medium.

(A) Insulin consumption was comparable in all media tested. n=4 samples, one biological replicate per condition. (B) Glucose consumption of differentiated, expanded P0 airway epithelial cells of mixed tracheal/bronchial origin. Red triangles and squares indicate cells cultured in E-ALI medium and blue triangles and squares indicate cells cultured in 2% Ultroser G (2% UG) medium. High glucose = 300 mg/dL glucose in the base media (triangles); Normal resting glucose = 150 mg/dL glucose in the base media (squares). Glucose consumption was significantly higher for cells in high glucose E-ALI as compared with cells in high glucose 2% UG (n=4 samples, one biological replicate; ****P < 0.0001; **P = 0.0085; *P = 0.014, by two way ANOVA). (C) Cells differentiated using E-ALI medium containing normal resting glucose elicited a significant increase in insulin stimulated [3 H]-2-D-glucose uptake. n = 3-6 samples from n = 1 (E-ALI high

glucose, 2% UG normal glucose), 3 (2% UG High glucose) or 4 (E-ALI normal glucose) biological replicates; ***P = 0.0001; ****P < 0.0001, by one-way ANOVA. (D) Cells cultured in E-ALI showed significant increases in relative transepithelial resistance (TER) in response to insulin regardless of glucose content, cells cultured in 2% UG did not. n = 4—11 samples from n = 3 (E-ALI normal glucose) or 2 (all others) biological replicates; *P = 0.015, ****P < 0.0001 by one-way ANOVA. All data is plotted as mean \pm SD.

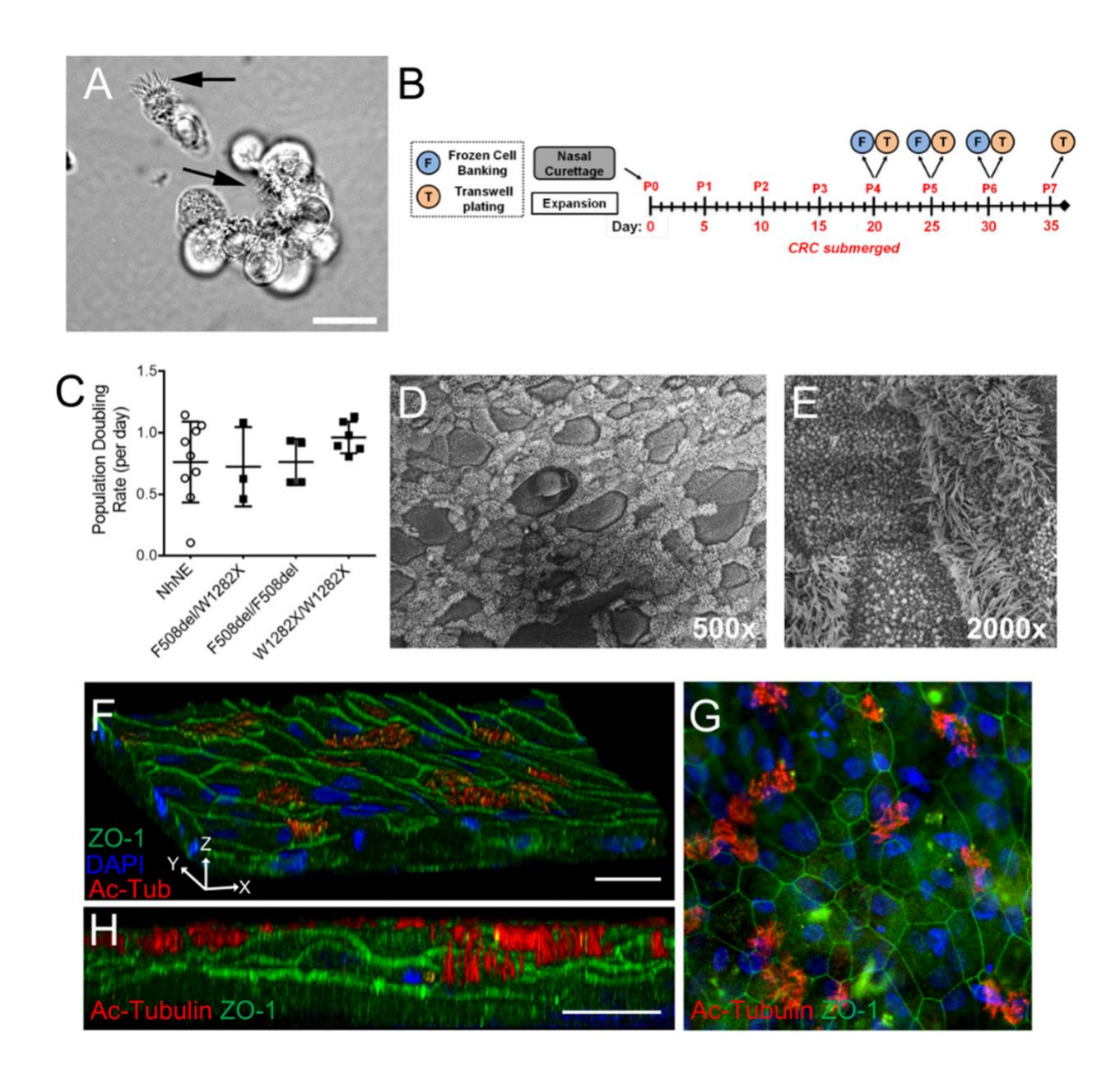


Figure 2.5 Expansion and differentiation of non-CF and CF nasal epithelial cells.

(A) Ciliated cells (black arrows) are observed in freshly isolated CF nasal cultures by phase contrast microscopy. Bar, 20 μm. (B) Timeline for processing of nasal curettage samples showing frozen cell banking (F), plating for differentiation on Transwell permeable supports (T) or plating for expansion in FYRM submerged culture. Due to the small initial sample size, cells were not banked or plated for differentiation until P4. Cells beyond P7 are not typically used to generate

differentiated cultures for experimental analysis. Detail related to culture on Transwells (T) is shown in Fig. 2. (C) Non-CF and CF nasal epithelial cells with 3 different genotypes had a comparable doubling time when cultured in CRC conditions. n=3-6 wells for CF cells; doubling data for NhNE cells is from Fig. 2. (D, E) Cilia and mucus producing CF nasal epithelial cells as observed by scanning electron microscopy at 500x (D) and 2000x (E) magnification. (F–H) Immunofluorescence confocal microscopy of CF nasal airway cells showed tight junctions (green, ZO-1) and cilia (red, Ac-Tubulin). Nuclei were labeled with DAPI (blue). Bar, 20 μ m (F, H).

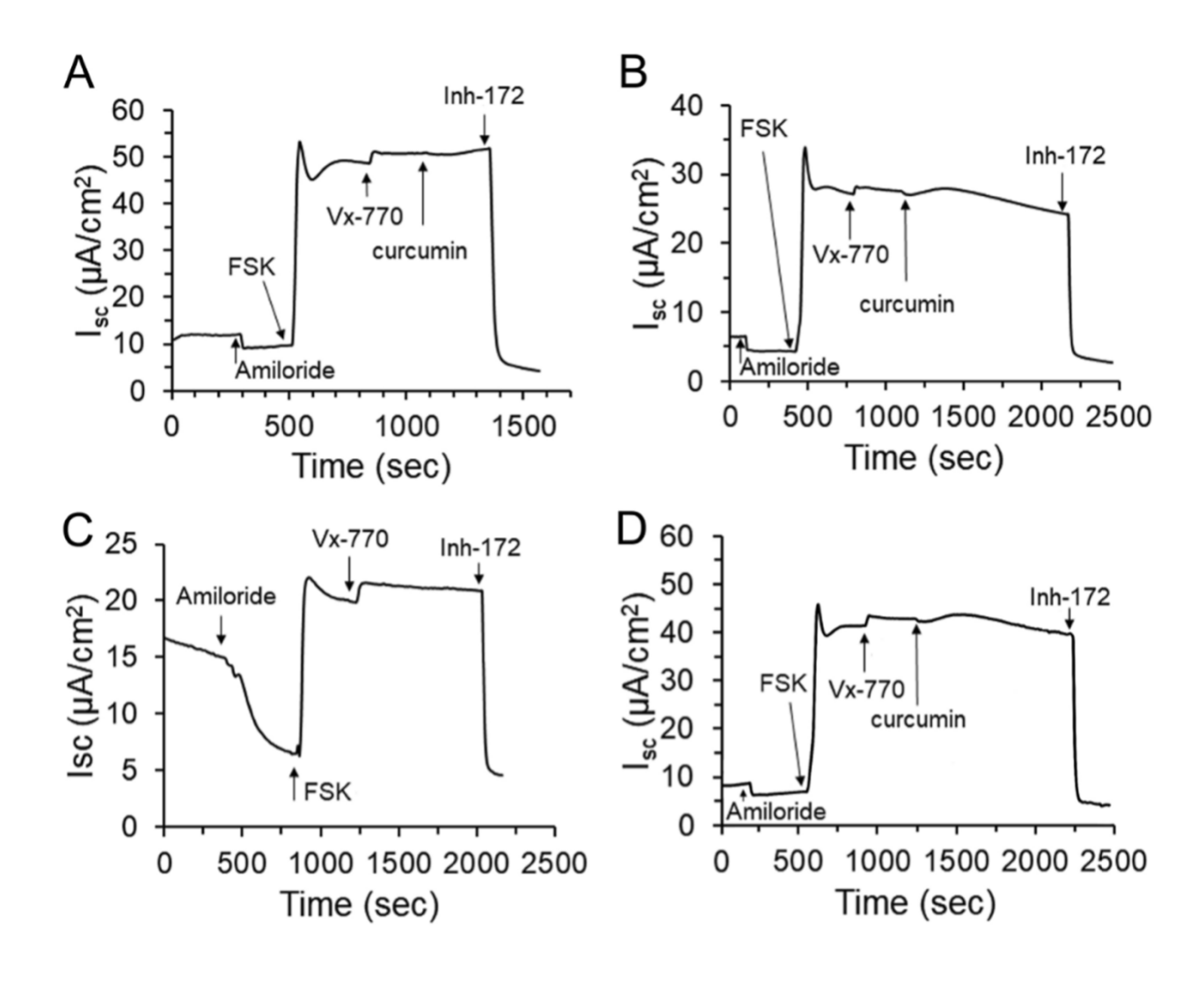


Figure 2.6 Representative electrophysiological analysis of primary tracheal and nasal airway epithelia expanded using CRC conditions and differentiated in E-ALI.

(A, B) P0 NhTEC cultured in E-ALI for 16 weeks (A) or 21 weeks (B) show comparable response profiles to the ENaC inhibitor amiloride and agents that stimulate or inhibit CFTR currents. (C, D) NhNE cells that were expanded using CRC conditions to P4 and then differentiated with E-ALI for 2 weeks (C) or 7 weeks (D), also exhibited comparable ENaC and CFTR current profiles. FSK, Forskolin; Vx-770, Ivacaftor; CFTRinh172, CFTR channel inhibitor.

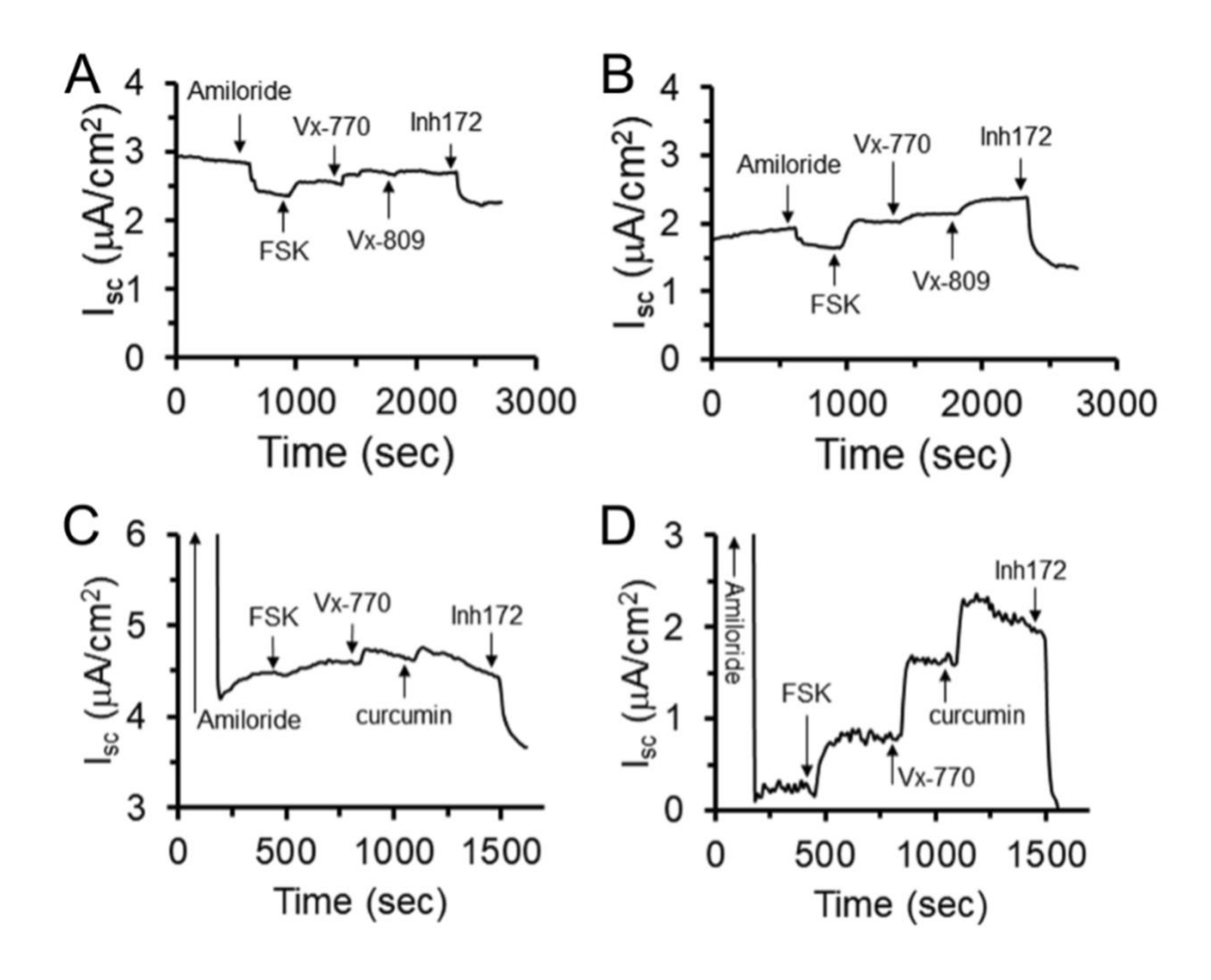


Figure 2.7 Representative electrophysiological analysis of primary nasal CF airway epithelia expanded using CRC conditions and differentiated in E-ALI.

(A, B) CFhNE cells with the G551D/F508del genotype were expanded using CRC conditions to P4 and differentiated in E-ALI for 14 days. Shown are two representative traces demonstrating low levels of CFTR currents and modest responses to Vx-770 and Vx-809. (C, D) CFhNE cells with the W1282X/F508del genotype were expanded and differentiated as described above. Shown are two representative traces demonstrating low levels of CFTR currents and responses to Vx-770 and curcumin. FSK, Forskolin; inh172, CFTR channel inhibitor; Vx-770, Ivacaftor; Vx-809, Lumacaftor.

	Reagent	Final Conc. (For 1000 mL)	Supplier	Catalog #
Base Medium	DMEM 1.0 g/L glucose (w/L-glutamine and w/sodium pyruvate)	225 mL	Corning	10-014-CV
	Ham's F12	725 mL	Cytiva	SH30026.01
Biologics	Fetal Bovine Serum	50 mL	R&D Systems	S11150
	Insulin	5 μg/mL	Gemini Bio	800-112P
	Epidermal Growth Factor	10 ng/mL	StemCell Tech	78006.2
	Hydrocortisone	480 ng/mL	StemCell Tech	74142
	Adenine	24 μg/mL	Sigma-Aldrich	A2786
Agents	Y-27632	10 μΜ	Tocris	1254
	Cholera Toxin	8.33 ng/mL	Sigma-Aldrich	C8052
Anti – infectives	Primocin	0.2% (2 mL)	Invivogen	ant-pm-1
	Plasmocin	0.1% (1 mL)	Invivogen	ant-mpp
	Vorconazole	200 ng/mL	Selleck Chemicals	S1442

Table 2.1 FYRM medium composition.

This formulation produces medium containing 150 mg/dL glucose as measured using a colorimetric assay. For details related to medium preparation, see Methods.

	Reagent		Final Conc. (For 1000 mL)	Supplier	Catalog #
Base Medium	DMEM 1.0 g/L glucose (w/o L-glutamine and w/se	odium pyruvate)	50% (500 mL)	Sigma-Aldrich	D5546
	LHC Basal Medium		50% (500 mL)	ThermoFisher	12677019
	L-glutamine		2.5 mM (12.5 mL)	Corning	25-005-CV
	Insulin		5 μg/mL	Gemini Bio	800-112P
	Epidermal Growth Factor		0.5 ng/mL	StemCell Tech	78006.2
	Hydrocortisone		960 ng/mL	StemCell Tech	74142
	Bovine Pituitary Extract		20 μg/mL	Gemini Bio	500-102
	Triiodothyronine (T3)		10 nM	Sigma-Aldrich	T6397
Biologics	Transferrin		125 nM	Gemini Bio	800-131P
	Epinephrine		2.7 μΜ	Sigma-Aldrich	E4250
	O-phosphorylethanolamine		0.5 μΜ	Sigma-Aldrich	P0503
	Ethanolamine		0.5 μΜ	Sigma-Aldrich	E0135
	Retanoic Acid		50 nM	StemCell Tech	72262
	Heparin		2 μg/mL	StemCell Tech	07980
	Bovine Serum Albumin, Fraction V		500 μg/mL	Gemini Bio	700-102P
CaCl ₂ stock	Calcium Chloride dihydrate		1 mM	Sigma-Aldrich	C3881
ZnSO ₄ stock	Zinc Sulfate heptahydrate		3 μΜ	Sigma-Aldrich	Z0251
	Ferrous Sulfate heptahydrate		1.51 μΜ	Sigma-Aldrich	F8633
	Magnesium Chloride hexahydrate		300 μM	Sigma-Aldrich	M2393
Mg/Fe stock	Magnesium Sulfate heptahydrate		195 μΜ	Sigma-Aldrich	M5921
	Hydrochloric Acid (12 M)		60 μM	ThermoFisher	A144-500
	Sodium Selenite		30 nM	Sigma-Aldrich	S5261
	Manganese(II) chloride tetrahydrate		1 nM	Sigma-Aldrich	M5005
	Sodium metasilicate nonahydrate		500 nM	Sigma-Aldrich	S5904
	Ammonium molybdate tetrahydrate		1 nM	Sigma-Aldrich	M1019
Trace Elements	Ammonium metavanadate		5 nM	Sigma-Aldrich	398128
	Nickel(II) sulfate hexahydrate		1 nM	Sigma-Aldrich	N4882
	Tin(II) chloride dihydrate		0.5 nM	Sigma-Aldrich	S9262
	Hydrochloric Acid (12 M)		12 μΜ	ThermoFisher	A144-500
	Primocin		0.2% (2 mL)	Invivogen	ant-pm-1
	Plasmocin		0.1% (1 mL)	Invivogen	ant-mpp
	A	Ceftazidime	7.7 μg/mL	ThermoFisher	AC461730050
		Gentamicin	5 μg/mL	Sigma-Aldrich	G1397
Anti-infectives (add A,B,C	В	Cilistatin/Imipenem	25 μg/mL	Astatech	42454
or D as needed)		Piperacillin	4.4 μg/mL	Alfa Aesar	J66143-ME
	C	Tazobactam	0.6 μg/mL	Alfa Aesar	J66226-03
		Azithromycin	5 μg/mL	Alfa Aesar	J66220-03 J66740-06
	D	Voriconazole	0.5 μg/mL	Selleck Chemicals	S1442

Table 2.2 E-ALI medium composition.

This formulation produces medium containing 150 mg/dL glucose as measured using a colorimetric assay. For details related to medium preparation, see Methods.

2.5 Acknowledgements

We thank Kirsten Cottrill and Ryan Chance Reed for critical reading of the manuscript. Cells were provided jointly by the Children's Healthcare of Atlanta, the Emory University CF Discovery Core and the CF@LANTA RDP Experimental Models Core. This research project was supported by the Emory University Integrated Cellular Imaging Microscopy Core, the Winship Research Pathology Core and SEM was done by the Robert P. Apkarian Integrated Electron Microscopy Core (IEMC) of Emory University School of Medicine. This project was also supported by CF@LANTA RDP Center Grant (MCCART15R0), R01-HL116958 and R01-AA025854 to M.K., T32-HL116271 to S.A.M., R01-HL139876 and R01-HL136414 to E.J.S., F31-AA029000 to K.F.E., and by the Emory+Children's Center for Cystic Fibrosis and Airways Disease Research.

2.6 Author Contributions

These authors contributed equally: Rachel Morgan, Candela Manfredi and Kristen F. Easley. S.A.M., E.J.S. and M.K. designed the scope of the study. S.L.G. and W.R.H. performed nasal curettage. W.R.H. obtained tissues from the Emory Transplant Center and CF@LANTA Clinical and Translational CF Biorepository. R.M., K.F.E., L.D.W. and S.A.M. cultured cells, tested medium formulations, performed immunofluorescence microscopy and barrier function measurements. S.A.M. and L.D.W. measured glucose uptake. C.M. and S.A.M. performed electrophysiological measurements. S.A.M., M.K. and K.F.E. analyzed the data, compiled the figures, and wrote the first draft of manuscript. All of the co-authors edited and approved the manuscript.

References

- 1. Schlingmann, B., Molina, S. A. & Koval, M. Claudins: Gatekeepers of lung epithelial function. *Semin. Cell Dev. Biol.* 42, 47–57. (2015).
- 2. Whitsett, J. A. & Alenghat, T. Respiratory epithelial cells orchestrate pulmonary innate immunity. *Nat. Immunol.* 16, 27–35. (2014).
- 3. Tam, A., Wadsworth, S., Dorscheid, D., Man, S. F. & Sin, D. D. The airway epithelium: more than just a structural barrier. *Ther. Adv. Respir. Dis.* 5, 255–273. (2011).
- 4. Suprynowicz, F. A. et al. Conditionally reprogrammed cells represent a stem-like state of adult epithelial cells. *Proc. Natl. Acad. Sci. U S A* 109, 20035–20040. (2012).
- 5. Nawroth, J. C., van der Does, A. M., Ryan Firth, A. & Kanso, E. Multiscale mechanics of mucociliary clearance in the lung. *Philos. Trans. R. Soc. Lond. B Biol. Sci.* 375, 20190160. (2020).
- 6. Jaramillo, A. M., Azzegagh, Z., Tuvim, M. J. & Dickey, B. F. Airway Mucin secretion.

 Ann. Am. Thorac. Soc. 15, S164–S170. (2018).
- 7. Widdicombe, J. H. & Wine, J. J. Airway gland structure and function. *Physiol. Rev.* 95, 1241–1319. (2015).
- 8. Sell, E. A., Ortiz-Carpena, J. F., Herbert, D. R. & Cohen, N. A. Tuft cells in the pathogenesis of chronic rhinosinusitis with nasal polyps and asthma. *Ann. Allergy Asthma Immunol.* 126, 143–151. (2021).
- 9. Plasschaert, L. W. et al. A single-cell atlas of the airway epithelium reveals the CFTR-rich pulmonary ionocyte. *Nature* 560, 377–381. (2018).
- 10. Montoro, D. T. et al. A revised airway epithelial hierarchy includes CFTR-expressing ionocytes. *Nature* 560, 319–324. (2018).

- 11. Schuler, B. A. et al. Age-determined expression of priming protease TMPRSS2 and localization of SARS-CoV-2 in lung epithelium. *J. Clin. Invest.* (2021).
- 12. Bergeron, C. & Cantin, A. M. Cystic fibrosis: pathophysiology of lung disease. *Semin. Respir. Crit. Care Med.* 40, 715–726. (2019).
- 13. Wallmeier, J. et al. Motile ciliopathies. *Nat. Rev. Dis. Primers* 6, 77. (2020).
- 14. Garnett, J. P. et al. Hyperglycemia and Pseudomonas aeruginosa acidify cystic fibrosis airway surface liquid by elevating epithelial monocarboxylate transporter 2 dependent lactate-H(+) secretion. *Sci. Rep.* 6, 37955. (2016).
- 15. Suzuki, S. et al. Highly efficient gene editing of cystic fibrosis patient-derived airway basal cells results in functional CFTR correction. *Mol. Ther.* 28, 1684–1695. (2020).
- 16. Brewington, J. J. et al. Brushed nasal epithelial cells are a surrogate for bronchial epithelial CFTR studies. *JCI Insight*. (2018).
- 17. Harris, C. M. et al. Assessment of CFTR localization in native airway epithelial cells obtained by nasal brushing. *J. Cyst. Fibros* 3(Suppl 2), 43–48. (2004).
- 18. Bengtson, C. D. et al. Hyperglycemia in cystic fibrosis adversely affects BK channel function critical for mucus clearance. *Eur. Respir. J.* (2021).
- 19. Bedi, B. et al. UPR modulation of host immunity by Pseudomonas aeruginosa in cystic fibrosis. *Clin. Sci. (Lond)* 134, 1911–1934. (2020).
- 20. Molina, S. A. et al. Insulin signaling via the PI3K/Akt pathway regulates airway glucose uptake and barrier function in a CFTR dependent manner. *Am. J. Physiol. Lung Cell Mol. Physiol.* 312, L688–L702. (2017).
- 21. Wu, Y. S. et al. ORKAMBI-mediated rescue of mucociliary clearance in cystic fibrosis primary respiratory cultures is enhanced by arginine uptake, arginase inhibition, and

- promotion of nitric oxide signaling to the cystic fibrosis transmembrane conductance regulator channel. *Mol. Pharmacol.* 96, 515–525. (2019).
- 22. Lan, B. et al. Airway epithelial compression promotes airway smooth muscle proliferation and contraction. *Am. J. Physiol. Lung Cell Mol. Physiol.* 315, L645–L652. (2018).
- 23. Mitchel, J. A. et al. In primary airway epithelial cells, the unjamming transition is distinct from the epithelial-to-mesenchymal transition. *Nat. Commun.* 11, 5053. (2020).
- 24. Kim, M. D. et al. Losartan reduces cigarette smoke-induced airway inflammation and mucus hypersecretion. *ERJ Open Res.* 7, 149. (2021).
- 25. Hou, Y. J. et al. SARS-CoV-2 D614G variant exhibits efficient replication ex vivo and transmission in vivo. *Science* 370, 1464–1468. (2020).
- 26. Vanderheiden, A. et al. Type I and Type III interferons restrict SARS-CoV-2 infection of human airway epithelial cultures. *J. Virol.* (2020).
- 27. Schweitzer, K. S. et al. Influenza virus infection increases ACE2 expression and shedding in human small airway epithelial cells. *Eur. Respir. J.* (2021).
- 28. Liu, X. et al. Conditional reprogramming and long-term expansion of normal and tumor cells from human biospecimens. *Nat. Protoc.* 12, 439–451. (2017).
- 29. Mou, H. et al. Dual SMAD signaling inhibition enables long-term expansion of diverse epithelial basal cells. *Cell Stem Cell* 19, 217–231. (2016).
- 30. Cantor, J. R. et al. Physiologic medium rewires cellular metabolism and reveals uric acid as an endogenous inhibitor of UMP synthase. *Cell* 169, 258-272 e217. (2017).
- 31. Clancy, J. P. et al. CFTR modulator theratyping: current status, gaps and future directions. *J. Cyst. Fibros* 18, 22–34. (2019).
- 32. Zuo, W. L. et al. Ontogeny and biology of human small airway epithelial club cells. *Am. J.*

- Respir. Crit. Care Med. 198, 1375–1388. (2018).
- 33. Hawkins, F. J. et al. Derivation of airway basal stem cells from human pluripotent stem cells. *Cell Stem Cell* 28, 79-95 e78. (2021).
- 34. Martinovich, K. M. et al. Conditionally reprogrammed primary airway epithelial cells maintain morphology, lineage and disease specific functional characteristics. *Sci. Rep.* 7, 17971. (2017).
- 35. Wolf, S. et al. Conditional reprogramming of pediatric airway epithelial cells: a new human model to investigate early-life respiratory disorders. *Pediatr. Allergy Immunol.* 28, 810–817. (2017).
- 36. Reynolds, S. D. et al. Airway progenitor clone formation is enhanced by Y-27632-dependent changes in the transcriptome. *Am. J. Respir. Cell Mol. Biol.* 55, 323–336. (2016).
- 37. Zhang, Z. et al. Conditionally reprogrammed human normal bronchial epithelial cells express comparable levels of cytochromes p450 and are sensitive to BaP induction. *Biochem. Biophys. Res. Commun.* 503, 2132–2138. (2018).
- 38. Tadokoro, T., Gao, X., Hong, C. C., Hotten, D. & Hogan, B. L. BMP signaling and cellular dynamics during regeneration of airway epithelium from basal progenitors. *Development* 143, 764–773. (2016).
- 39. Miller, A. J. et al. In vitro and in vivo development of the human airway at single-cell resolution. *Dev. Cell* 53, 117-128 e116. (2020).
- 40. Awatade, N. T. et al. Significant functional differences in differentiated conditionally reprogrammed (CRC)- and feeder-free dual SMAD inhibited-expanded human nasal epithelial cells. *J. Cyst. Fibros* (2021).

- 41. Gewolb, I. H. & Torday, J. S. High glucose inhibits maturation of the fetal lung in vitro. Morphometric analysis of lamellar bodies and fibroblast lipid inclusions. *Lab. Invest.* 73, 59–63 (1995).
- 42. Mboge, M. Y. & Bissell, M. J. The not-so-sweet side of sugar: influence of the microenvironment on the processes that unleash cancer. *Biochim. Biophys. Acta Mol. Basis Dis.* 1866, 165960. (2020).
- 43. Garnett, J. P. et al. Proinflammatory mediators disrupt glucose homeostasis in airway surface liquid. *J. Immunol.* 189, 373–380. (2012).
- 44. Bearham, J., Garnett, J. P., Schroeder, V., Biggart, M. G. S. & Baines, D. L. Effective glucose metabolism maintains low intracellular glucose in airway epithelial cells after exposure to hyperglycemia. *Am. J. Physiol. Cell Physiol.* 317, C983–C992. (2019).
- 45. Li, K. et al. Airway epithelial regeneration requires autophagy and glucose metabolism.

 *Cell Death Dis. 10, 875. (2019).
- 46. Saint-Criq, V. et al. Choice of differentiation media significantly impacts cell lineage and response to CFTR modulators in fully differentiated primary cultures of cystic fibrosis human airway epithelial cells. *Cells*. (2020).
- 47. Fulcher, M. L. & Randell, S. H. Human nasal and tracheo-bronchial respiratory epithelial cell culture. *Methods Mol. Biol.* 945, 109–121. (2013).
- 48. Bovard, D. et al. A lung/liver-on-a-chip platform for acute and chronic toxicity studies.

 **Lab. Chip 18, 3814–3829. (2018).
- 49. Zoso, A., Sofoluwe, A., Bacchetta, M. & Chanson, M. Transcriptomic profile of cystic fibrosis airway epithelial cells undergoing repair. *Sci. Data* 6, 240. (2019).
- 50. Deprez, M. et al. A single-cell atlas of the human healthy airways. Am. J. Respir. Crit. Care

- Med. 202, 1636–1645. (2020).
- 51. Inman, T. B., Proudfoot, J. A., Lim, M. & Demeterco-Berggren, C. Continuous glucose monitoring in a cystic fibrosis patient to predict pulmonary exacerbation. *J. Cyst. Fibros* 16, 628–630. (2017).
- 52. Hunt, W. R. et al. Hyperglycemia impedes lung bacterial clearance in a murine model of cystic fibrosis-related diabetes. *Am. J. Physiol. Lung Cell Mol. Physiol.* 306, L43-49. (2014).
- 53. Giri, B. et al. Chronic hyperglycemia mediated physiological alteration and metabolic distortion leads to organ dysfunction, infection, cancer progression and other pathophysiological consequences: an update on glucose toxicity. *Biomed. Pharmacother*. 107, 306–328. (2018).
- 54. Ghosh, B. et al. Strong correlation between air-liquid interface cultures and in vivo transcriptomics of nasal brush biopsy. *Am. J. Physiol. Lung Cell Mol. Physiol.* 318, L1056–L1062. (2020).
- 55. Mall, M. A., Mayer-Hamblett, N. & Rowe, S. M. Cystic fibrosis: emergence of highly effective targeted therapeutics and potential clinical implications. *Am. J. Respir. Crit. Care Med.* 201, 1193–1208. (2020).
- 56. Joshi, D., Ehrhardt, A., Hong, J. S. & Sorscher, E. J. Cystic fibrosis precision therapeutics: emerging considerations. *Pediatr. Pulmonol.* 54(Suppl 3), S13–S17. (2019).
- 57. Wang, W., Hong, J. S., Rab, A., Sorscher, E. J. & Kirk, K. L. Robust stimulation of W1282X-CFTR channel activity by a combination of allosteric modulators. *PLoS ONE* 11, e0152232. (2016).
- 58. Baglole, C. J. et al. Isolation and phenotypic characterization of lung fibroblasts. *Methods*

- Mol. Med. 117, 115-127. (2005).
- 59. Liu, X. et al. ROCK inhibitor and feeder cells induce the conditional reprogramming of epithelial cells. *Am. J. Pathol.* 180, 599–607. (2012).
- 60. Terunuma, A., Limgala, R. P., Park, C. J., Choudhary, I. & Vogel, J. C. Efficient procurement of epithelial stem cells from human tissue specimens using a Rho-associated protein kinase inhibitor Y-27632. *Tissue Eng. Part A* 16, 1363–1368. (2010).
- 61. Molina, S. A. et al. Junctional abnormalities in human airway epithelial cells expressing F508del CFTR. *Am. J. Physiol. Lung Cell Mol. Physiol.* 309, L475-487. (2015).

Chapter 3: Chronic alcohol use primes bronchial cells for barrier dysfunction and altered inflammatory response during SARS-CoV-2 infection

Kristen F. Easley, R. Clayton Edenfield, Megan Jane Lott, Ryan C. Reed, Cheryl A. Jones, Scott
K. Johnson, In Ki Cho, Jayasri Das Sarma, Ashish J. Mehta, Bashar S. Staitieh, Erin K. Lipp,
Anne-Gaelle Bebin-Blackwell, Joshua M. Levy, S. Mark Tompkins, Charles A. Easley 4th,
Michael Koval

This work was submitted to *American Journal of Physiology: Lung Cellular and Molecular Physiology* in November 2022, and was returned with revisions. Expected resubmission June 2023.

3.1 Abstract

Alcohol Use Disorder (AUD) is a significant public health concern and people with AUD are more likely to develop severe acute respiratory distress syndrome (ARDS) in response to respiratory infections. To examine whether AUD was a risk factor for more severe outcome in response to SARS-CoV-2 infection, we examined early responses to infection using cultured differentiated bronchial epithelial cells derived from brushings obtained from people with AUD or without AUD. Bronchial epithelial cells from AUD patients showed a significant decrease in barrier function 72 h post infection, as determined by transepithelial electrical resistance. In contrast, barrier function of non-AUD cells was not impaired 72 h after SARS-CoV-2 infection.

Immunofluorescence of β -catenin revealed that it decreased in response to infection, regardless of AUD status. To determine the impact of AUD on the inflammatory response to SARS-CoV-2 infection, cytokine secretion was measured by multiplex analysis. SARS-CoV-2-infected AUD bronchial cells had enhanced secretion of multiple pro-inflammatory cytokines including TNF α , IL-1 β and interferon- γ as opposed to non-AUD cells. By contrast, secretion of EGF and GM-CSF, cytokines that can be barrier protective, was enhanced for non-AUD bronchial cells. RNA-seq of non-AUD and AUD cells revealed that AUD cells have up-regulated expression of ACE2 and adapted an epidermal gene expression profile. Taken together, these data support the hypothesis that AUD is a risk factor for COVID-19, where alcohol primes airway epithelial cells for increased barrier dysfunction and increased inflammation in response to infection by SARS-CoV-2.

3.2 Introduction

COVID-19 is caused by severe acute respiratory syndrome coronavirus 2 (SARS-CoV-2) and is associated with respiratory failure in the most severe cases (33, 62). It is estimated that a third of COVID-19 patients requiring mechanical ventilation do not survive (36). Several comorbidities are associated with increased COVID-19 severity, including obesity, diabetes and other chronic diseases (7). It has long been appreciated that alcohol use disorder (AUD) is a risk factor for increased severity of lung disease (42, 47, 82). This includes increased susceptibility to infectious pneumonia (19, 22, 58, 79) and poor outcomes in acute respiratory distress syndrome (ARDS) (5). As ARDS is a significant pathological consequence of SARS-CoV-2 infection (75), it is noteworthy that people with AUD and COVID-19 have been shown to have a higher rate of hospitalization and mortality (3), suggesting that AUD is a risk factor for increased severity of COVID-19 related illness (2). Compounding the potential impact of AUD on patient outcomes is

the added stress of experiencing the COVID-19 pandemic, which has been associated with substance abuse, including increased alcohol consumption (13, 68). However, the mechanisms by which AUD influences lung epithelial responses to SARS-CoV-2 are not known at present.

Numerous factors associated with AUD contribute to increased inflammation and overall poor lung health. Patients with AUD and animal models of AUD show higher levels of inflammatory cytokines and chemokines in the airway (1, 14, 44, 51), alveolar macrophage dysfunction (67, 81) and disruption of the lung microbiome (59). Additionally, chronic alcohol exposure results in lung epithelial barrier dysfunction, which predisposes ARDS patients to more severe pulmonary edema (11, 66). For instance, lung epithelial barrier permeability is regulated by the apical junctional complex, composed of tight junctions and adherens junctions (32, 37, 77). The impact of alcohol exposure on the expression, organization, and function of lung epithelial tight junction proteins can be demonstrated using in vitro models (39, 51, 61, 65). Of note, alveolar epithelial cells isolated from alcohol-fed animals have barrier dysfunction that persists in tissue culture, even in the absence of added ethanol (21).

It is clear that SARS-CoV-2 has the capacity to infect multiple epithelia throughout the respiratory tree (25). However, whether the impact of AUD on SARS-CoV-2 infection is due to the effects of alcohol on lung epithelia has not been determined. Since AUD is a significant risk factor for ARDS in general, we hypothesize that AUD would sensitize lung epithelial cells to the effects of SARS-CoV-2 infection.

It is well established that cultured human lung epithelial cells have significant utility for the study of the effects of SARS-CoV-2 infection (23, 29, 34, 48, 55, 74, 76, 83), suggesting that an in vitro model would shed light on the impact of AUD on the effects of SARS-CoV-2 infection on lung epithelial cells. To do this, we isolated bronchial brushings from patients with and without

AUD, expanded them in a basal cell state and then differentiated them using an air-liquid interface (ALI) culture system using methods previously established by our laboratory (46). The cells were infected with SARS-CoV-2 and the effect on barrier function, junction protein expression and inflammatory cytokine production were measured. We found that after infection, cells from patients with AUD had a significant decrease in TER and showed enhanced secretion of several pro-inflammatory cytokines including IL-6, TNFα, IL-1β and IFNγ as compared with non-AUD cells. By contrast, infected non-AUD cells produced significantly higher levels of GM-CSF and EGF than AUD cells, which can have an anti-inflammatory, barrier protective effect on epithelial cells. RNA-seq revealed that AUD cells have increased expression of ACE2 and decreased expression of glutathione S-transferase alpha 1 (GSTA1), which promotes antioxidant defenses. GO enrichment analysis suggested that AUD cells adapted an epidermal differentiation profile. Taken together, these data support the hypothesis that AUD is a risk factor for COVID-19 and that this is, in part, due to an effect of chronic alcohol exposure on airway epithelial cells.

3.3 Material and Methods

3.3.1 Donor Consent

Research involving human research participants was performed in accordance with the Declaration of Helsinki guidelines. All human subject protocols were reviewed and approved by the Emory University Institutional Review Board and the Atlanta Veterans Affairs Health Care System Research and Development Committee. Potential subjects for study enrollment were screened using the Short Michigan Alcohol Screening Test and AUD Identification Test (60, 63). Individuals with a history of AUD were recruited from the Substance Abuse Treatment Program at the Atlanta Veterans Affairs Health Care System, and otherwise healthy control subjects were

recruited from general Veterans Affairs medical clinics (43). Additional subject inclusion criteria included active alcohol abuse, in which the last alcoholic drink was <8d prior to bronchoscopy. Subjects were excluded if they primarily abused substances other than alcohol, were HIV positive, were >55 y old, or had abnormal chest radiographs.

3.3.2 Airway epithelial cell culture and infection

Cells from bronchial brushings were expanded in co-culture with irradiated 3T3 fibroblast feeder cells in F+Y reprogramming media (FYRM) as previously described (46). FYRM was changed every other day until the cells were ~70-90% confluent and then the cells were isolated by first removing the 3T3 feeder layer using calcium/magnesium-free phosphate buffered saline supplemented with 1 mM EDTA (PBS/EDTA), followed by detaching epithelial cells by incubating with Accutase (Sigma-Aldrich #A6964) at RT for 10 minutes. Cells were then centrifuged and frozen as P1 stocks. For experiments, cells were thawed, expanded using FYRM and then seeded on Transwell permeable supports pre-coated with type IV collagen (Sigma-Aldrich #C7521) at a density of 150,000 cells per 6.5 mm Transwell (Costar #3450, 24 well) or 350,000 cells per 12 mm Transwell (Costar # 3460, 12 well) in E-ALI medium (46). E-ALI medium was based on previous formulations with modifications to glucose (150 mg/dl; 8.3 mM), CaCl₂ (1 mM), heparin (2 µg/ml), L-glutamine (2.5 mM), hydrocortisone (960 mg/ml), bovine pituitary extract (20 µg/ml), and Mg²⁺ (0.5 µM). E-ALI medium is changed every other day with washing of the apical surface. Using this protocol, monolayers were fully differentiated 14 days after transitioning to ALI, ehich occurs two days after plating.

Differentiated cells were infected at MOI 0.1 for 6h with SARS-CoV-2 USA-WA1/2020 (BEI Resources, # NR-52281), consistent with previously used conditions (83). The cells were

then washed with ALI medium and further incubated for 72h. At 6, 24, 48 and 72h post infection, apical surfaces were washed with 0.2 ml E-ALI and 0.5 ml basal medium was collected, banked at -20°C for further analysis and the cells were re-fed. Virus production by infected cells was confirmed by analysis of medium using a LAMP assay kit (New England BioLabs, # E2019S) according to the manufacturer's instructions.

3.3.3 RNA-seq Analysis

Non-infected AUD and non-AUD cells were flash frozen and submitted to Azenta Life Sciences for RNA extraction and Standard RNA-Seq. Sequencing Configuration: library preparation, Illumina, 2x150bp, ~350M raw paired-end reads (~105GB), single index, per lane. RNA-seq reads were analyzed for differential gene expression, alternative splicing and gene ontology (GO) enrichment analysis. Heat map of differentially expressed genes (p-adj. value < 0.05) was generated using Galaxy Project. All samples had a similar distribution of normalized read counts (Supplemental Figure 3.1).

3.3.4 Transepithelial Resistance (TER)

TER was measured using an EVOM Voltohmmeter (World Precision Instruments, #EVOM2). Before measuring, cells were washed with Dulbecco's Phosphate Buffered Saline containing Ca⁺² and Mg⁺² (DPBS, Corning # 21-030-CV) followed by a 15-minute incubation at 37°C in Ringer's solution (140 mM NaCl, 5 mM KCl, 0.36 mM K₂HPO₄, 0.44mM KH₂PO₄, 1.3 mM CaCl₂ • 2 H₂O, 0.5 mM MgCl₂ • 6 H₂O, 4.2 mM NaHCO₃, 10 mM Na HEPES, 10 mM glucose). Cells that had a pre-infection TER of at least 500 Ohm x cm² or higher were used for further analysis. To facilitate comparison between different cells, TER values were normalized to

pre-infection values obtained at t = 0 h for each condition examined.

3.3.5 Immunofluorescence Microscopy

Cells on Transwell permeable supports were rinsed with DPBS then fixed with 4% paraformaldehyde (PFA) for 10 minutes at RT in the dark. This was followed by a DPBS rinse and 2 minutes of fixation in 1:1 methanol/acetone at RT. Cells were then washed 3x with DPBS. Cells were permeabilized in 0.5% Triton X-100/DPBS++ for 5 minutes, followed by two 5-minute incubations in blocking solution (0.5% Triton X-100 and 5% Goat serum in DPBS). Primary antibodies were added (diluted in 3% BSA in DPBS) and incubated overnight at 4°C. The cells were washed 3x with DPBS and then incubated for 1h at RT with fluorescent secondary antibodies diluted in 3% BSA. The secondary antibodies were removed and the cells were further incubated for 10 minutes in Hoechst 33342 (ThermoFIsher # 62249) diluted 1:1000 in DPBS to stain nuclei. Cells were washed 3x with DPBS, and Transwells were mounted on slides using Vectashield mounting solution (Vector Labs #H-1000-10).

Primary antibodies used for immunofluorescence were: mouse anti-ZO-1 (Invitrogen #339100, 1:500 dilution), rabbit anti-β-catenin (Abcam ab32572, 1:400 dilution), Rabbit anticlaudin 7 (Abcam #ab27487, 1:200 dilution). Secondary antibodies used for immunofluorescence were: Alexa fluor 568 goat anti-mouse (Invitrogen A11031, 1:1500 dilution), Alexa fluor 488 goat anti-rabbit (Invitrogen #A11034, 1:1500 dilution), Alexa fluor 488 anti-mouse (Invitrogen #A11029, 1:1500 dilution), Alexa fluor 568 anti-rabbit (Invitrogen #A11036, 1:1500 dilution). Images were taken using either a Nikon Ti Eclipse with epifluorescence and processed using 3D deconvolution or a Nikon A1R confocal and processed using Nikon Elements and Image J.

3.3.6 Cytokine Analysis

Apical washes and basolateral medium that were collected at 6, 24, 48 and 72h after SARS-CoV-2 infection were analyzed and the total amount of cytokine secreted was determined by measuring cytokine concentration multiplied by total volume. E-ALI medium collected at each time-point following SARS-CoV-2 infection was analyzed using the MILLIPLEX Human Cytokine / Chemokine / Growth Factor Panel A kit (Cat # HCYTA-60K-PX38) according to the manufacturer's instructions, modified to accommodate the BSL-3 facility. After Streptavidin-Phycoerythrin incubation, all wells on the assay plate were washed twice with assay buffer followed by the addition of 200 μ l 4% PFA and the samples were further incubated for 17 h 4°C to denature any virus that was present prior to analysis. Data represent the combined total pg secreted over a 72h period.

3.3.7 Statistics

Statistics were calculated using Graphpad Prism 8.0 and significance was determined using ordinary one-way ANOVA with Sidak's multiple comparison test (baseline barrier function analysis). the Kruskal Wallis one-way ANOVA test (cytokine analysis) or the one-way ANOVA test with Fisher's LSD Test (barrier function analysis of infected samples).

3.4 Results

3.4.1 RNA-seq reveals differentially expressed genes between non-AUD cells and AUD cells

In this study, we used cells obtained from three individuals with AUD and three non-AUD individuals matched as closely as possible by sex, race and age. The demographic characteristics of the donors are shown in Table 3.1. Smoking status varied for each subject but was comparable

overall when comparing AUD and non-AUD subjects. These cells were proliferated as basal cells and then differentiated using ALI cultures as described in Methods.

To determine whether there were AUD dependent differences in gene expression, we analyzed the cultures by RNA-seq. Normalized read counts were comparable for all six different samples (Supplemental Figure 3.2). As shown by hierarchical clustering in Figure 3.1A, the samples stratified by AUD status showed distinct patterns of upregulated and downregulated genes. Further analysis by volcano plot shows the 117 up-regulated genes and 47 down-regulated genes in AUD cells compared to non-AUD cells (Figure 3.1B). All differentially expressed (DE) genes are listed in Supplemental Table 3.1. Among the up-regulated genes are several that have been implicated in SARS-CoV-2 infection, including ACE2, which encodes the receptor that binds the virus spike protein, and two TMPRSS isoforms: TMPRSS11B and TMPRSS11E. While the TMPRSS2 isoform is best known for activating the SARS-CoV-2 spike protein, one study found enhanced fusion between 293 cells expressing SARS-CoV-2 S and 293 cells expressing hACE2 and TMPRSS11E (84). AUD cells have decreased expression of glutathione S-transferase alpha 1 (GSTA1), WNT3A and MUC5B, which play roles in protection from oxidative stress, airway repair and clearance of respiratory particulates and pathogens, respectively (85, 86).

Gene Ontology (GO) enrichment analysis reveals the top 11 GO terms, 5 that relate to epidermal processes and 2 that relate to inflammation (Figure 3.1C). The DE genes from these GO terms can be found in Table 3.2. All GO terms with associated enriched DE genes are found in Supplemental Table 3.2. Small proline rich proteins (SPRRs) are largely expressed in the epidermis and have bactericidal properties (87). However, SPRR3 was found to play a role in allergic airway inflammation, and knockdown of SPRR3 reduced the number of inflammatory cells in the BAL fluid (87). S100A8, S100A9 and S100A12 are associated with inflammatory

diseases (88), including severe asthma (89, 90).

Taken together, these data suggest that AUD status of donor cells is an independent determinant of gene expression of bronchial epithelial cells in our model system that may impact their response to SARS-CoV-2 infection.

3.4.2 SARS-CoV-2 infection impairs barrier function of AUD cells

We measured transepithelial resistance (TER) as an index of barrier integrity. TER values were measured for cultured, differentiated bronchial epithelial cells originally isolated from people with or without AUD. The cells were then infected with the Washington strain of SARS-CoV-2 at 0.1 MOI and TER values were measured at intervals over the course of a 72h time course and normalized to baseline values to facilitate comparisons for each condition examined (Figure 3.2).

In bronchial epithelial cells derived from three different AUD isolates, SARS-CoV-2 infection caused a significant decrease in TER (Figure 3.2A-C). On the other hand, three different non-AUD cell isolates showed an increase in TER 72 h following infection (Figure 3.2D-F). All samples had a similar baseline TER (Figure 3.2G) except for non-AUD 1, which had a significantly lower TER compared to AUD 1 and AUD 2. Taken together, these data support a model where the ability of AUD bronchial epithelial cell barrier function is more sensitive to SARS-CoV-2 infection than non-AUD cells.

To determine whether the differential effects of SARS-CoV-2 infection on TER were due to differences between AUD and non-AUD cells in epithelial junction organization, we used confocal and deconvolution immunofluorescence microscopy (Figure 3.3). Over the course of our experiments, the tight junction scaffold protein zonula occludens-1 (ZO-1) remained predominantly tight junction-associated. Also, total levels of ZO-1 were unchanged by SARS-

CoV-2 infection (Figure 3.3E).

We also examined one of the major transmembrane tight junction proteins responsible for bronchial epithelial barrier function, claudin-7 (45). At baseline, there was significantly more claudin-7 present in AUD than in non-AUD bronchial epithelial cells (Figure 3.3F), potentially rendering the AUD cells more sensitive to barrier dysfunction. Note that most of the claudin-7 expressed by bronchial cells is present on the lateral plasma membrane (Figure 3.3A, xz), that is not colocalized with ZO-1 and does not contribute to barrier function (38). Infection eliminated the significance of the difference in total claudin-7, however, having less ZO-1 associated with tight junctions in infected AUD cells (Figure 3.3C) is anticipated to result in decreased barrier function.

In contrast to ZO-1 and claudin-7, levels of β -catenin, an adherens junction scaffold protein, were significantly diminished in response to SARS-CoV-2 infection (Figure 3.3B, D, G). A similar effect of SARS-CoV-2 on β -catenin expression has been reported for infected endothelial cells (24, 54) and has been implicated in the disruption of vascular barrier function due to COVID-19. However, infection had a similar effect on total β -catenin in AUD and non-AUD cells, suggesting that this does not account for the differential effect of infection on barrier function of bronchial epithelial cells. Instead, the decrease in airway epithelial β -catenin following SARS-CoV-2 infection more likely reflects another cell response that is unaffected by AUD, such as translocation of junction localized β -catenin to mediate wnt signaling (73).

3.4.3 Differential secretion of cytokines by infected AUD and non-AUD cells

Multiplex analysis of cytokine secretion by SARS-CoV-2 infected cells revealed that most pro-inflammatory cytokines showed higher levels of secretion by AUD cells during the initial 72h

period post-infection as compared to non-AUD cells (Figure 3.4, Supp. Figure 3.2). Notable among these cytokines are TNF α , IL-1 β and IFN γ (Figure 3.4A-C), although there was only a trending increase in secretion of TNF α by AUD cells at 6 and 24 h after infection. These cytokines were found to be up-regulated in COVID-19 patients (92) and cause barrier dysfunction in barrier-forming cells (17, 93). This is consistent with the effect we observed on barrier function in Figure 1. Non-AUD cells secreted more Epidermal Growth Factor (EGF) over the 72h time course compared to AUD cells (Figure 3.4D). In addition, there was an appreciable, although not significant increase, in Granulocyte Macrophage Colony Stimulating Factor (GM-CSF) secretion in non-AUD cells compared to AUD cells (Figure 3.4E). Both EGF (16, 70) and GM-CSF (51) have been associated with improved lung epithelial barrier function, which is consistent with the effect we observed on barrier function in Figure 1.

We assessed apical and basolateral secretion of the abovementioned cytokines and found that AUD cells had a significant increase in basolateral secretion of IFN γ and IL-1 β , while TNF α EGF, GM-CSF were secreted in a non-polarized manner in both AUD and non-AUD cells (Figure 3.4F-J). Taken together, these results support a model in which AUD cells were primed for an enhanced innate immune response to SARS-CoV-2 infection when compared with non-AUD cells.

An additional 16 cytokines were preferentially secreted by AUD cells at least at one timepoint (Supplemental Figure 3.1), except for CCL3/MIP-1 α , which was preferentially secreted by non-AUD cells at 6 h and 72 h post infection (Supplemental Figure 3.2A). It is noteworthy that AUD cells secreted more IL-17A, IL-17F and IL-25/IL-17E (Supplemental Figure 3.2L, M, P), as IL-17 strongly correlates with severe COVID-19 (94). Nine additional cytokines were found to be equivalently secreted from AUD and non-AUD cells during the 72 h time course, including IL-6, IL-1 α and IL-13 (Supplemental Figure 3.3).

Seventeen cytokines from our multiplex analysis were secreted in a polarized manner from either AUD cells or non-AUD cells (Supplemental Figure 3.4). We observed a variety of profiles, including 8 cytokines that were significantly secreted basolaterally from AUD cells while 5 cytokines were significantly secreted basolaterally from non-AUD cells. CCL5/RANTES and M-CSF were significantly secreted apically from AUD cells while IL-7 and IL-22 were significantly secreted basolaterally in both AUD and non-AUD cells. Eight cytokines displayed equal bidirectional secretion (Supplemental Figure 3.5).

3.5 Discussion

The effect of SARS-CoV-2 infection on human primary bronchial cells in culture has been examined by others (23, 48, 55, 74, 76, 83), however, this study is the first analysis of the effects of AUD on cell responses to SARS-CoV-2 infection. Together, our data support a model where AUD and non-AUD differ in their inflammatory response to SARS-CoV-2 infection. We found that AUD cells showed a significant decrease in TER in response to SARS-CoV-2 infection, however non-AUD cells showed an increase in TER. Previous analysis of infected airway cells has shown a minimal effect of SARS-CoV-2 infection on TER over a 6 day period (83) or over a 30 day period following an initial drop, with some fluctuations (23). Although the enhancement of TER by non-AUD cells was unexpected, it was consistent with another study demonstrating that SARS-CoV-2 infection of bronchial epithelial cells showed a transient decrease in TER followed by a rebound to higher TER when measured over a 7-day time course post infection (57).

In general, TER is largely preserved but it can decrease when virus shedding is high, most likely due to focal overt damage to the monolayer (57). Another likely mechanism of diminished barrier function is influence of viral proteins on assembly of the tight junction complex, even in

the absence of viral shedding. In particular, interference of the SARS-CoV envelope protein (E protein) with ZO-1 association with tight junctions was originally demonstrated for SARS-CoV-1 (69). Subsequently SARS-CoV-2 E protein has been found to bind to ZO-1 as well (12, 18, 64, 72). Whether this is occurring in SARS-CoV-2 infected airway cells to interfere with tight junctions remains to be determined. Disruption of ZO-1 can also influence the distribution of claudin-7 between the tight junction (barrier forming) and lateral (non-barrier forming) pools. Regardless of the mechanism, cell polarity is largely retained, since infected airway cells *in vitro* show low levels of basolateral virus shedding relative to apical shedding (23, 57) and cytokine secretion is also polarized, as seen here and in other reports (74, 76).

Surprisingly, we found that non-AUD cells secreted two protective cytokines, EGF and GM-CSF, in response to SARS-CoV-2 that were less prominent in infected AUD cells. EGF in particular has been shown to promote lung epithelial cell barrier function (16, 70). Moreover, administration of EGF to septic mice has been shown to lessen the severity of sepsis, even in alcohol fed mice, in part by protecting gut barrier function (31).

Interpreting roles for GM-CSF in bronchial epithelial cell behavior is more complex, since it has both pro- and anti- inflammatory effects, depending on the amount, context and presence of other inflammatory mediators (6). Consistent with the protective effect of GM-CSF, GM-CSF deficient mice exhibit pulmonary alveolar proteinosis (PAP) (20), which ultimately led to therapies including inhaled GM-CSF to treat this disease (30). There is also evidence that ARDS survival correlates with the amount of GM-CSF present in lung lavage fluid (40, 51). This is due to stimulation of the PU.1 transcription factor by autocrine stimulation of lung epithelial cells by GM-CSF and this pathway was found to be impaired as a result of chronic alcohol ingestion in a rodent model (27). This would be consistent with impairment of GM-CSF signaling by AUD cells

as a contributor to barrier dysfunction due to SARS-CoV-2 (Figure 3.2) and supports the potential for GM-CSF administration as a therapeutic approach in severe COVID-19 (35, 41). However, the use of administered GM-CSF to treat non-COVID ARDS has had mixed success, where it was shown to improve the ratio of arterial oxygen partial pressure to fractional inspired oxygen (PaO2/FIO2) (53), but it did not increase the number of ventilator-free days in ARDS patients (52).

IL-6 is a highly investigated COVID-19-associated cytokine that correlates with more severe outcomes (8,15). Other studies examining SARS-CoV-2-exposed bronchial cells have also shown that IL-6 was produced at 72 h after infection (55, 74, 76), consistent with the response we observed in AUD and non-AUD cells (Supplemental Figure 3.3). We found that in general AUD cells had a stronger inflammatory response than non-AUD cells in response to SARS-CoV-2 infection. Although IL-6 secretion is potentially an epithelial protective response to infection (78), IL-6 is also associated with vascular barrier dysfunction, including COVID-19 associated vascular disease (71, 80).

Our study is the first to focus on the Black or African American patient population concerning the effects of AUD on SARS-CoV-2 infection (Table 3.3). In the United States, African American/Black populations have disproportionally higher rates of SARS-CoV-2 infection, hospitalization, and COVID-19-related mortality, according to a systematic review of numerous studies (97). This is a multifactorial issue due in part to adverse social determinants of health and increased prevalence of comorbidities (98). While we were unable to adjust for smoking in our study, we did have 2 smokers among both the AUD and non-AUD patients, making the percentage of smokers 66%. This percentage of smokers in the AUD patient samples is equivalent to the percentage of chronic alcohol users who smoke at least one pack of cigarettes a day, which is 70% (95).

RNA-seq analysis revealed 164 DE genes with the majority up-regulated in AUD cells. Critically, there were few proinflammatory genes that were upregulated by AUD, including TNFα, IL-1β, and IFNγ, indicating that cells from AUD subjects were not classically inflamed prior to infection. We also compared our RNA-seq results with those from Bailey et al. who performed RNA-seq analysis of unexpanded bronchial brushings from 19 non-AUD samples and 18 AUD samples (96). In samples which were not corrected for smoking status, we identified 19 genes that were differentially expressed in both studies (Table 3.2), however, this required using a less stringent measure of significance for the Bailey dataset, raw p value as opposed to adj p value. Notably, S100A8 and MUC5B are among these common DE genes. In addition, CEACAM5 is an adhesion protein that is upregulated in bronchial cells from patients with type-2 severe asthma (91). Together, these findings suggest that AUD cells adapted an inflammatory, epidermal profile. This may explain why AUD cells have an altered barrier function and inflammatory response to SARS-CoV-2 infection.

We found that the effects of AUD on human airway epithelial cell responses to SARS-CoV-2 infection were maintained by cultured cells and did not require the presence of alcohol in the culture medium. This finding is consistent with our data using lung epithelial cells isolated from alcohol fed rodents (21, 39, 61) and suggests that the cells may by epigenetically reprogrammed in response to chronic alcohol exposure. In fact, alcohol consumption has been linked to epigenetic modification of the central nervous system as a mechanism underlying addiction (4), which further suggests that epigenetic reprogramming also can occur in the lung in response to AUD. Consistent with this possibility, it has previously been shown that alcohol inhibits Thy-1 expression by lung fibroblasts by DNA methylation induced by TGF-β1 (49, 50). The effects of epigenetic reprogramming of lung epithelia by alcohol remains to be determined.

Our findings that non-AUD cells had a relatively mild response to SARS-CoV-2 infection is likely to reflect the cell culture conditions we used. Here we used medium that supports bronchial cell differentiation and also contains normal resting glucose levels (46). However, several media commonly used to support airway epithelial cell differentiation have high glucose concentrations, including media based on LHC Basal:DMEM-H and Pneumocult-ALI both of which contain ~ 300 mg/dL glucose (46). Thus, one consideration in interpreting results obtained with cultured airway epithelial cells is that their response to SARS-CoV-2 infection may be sensitive to medium glucose content, which would be consistent with diabetes as a risk factor for increased severity of COVID-19 (10).

Here we compared primary bronchial epithelial cells derived from AUD and non-AUD patients that were grown, differentiated, and treated under the same conditions to demonstrate that AUD cells showed early sensitivity to SARS-CoV-2 infection. As early onset of severe disease is a likely determinant of further disease progression, our data add AUD as a risk factor for increased severity of COVID-19 related illness (2) due to the combined impact of alcohol and SARS-CoV-2 infection on airway epithelial barrier function and inflammation. This underscores the importance of considering AUD status when treating COVID-19 patients and the likely utility of targeting the lung epithelium when considering treatment options.

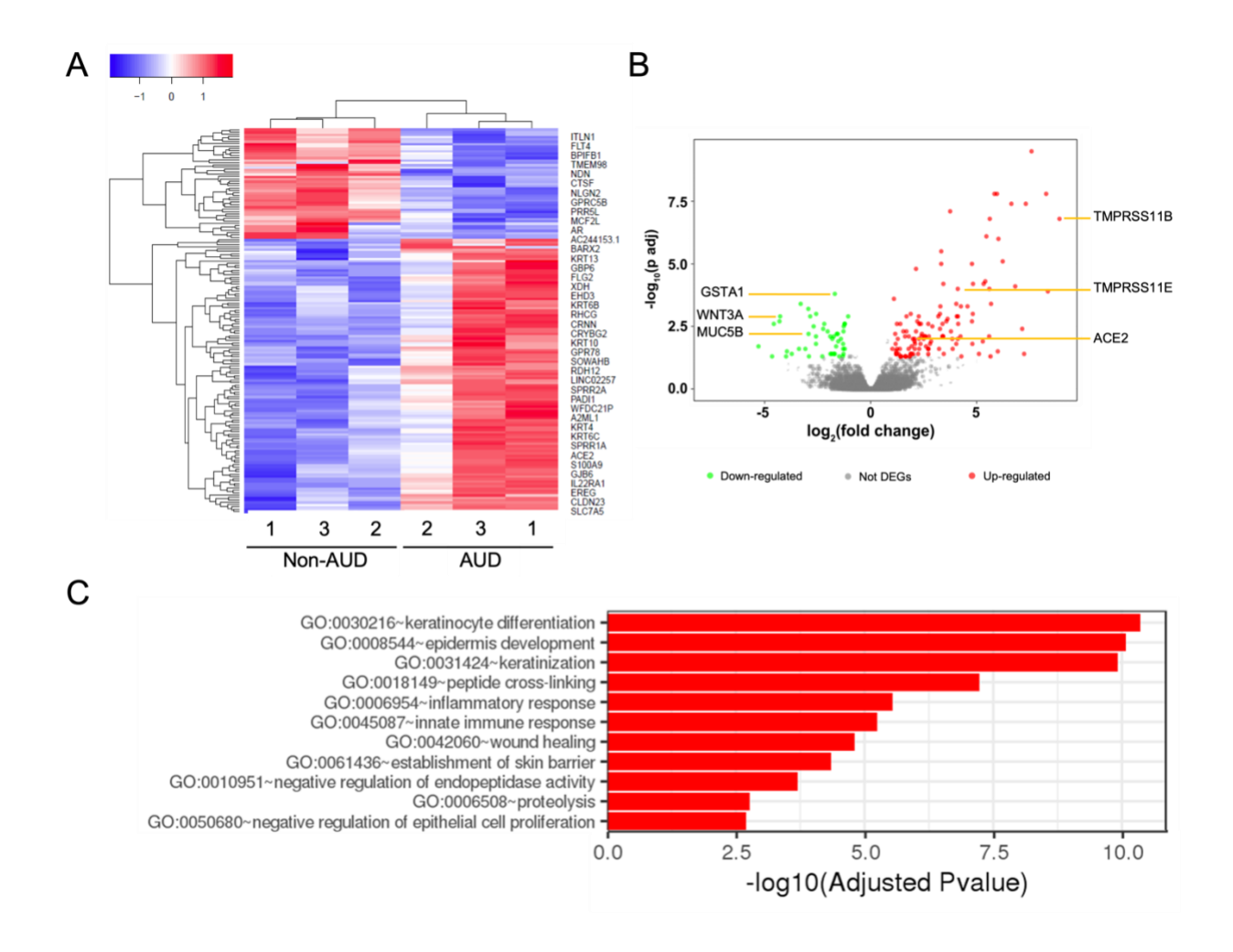


Figure 3.1 Summary of RNA-seq analysis of AUD and non-AUD cells.

Differentiated bronchial cells from non-AUD and AUD patients were subject to RNA sequencing.

(A) Heat map representation of all 164 differentially expressed genes. Down-regulated genes are in blue and up-regulated genes are in red, in respect to AUD cells. Select DE genes are located on right. (B) Volcano plot representation of all genes. Green dots represent down-regulated genes in AUD cells, red dots represent up-regulated genes in AUD cells and grey dots represent genes that were not differentially expressed. SARS-CoV-2 receptor genes were upregulated in AUD cells. Genes required for proper function and maintenance of bronchial cells were down-regulated in AUD cells. (C) Differentially expressed genes were clustered by their gene ontology. Enrichment

of gene ontology terms was tested using Fisher exact test (GeneSCF v1.1-p2). Shown are top 11 significantly enriched gene ontology terms with an adjusted P-value less than 0.05 in the differentially expressed gene set.

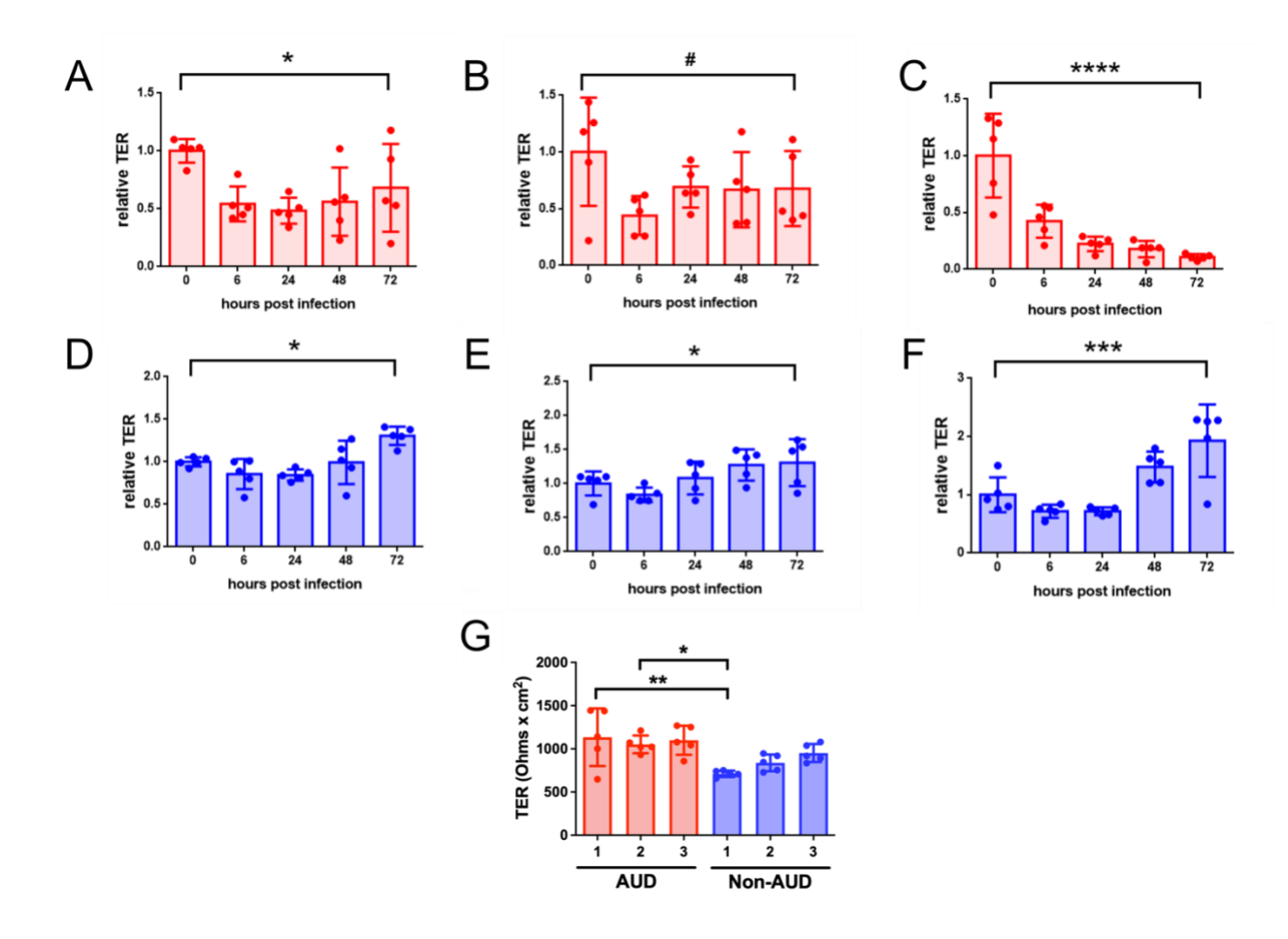


Figure 3.2 AUD cells have impaired barrier function following SARS-CoV-2 infection.

Differentiated bronchial cells from AUD (A-C, red) and non-AUD (D-F, blue) subjects were infected with SARS-CoV-2. TER was measured immediately prior to infection (t=0) and at 6, 24, 48 and 72 h post infection, normalized to values at t=0. AUD cells showed decreased barrier function 72h after infection (A, * p=0.04; B, # p=0.12; C, **** p<0.0001). By contrast, non-AUD cells showed increased barrier function 72 h after infection (D, ** p=0.0047; E, # p=0.051; F, *** p=0.0003). G. Actual TER values of all samples immediately prior to infection. Non-AUD 1 had a lower TER compared to AUD 1 (**p=0.0087) and AUD 2 (*p=0.02). n=3 biological replicates consisting of 5 Transwells per group. Values represent mean ± SD in each case.

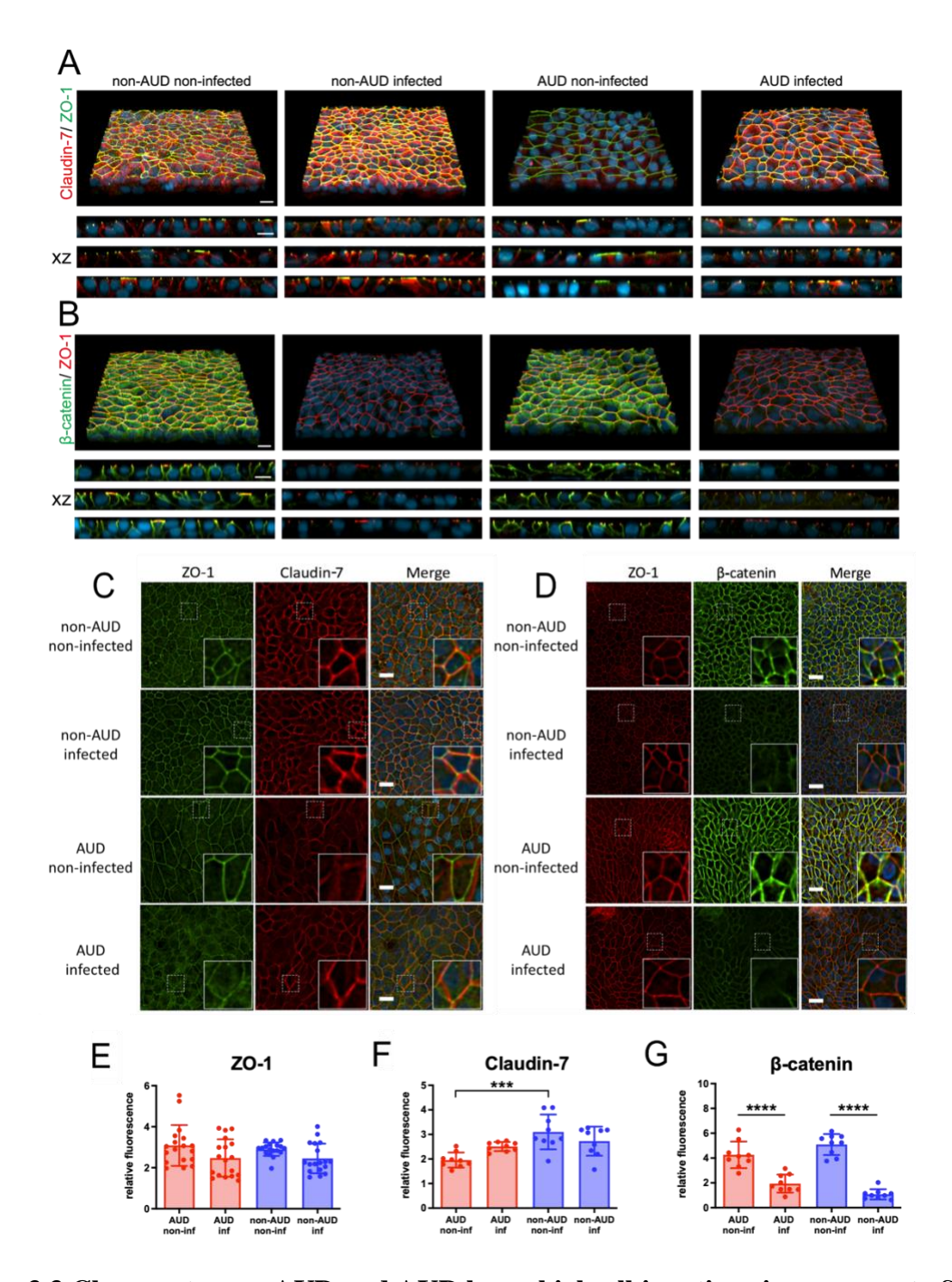


Figure 3.3 Changes to non-AUD and AUD bronchial cell junctions in response to SARS-CoV-2 infection.

A-D. Cells 72h post infection or mock infection were fixed and immunostained for ZO-1 (green) and claudin-7 (red) and DAPI (blue) (A,C) or ZO-1 (red), β -catenin (green) and DAPI (blue) (B,D) and imaged by confocal (A,B) and deconvolution (C,D) fluorescence microscopy. A,B. Top panels

show a 3D projection, the bottom panels represent xz projections from three biological replicates for each condition. Bar, 10 micron. C,D. xy projections of representative images. White dotted squares represent the location of insets in the bottom right corner of each image. Bar, 20 micron. E-G. Relative fluorescence measurements for showed little effect SARS-CoV-2 infection on total intensity of ZO-1 (C) and claudin-7 (D), however there was a significant decrease in total β -catenin 72 h post-infection (****, p<0.0001, n= 3 fields each from 3 biological replicates). Also, there was significantly less claudin-7 in non-infected AUD cells compared to non-infected non-AUD cells (****, p=0.001, n= 3 fields each from 3 biological replicates), although this difference diminished 72h post-infection. Values represent mean \pm SD in each case.

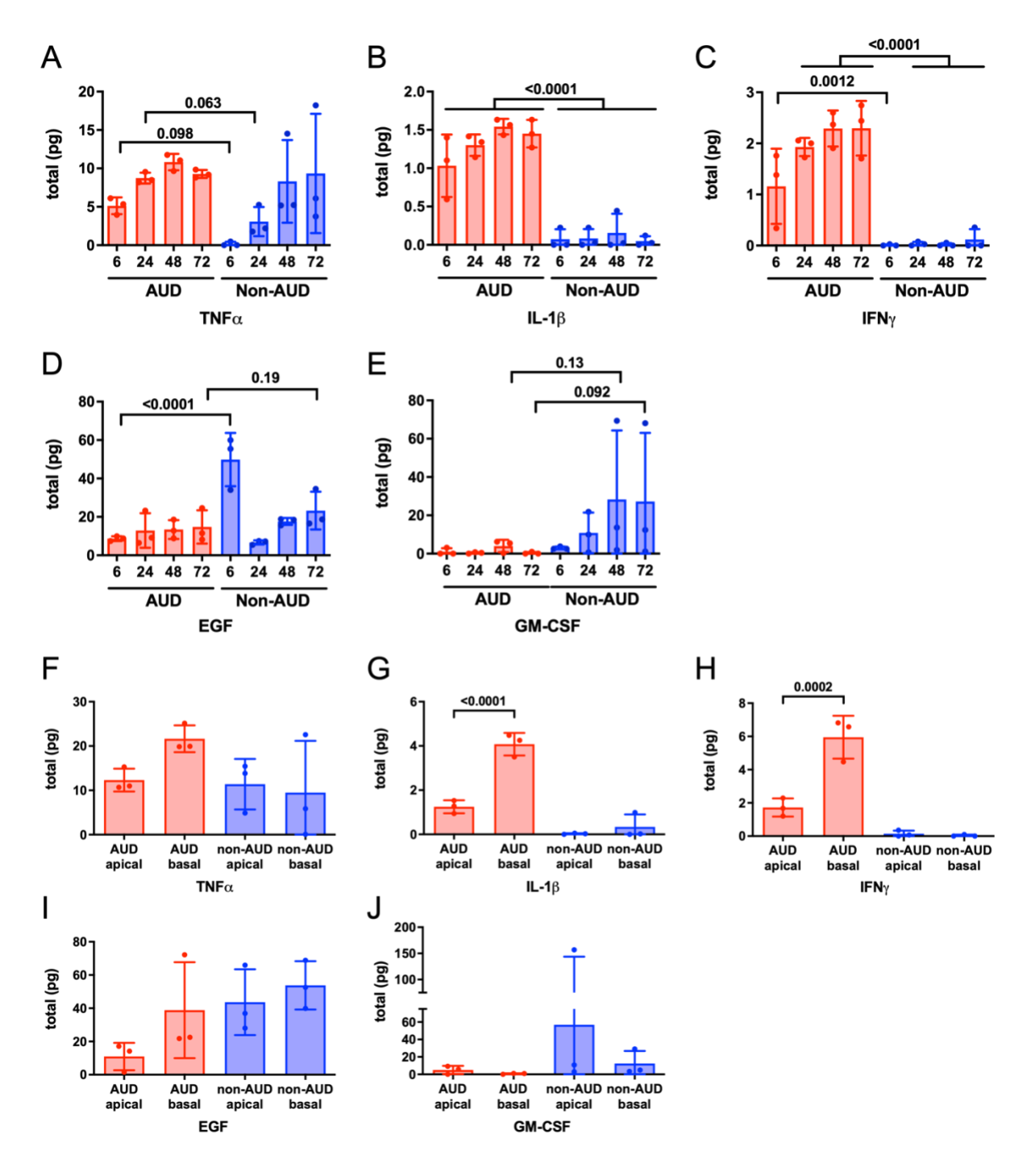


Figure 3.4 Pro-inflammatory cytokines were preferentially secreted by AUD cells in a polarized manner in response to infection.

Differentiated bronchial cells from non-AUD and AUD patients were infected with SARS-CoV-2 and analyzed for cytokine secretion at 6, 24, 48 and 72 h post infection (A-E) or analyzed for apical

and basolateral secretion over the entire time course (F-J). There was a trending or significant increase in pro-inflammatory cytokine secretion (TNF α , IL-1 β , and IFN γ) by AUD cells at some or all timepoints. There was a trending or significant increase in anti-inflammatory cytokines by non-AUD cells at some timepoints. AUD cells secreted significantly more basolateral IL-1 β , and IFN γ . There was equivalent apical and basolateral secretion of TNF α , EGF and GM-CSF by AUD cells. For all 5 cytokines, non-AUD cells secreted equal amounts apically and basolaterally. n=3 biological replicates consisting of samples from 3 Transwells per group. Values represent mean \pm SD in each case.

Enrollment ID	Age	Gender	Height (inches)	Weight (lbs)	ВМІ	Race	Ethnicity	current smoker?	Pack year history
AUD 1	50	Male	65	145	24.1	Black or African American	NOT Hispanic or Latino	Yes	3
AUD 2	53	Male	71	201	28.0	Black or African American	NOT Hispanic or Latino	Yes	26
AUD 3	51	Male	71	173	24.1	Black or African American	NOT Hispanic or Latino	No	0
Non-AUD 1	20	Male	77	195	23.1	Black or African American	n/a	No	0
Non-AUD 2	29	Male	66	172	27.8	Black or African American	NOT Hispanic or Latino	Yes	4
Non-AUD 3	58	Male	66	135	21.8	Black or African American	NOT Hispanic or Latino	Yes	45

Table 3.1 Subject Characteristics.

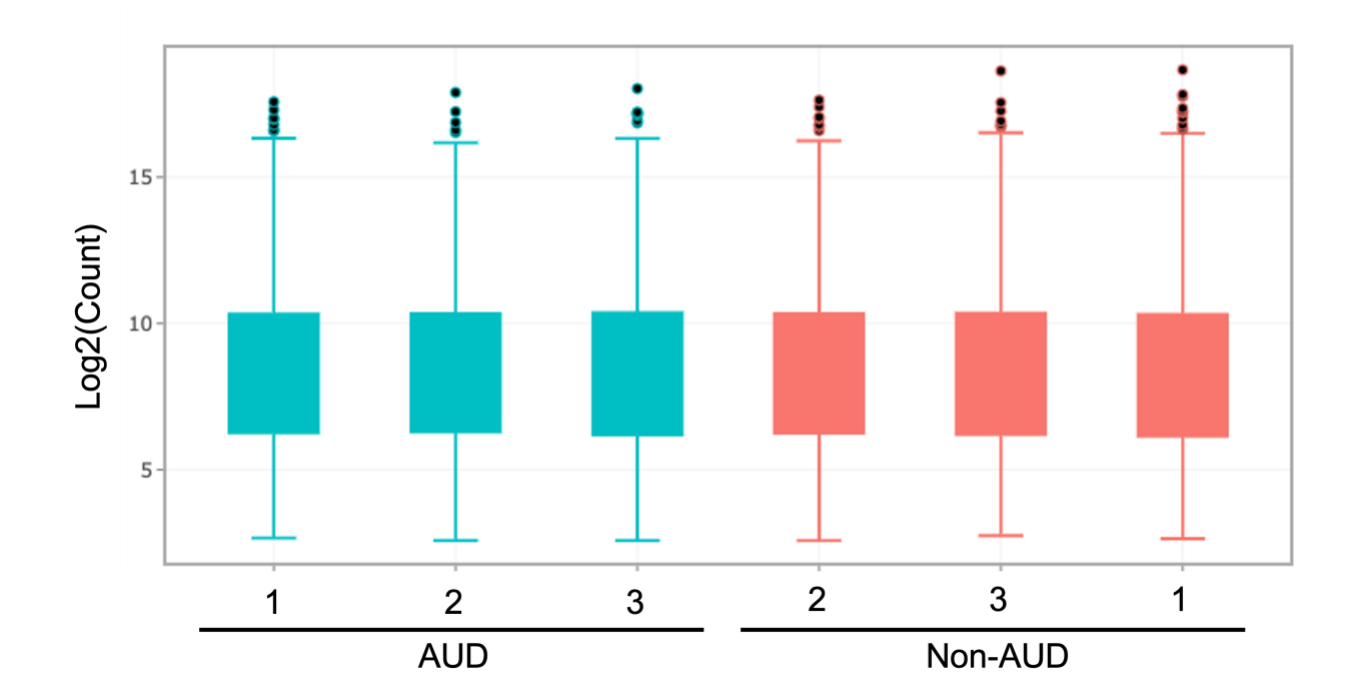
Gene Ontology Analysis	Genes
Genes related to epidermal regulation	ABCA12; CALML5; EMP1; EREG; FLG2; GRHL3; KLK7; KRT10; KRT16; SCEL; SPRR1A; SPRR2A; SPRR1B; SPRR2D; SPRR2E; SPRR3; TGM1
Genes related to Inflammation	BDKRB2; BMPR1B; C4B; C6; CLEC7A; ECM1; IL1RN; IL22RA; IL36RN; IL36A; KRT16; MGLL; PGLYRP4; S100A8; S100A9; S100A12; SUSD4

Table 3.2 Differentially expressed genes related to epidermal regulation and inflammation identified in the Gene Ontology analysis.

	Ours			Bailey et al.	(ref)	
Gene name	log 2 fold change	p Value	adj. p Val	log 2 fold change	p Value	adj. p Val
CEACAM7	4.82	0.00	0.00	2.58	0.01	0.18
S100A8	4.78	0.00	0.00	2.10	0.02	0.21
CYSRT1	3.43	0.00	0.00	1.06	0.02	0.20
CEACAM5	3.39	0.00	0.01	4.18	0.00	0.06
PADI1	3.33	0.00	0.00	1.55	0.02	0.19
ABCA12	2.09	0.00	0.02	2.34	0.01	0.16
CRYBG2	1.62	0.00	0.01	1.32	0.02	0.19
PLBD1	1.41	0.00	0.05	0.77	0.01	0.14
BDKRB2	1.24	0.00	0.00	0.42	0.05	0.31
GPRC5B	-1.63	0.00	0.02	-0.84	0.02	0.22
MUC5B	-2.93	0.00	0.01	-2.05	0.00	0.10
CYP2A13	-3.99	0.00	0.05	-2.09	0.00	0.08
ITLN1	-4.57	0.00	0.00	-3.18	0.01	0.16

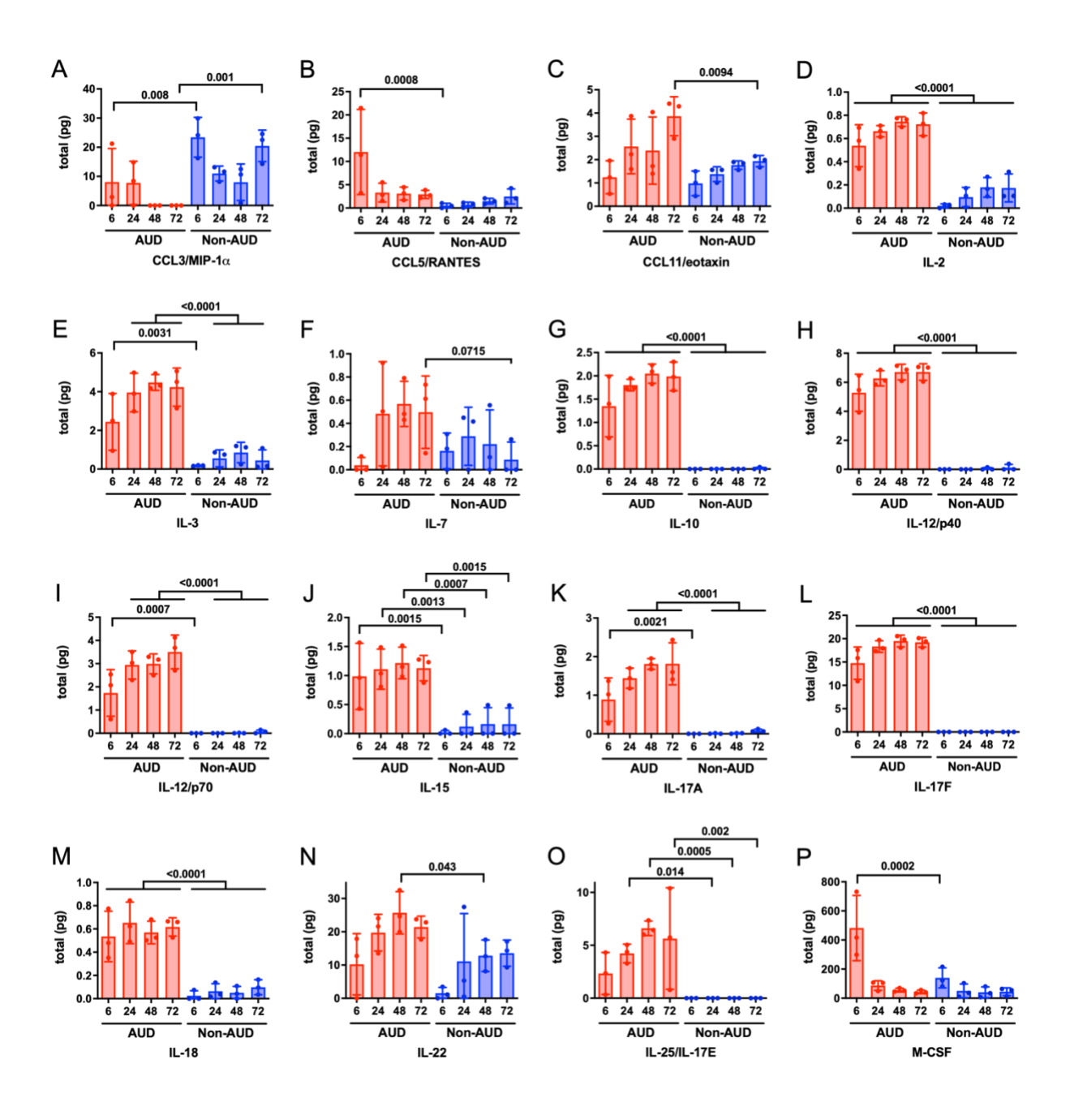
Table 3.3 Differentially expressed genes by AUD and non-AUD bronchial cells that were identified in both our study and by Bailey et al.

We compared our RNA sequencing results to those in Bailey et al. and identified 13 genes that were differentially expressed in both studies (96). Bailey et al. evaluated 19 non-AUD and 18 AUD bronchial brushing samples and identified 520 differentially expressed genes.



Supplemental Figure 3.1 Distribution of normalized read counts.

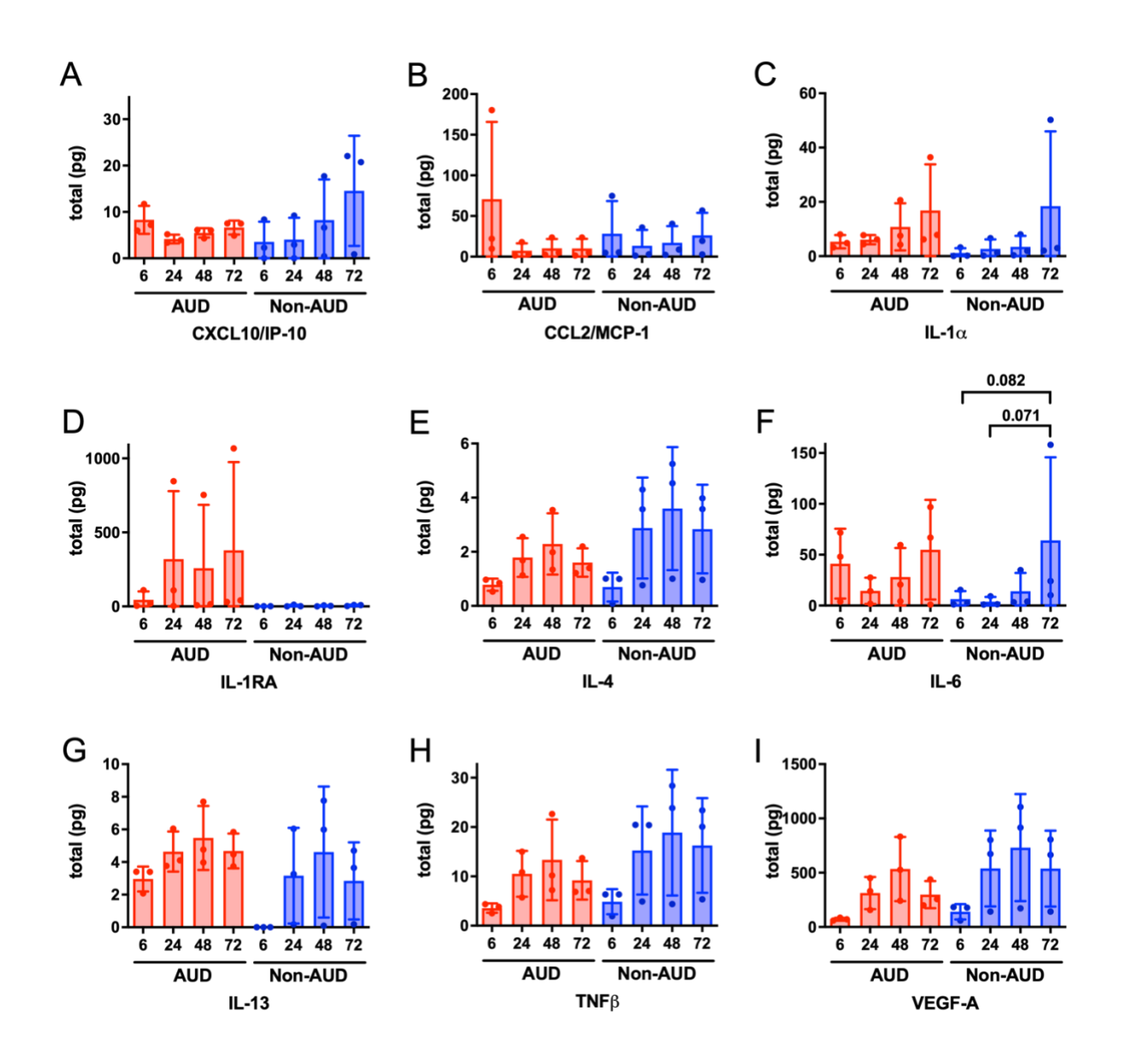
The original read counts were normalized to adjust for various factors and used to accurately determine differentially expressed genes.



Supplemental Figure 3.2 Cytokines that were preferentially secreted by AUD cells in response to infection.

Differentiated bronchial cells from non-AUD and AUD patients were infected with SARS-CoV-2 and analyzed for cytokine secretion using a multiplex assay. Shown is cytokine secretion at 6, 24,

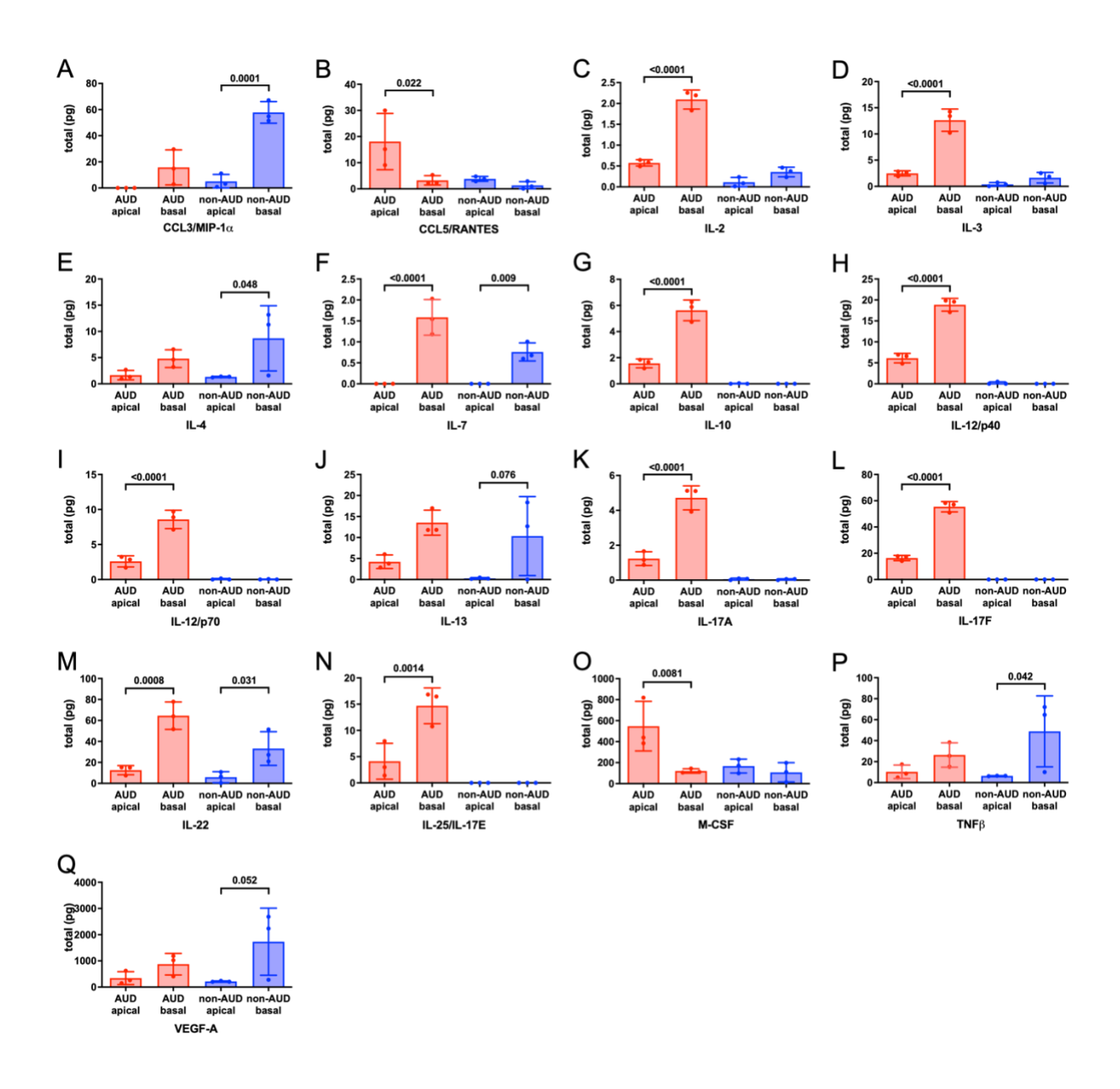
48 and 72 h post infection. n=3 biological replicates consisting of samples from 3 Transwells per group. Values represent mean \pm SD in each case.



Supplemental Figure 3.3 Cytokines that were equivalently secreted by AUD cells and non-AUD cells in response to infection.

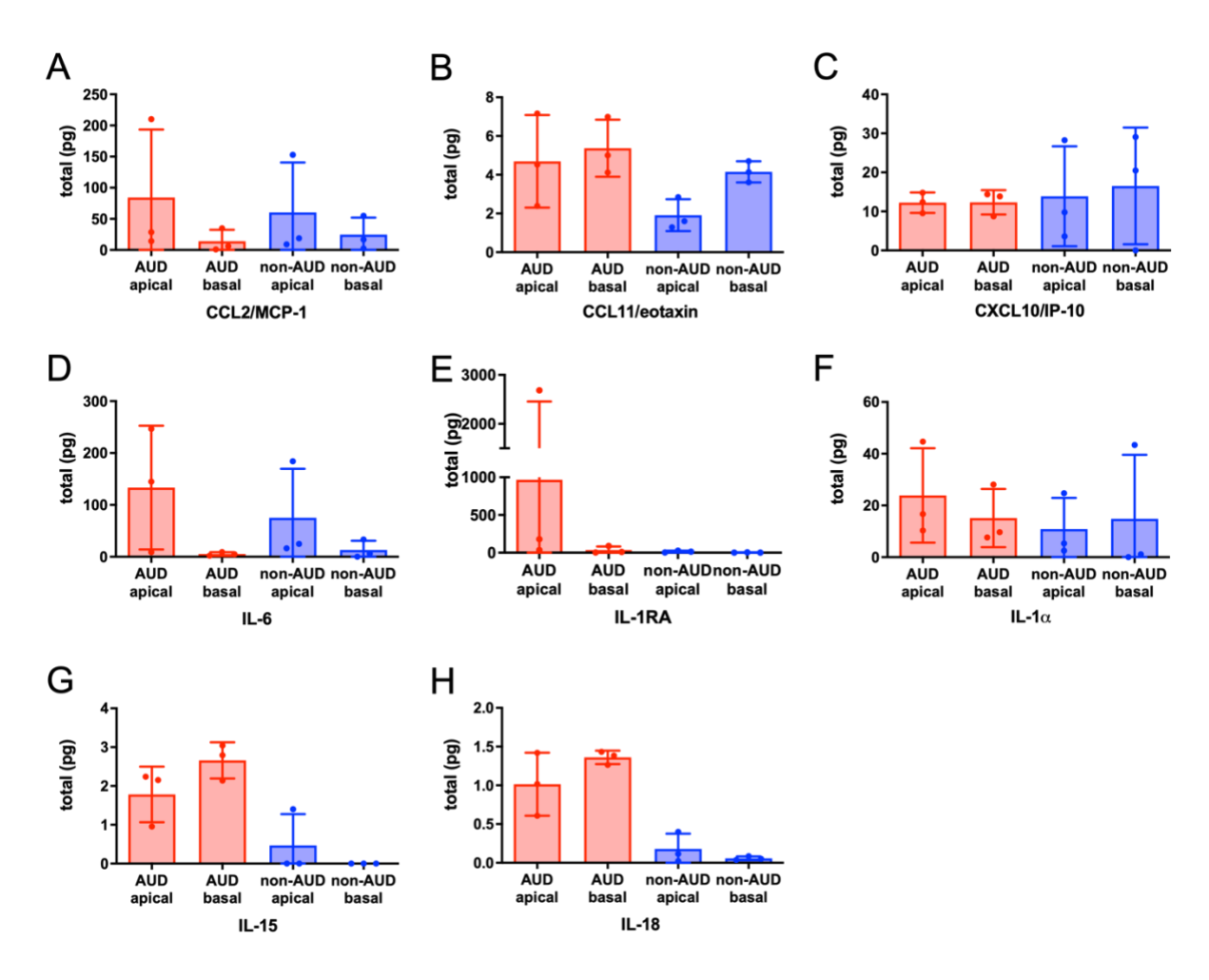
Differentiated bronchial cells from non-AUD and AUD patients were infected with SARS-CoV-2 and analyzed for cytokine secretion using a multiplex assay. Shown is cytokine secretion at 6, 24, 48 and 72 h post infection. Shown are cytokines that were equivalently secreted by AUD cells and

non-AUD cells at each timepoint. n=3 biological replicates consisting of samples from 3 Transwells per group. Values represent mean \pm SD in each case.



Supplemental Figure 3.4 Polarized secretion of cytokines by AUD and non-AUD cells in response to infection.

Differentiated bronchial cells from non-AUD and AUD patients were infected with SARS-CoV-2 and analyzed for cytokine secretion using a multiplex assay. Shown is apical and basolateral cytokine secretion over the entire time course. Shown are cytokines that were significantly secreted either apically or basolaterally by either AUD or non-AUD cells.



Supplemental Figure 3.5 Equal apical and basolateral secretion of cytokines by AUD and non-AUD cells in response to infection.

Differentiated bronchial cells from non-AUD and AUD patients were infected with SARS-CoV-2 and analyzed for cytokine secretion using a multiplex assay. Shown is apical and basolateral cytokine secretion over the entire time course. Shown are cytokines that were secreted in equal amounts into the apical and basolateral chambers.

GeneID	GeneName	log2FoldChange	P-value	P-adj
ENSG00000185873	TMPRSS11B	8.91	0	0
ENSG00000167916	KRT24	8.36	0	0
ENSG00000172005	MAL	8.28	0	0
ENSG00000163209	SPRR3	7.59	0	0
ENSG00000143536	CRNN	7.32	0	0
ENSG00000170426	SDR9C7	7.24	0	0.04
ENSG00000126233	SLURP1	7.15	0	0
ENSG00000136694	IL36A	6.82	0	0
ENSG00000170423	KRT78	6.64	0	0
ENSG00000169474	SPRR1A	6.23	0	0
ENSG00000189001	SBSN	6.03	0	0
ENSG00000155269	GPR78	6	0	0.03
ENSG00000241794	SPRR2A	5.96	0	0
ENSG00000249307	LINC01088	5.84	0	0
ENSG00000203785	SPRR2E	5.68	0	0
ENSG00000145879	SPINK7	5.66	0	0.05
ENSG00000163216	SPRR2D	5.62	0	0
ENSG00000166535	A2ML1	5.6	0	0
ENSG00000280071	FP565260.6	5.59	0	0.01
ENSG00000214711	CAPN14	5.46	0	0
ENSG00000140519	RHCG	5.41	0	0
ENSG00000129455	KLK8	5.33	0	0
ENSG00000166183	ASPG	5.29	0	0.01
ENSG00000143520	FLG2	5.11	0	0.04
ENSG00000133710	SPINK5	4.83	0	0
ENSG00000007306	CEACAM7	4.82	0	0
ENSG00000200033	RNU6-403P	4.8	0	0.01
ENSG00000143546	S100A8	4.78	0	0

ENSG00000174226	SNX31	4.78	0	0
ENSG00000178372	CALML5	4.57	0	0
ENSG00000183671	GPR1	4.28	0	0.05
ENSG00000130600	H19	4.26	0	0
ENSG00000090512	FETUB	4.24	0	0.01
ENSG00000163221	S100A12	4.13	0	0
ENSG00000171476	HOPX	4.12	0	0
ENSG00000087128	TMPRSS11E	4.11	0	0
ENSG00000125998	FAM83C	4.11	0	0.01
ENSG00000169469	SPRR1B	4.06	0	0
ENSG00000238042	LINC02257	4.04	0	0
ENSG00000136695	IL36RN	4.04	0	0.01
ENSG00000171401	KRT13	3.87	0	0.03
ENSG00000167755	KLK6	3.85	0	0.01
ENSG00000185479	KRT6B	3.79	0	0
ENSG00000169035	KLK7	3.75	0	0
ENSG00000170477	KRT4	3.63	0	0
ENSG00000143369	ECM1	3.57	0	0
ENSG00000198488	B3GNT6	3.45	0	0.04
ENSG00000197191	CYSRT1	3.43	0	0
ENSG00000139988	RDH12	3.42	0	0.01
ENSG00000158125	XDH	3.4	0	0.01
ENSG00000071991	CDH19	3.39	0	0
ENSG00000105388	CEACAM5	3.39	0	0.01
ENSG00000142623	PADI1	3.33	0	0
ENSG00000172382	PRSS27	3.33	0	0
ENSG00000214049	UCA1	3.29	0	0
ENSG00000121742	GJB6	3.27	0	0
ENSG00000170465	KRT6C	3.27	0	0

ENSG00000186832	KRT16	3.23	0	0.02
ENSG00000166736	HTR3A	3.19	0	0
ENSG00000161249	DMKN	2.91	0	0
ENSG00000124466	LYPD3	2.85	0	0.01
ENSG00000186806	VSIG10L	2.8	0	0.02
ENSG00000039537	C6	2.75	0	0.01
ENSG00000092295	TGM1	2.73	0	0.02
ENSG00000142677	IL22RA1	2.72	0	0
ENSG00000280693	SH3PXD2A-AS	2.72	0	0.04
ENSG00000173212	MAB21L3	2.71	0	0.02
ENSG00000197632	SERPINB2	2.61	0	0.02
ENSG00000109321	AREG	2.58	0	0.01
ENSG00000253368	TRNP1	2.55	0	0.01
ENSG00000165794	SLC39A2	2.5	0	0.01
ENSG00000136155	SCEL	2.42	0	0.01
ENSG00000177494	ZBED2	2.4	0	0.01
ENSG00000261040	WFDC21P	2.37	0	0
ENSG00000074211	PPP2R2C	2.35	0	0.02
ENSG00000074416	MGLL	2.29	0	0
ENSG00000134531	EMP1	2.29	0	0.03
ENSG00000163220	S100A9	2.28	0	0.01
ENSG00000158055	GRHL3	2.27	0	0
ENSG00000225833	AC097625.1	2.24	0	0.04
ENSG00000124882	EREG	2.2	0	0
ENSG00000064787	BCAS1	2.14	0	0
ENSG00000144063	MALL	2.14	0	0.01
ENSG00000144452	ABCA12	2.09	0	0.02
ENSG00000197353	LYPD2	2.08	0	0.03
ENSG00000173210	ABLIM3	2.07	0	0.01

ENSG00000136689	IL1RN	2.07	0	0.01
ENSG00000013016	EHD3	2	0	0.04
ENSG00000130234	ACE2	1.99	0	0.01
ENSG00000183347	GBP6	1.93	0	0.02
ENSG00000109846	CRYAB	1.92	0	0.04
ENSG00000111344	RASAL1	1.89	0	0
ENSG00000124102	PI3	1.88	0	0.04
ENSG00000089127	OAS1	1.84	0	0.05
ENSG00000166396	SERPINB7	1.8	0	0.01
ENSG00000143382	ADAMTSL4	1.79	0	0.03
ENSG00000134955	SLC37A2	1.69	0	0
ENSG00000183018	SPNS2	1.69	0	0.01
ENSG00000186395	KRT10	1.66	0	0.05
ENSG00000143412	ANXA9	1.63	0	0.05
ENSG00000176092	CRYBG2	1.62	0	0.01
ENSG00000103257	SLC7A5	1.54	0	0
ENSG00000149948	HMGA2	1.43	0	0.05
ENSG00000121316	PLBD1	1.41	0	0.05
ENSG00000261104	AC093904.4	1.4	0	0
ENSG00000276170	AC244153.1	1.38	0	0.02
ENSG00000043039	BARX2	1.32	0	0.04
ENSG00000172243	CLEC7A	1.28	0	0.01
ENSG00000168398	BDKRB2	1.24	0	0
ENSG00000006555	TTC22	1.24	0	0.03
ENSG00000163218	PGLYRP4	1.22	0	0.04
ENSG00000151012	SLC7A11	1.2	0	0.03
ENSG00000140297	GCNT3	1.2	0	0.04
ENSG00000206337	HCP5	1.18	0	0.01
ENSG00000177191	B3GNT8	1.16	0	0.01

ENSG00000253958	CLDN23	1.1	0	0
ENSG00000186212	SOWAHB	1.03	0	0.02
ENSG00000144724	PTPRG	-1.06	0	0
ENSG00000169992	NLGN2	-1.22	0	0
ENSG00000174080	CTSF	-1.22	0	0.03
ENSG00000121064	SCPEP1	-1.23	0	0
ENSG00000135362	PRR5L	-1.27	0	0
ENSG00000138696	BMPR1B	-1.28	0	0
ENSG00000143502	SUSD4	-1.28	0	0.04
ENSG00000145284	SCD5	-1.3	0	0.02
ENSG00000184144	CNTN2	-1.3	0	0.02
ENSG00000006042	TMEM98	-1.31	0	0.05
ENSG00000182636	NDN	-1.4	0	0.01
ENSG00000113594	LIFR	-1.48	0	0.05
ENSG00000065989	PDE4A	-1.53	0	0.01
ENSG00000160180	TFF3	-1.55	0	0.01
ENSG00000115325	DOK1	-1.6	0	0.01
ENSG00000167191	GPRC5B	-1.63	0	0.02
ENSG00000243955	GSTA1	-1.69	0	0
ENSG00000234390	USP27X-AS1	-1.69	0	0.04
ENSG00000198892	SHISA4	-1.74	0	0.01
ENSG00000126217	MCF2L	-1.74	0	0.04
ENSG00000099864	PALM	-1.81	0	0.01
ENSG00000165238	WNK2	-1.83	0	0.04
ENSG00000164199	ADGRV1	-1.9	0	0.04
ENSG00000182853	VMO1	-1.91	0	0.01
ENSG00000116299	KIAA1324	-2.03	0	0
ENSG00000105088	OLFM2	-2.19	0	0
ENSG00000233725	LINC00284	-2.24	0	0

ENSG00000224389	C4B	-2.28	0	0.05
ENSG00000127324	TSPAN8	-2.57	0	0
ENSG00000117507	FMO6P	-2.58	0	0.01
ENSG00000272512	AL645608.8	-2.58	0	0.02
ENSG00000176533	GNG7	-2.69	0	0
ENSG00000162373	BEND5	-2.85	0	0
ENSG00000175344	CHRNA7	-2.91	0	0.05
ENSG00000117983	MUC5B	-2.93	0	0.01
ENSG00000125999	BPIFB1	-2.94	0	0
ENSG00000020633	RUNX3	-3.08	0	0.02
ENSG00000153822	KCNJ16	-3.3	0	0
ENSG00000124191	TOX2	-3.38	0	0.02
ENSG00000169083	AR	-3.72	0	0.04
ENSG00000037280	FLT4	-3.95	0	0.03
ENSG00000197838	CYP2A13	-3.99	0	0.05
ENSG00000154342	WNT3A	-4.27	0	0
ENSG00000215030	RPL13P12	-4.3	0	0
ENSG00000179914	ITLN1	-4.57	0	0
ENSG00000140937	CDH11	-4.65	0	0.05
ENSG00000221826	PSG3	-5.29	0	0.02

Supplemental Table 3.1 List of differentially expressed genes

		Significant	Total Genes	Percent		
		Genes	group	significant		
Genes	Process name	count	count	genes	P-value	Padj-value
EREG; SCEL; KRT16; KRT10; SPRR1B; SPRR2E; SPRR2D; TGM1; SPRR1A; SPRR2A; SPRR3;	GO:0030216~keratinocyte differentiation	11	76	14.47368	6.08E-14	4.41E-11
SCEL; KRT16; SPRR1B; SPRR2E; SPRR2D; SPRR1A; SPRR2A; KLK7; EMP1; GRHL3; CALML5; SPRR3;	GO:0008544~epidermis development	12	80	15	2.34E-13	8.50E-11
KRT16; SPRR1B; SPRR2E; SPRR2D; TGM1; SPRR1A; SPRR2A; ABCA12; SPRR3;	GO:0031424~keratinization	9	48	18.75	4.96E-13	1.20E-10
SPRR1B; SPRR2E; SPRR2D; TGM1; SPRR1A; SPRR2A; SPRR3;	GO:0018149~peptide cross- linking	7	49	14.28571	3.28E-10	5.94E-08
BMPR1B; S100A8; S100A9; KRT16; C4B; BDKRB2; S100A12; ECM1; MGLL; CLEC7A; IL36A;	GO:0006954~inflammatory response	11	370	2.972973	1.97E-08	2.86E-06
S100A8; S100A9; KRT16; C4B; C6; S100A12; SUSD4; PGLYRP4; CLEC7A; IL36RN; IL36A;	GO:0045087~innate immune response	11	404	2.722772	4.69E-08	5.67E-06
EREG; S100A8; SERPINB2; TFF3; GRHL3; SPRR3;	GO:0042060~wound healing	6	75	8	1.53E-07	1.59E-05
KRT16; FLG2; ABCA12; GRHL3;	GO:0061436~establishment of skin barrier	4	18	22.2222	4.92E-07	4.46E-05
A2ML1; SERPINB7; SERPINB2; C4B; PI3; FETUB;	GO:0010951~negative regulation of endopeptidase activity	6	124	4.83871	2.50E-06	0.000201423
CAPN14; KLK8; C4B; KLK7; ADAMTSL4; TMPRSS11B; PRSS27; CTSF; TMPRSS11E;	GO:0006508~proteolysis	9	508	1.771654	2.38E-05	0.001722206
EREG; AR; KRT4; RUNX3;	GO:0050680~negative regulation of epithelial cell proliferation	4	56	7.142857	3.01E-05	0.001982698
GCNT3; B3GNT6; B3GNT8; MUC5B;	GO:0016266~O-glycan processing	4	59	6.779661	3.65E-05	0.002205038
BMPR1B; EREG;	GO:0001550~ovarian cumulus expansion	2	2	100	5.07E-05	0.002448214

S100A8; S100A9; S100A12; GBP6; MUC5B;	GO:0042742~defense response to bacterium	5	127	3.937008	4.58E-05	0.002448214
S100A8; S100A9;	GO:0070488~neutrophil aggregation	2	2	100	5.07E-05	0.002448214
GSTA1; KRT4; SPINK5; RHCG;	GO:0030855~epithelial cell differentiation	4	67	5.970149	5.85E-05	0.002649057
S100A8; S100A9; S100A12; GPRC5B;	GO:0050729~positive regulation of inflammatory response	4	71	5.633803	7.25E-05	0.003090685
S100A8; S100A9;	GO:0032602~chemokine production	2	3	66.66667	8.43E-05	0.003223177
S100A8; S100A9; S100A12;	GO:0050832~defense response to fungus	3	26	11.53846	8.45E-05	0.003223177
C4B; C6; SUSD4;	GO:0030449~regulation of complement activation	3	29	10.34483	0.0001139	0.004129775
S100A8; S100A9;	GO:0002793~positive regulation of peptide secretion	2	4	50	0.0001261	0.004141277
PALM; KRT6B; KRT16; KRT13; KRT4;	GO:0007010~cytoskeleton organization	5	160	3.125	0.0001314	0.004141277
S100A8; S100A9;	GO:0032119~sequestering of zinc ion	2	4	50	0.0001261	0.004141277
PTPRG; BDKRB2; FLT4; DOK1;	GO:0007169~transmembrane receptor protein tyrosine kinase signaling pathway	4	87	4.597701	0.0001537	0.004642456
MAL; MALL;	GO:0001766~membrane raft polarization	2	8	25	0.0003755	0.009939799
ECM1; IL36RN;	GO:0001960~negative regulation of cytokine-mediated signaling pathway	2	8	25	0.0003755	0.009939799
PGLYRP4; CLEC7A;	GO:0002221~pattern recognition receptor signaling pathway	2	8	25	0.0003755	0.009939799
MAL; MALL; KLK6;	GO:0042552~myelination	3	45	6.666667	0.0003839	0.009939799
MAL; GRHL3; KLK6; NDN;	GO:0007417~central nervous system development	4	117	3.418803	0.0004564	0.011030585
EREG; AR; AREG; FLT4; CHRNA7; LIFR; WNT3A;	GO:0008284~positive regulation of cell proliferation	7	454	1.54185	0.0004416	0.011030585
SLURP1; LYPD2;	GO:0001775~cell activation	2	10	20	0.0005487	0.012030187
FLT4; WNT3A; PRR5L; ITLN1;	GO:0001934~positive regulation of protein phosphorylation	4	124	3.225806	0.0005642	0.012030187
S100A8; S100A9;	GO:0002523~leukocyte migration involved in inflammatory response	2	10	20	0.0005487	0.012030187
EREG; LIFR; IL22RA1; IL36A;	GO:0019221~cytokine-mediated signaling pathway	4	124	3.225806	0.0005642	0.012030187
SPINK7; SPINK5;	GO:1900004~negative regulation of serine-type endopeptidase activity	2	11	18.18182	0.0006472	0.013406106
FLT4; NDN;	GO:0003016~respiratory system process	2	12	16.66667	0.0007536	0.014378052
EREG; KLK8;	GO:0043616~keratinocyte proliferation	2	12	16.66667	0.0007536	0.014378052
S100A8; S100A9; AR; S100A12;	GO:0051092~positive regulation of NF-kappaB transcription factor activity	4	133	3.007519	0.0007278	0.014378052

TFF3; PSG3; HCP5;	GO:0006952~defense response	3	59	5.084746	0.0008147	0.015144285
KRT6B; GRHL3;	GO:0007398~ectoderm	2	13	15.38462	0.0008679	0.015730332
C100A9, C100A0,	development	า	62	4 02071	0.0000340	0.016211867
S100A8; S100A9; S100A12;	GO:0030593~neutrophil chemotaxis	3	62	4.83871	0.0009349	0.016311867
KRT16; KRT6C;	GO:0045104~intermediate filament cytoskeleton organization	2	14	14.28571	0.00099	0.016311867
AR; AREG;	GO:0060749~mammary gland alveolus development	2	14	14.28571	0.00099	0.016311867
BMPR1B; MAL;	GO:1902043~positive regulation of extrinsic apoptotic signaling pathway via death domain receptors	2	14	14.28571	0.00099	0.016311867
ANXA9; RASAL1; S100A9; AR; PDE4A; CHRNA7; HTR3A; ECM1; DOK1; CALML5;	GO:0007165~signal transduction	10	1073	0.931966	0.0013895	0.022386029
CDH11; RUNX3; ECM1;	GO:0001503~ossification	3	75	4	0.0015837	0.023432498
CNTN2; NDN;	GO:0007413~axonal fasciculation	2	18	11.11111	0.0015555	0.023432498
S100A8; S100A9;	GO:0014002~astrocyte development	2	18	11.11111	0.0015555	0.023432498
BDKRB2; ACE2;	GO:0019229~regulation of vasoconstriction	2	18	11.11111	0.0015555	0.023432498
S100A8; S100A9;	GO:0051493~regulation of cytoskeleton organization	2	19	10.52632	0.0017159	0.024880545
S100A8; S100A9; XDH;	GO:0006919~activation of cysteine-type endopeptidase activity involved in apoptotic process	3	78	3.846154	0.0017648	0.025088321
BMPR1B; BARX2;	GO:0001502~cartilage condensation	2	21	9.52381	0.0020593	0.028170257
OLFM2; SLURP1; GPRC5B;	GO:0007626~locomotory behavior	3	82	3.658537	0.0020257	0.028170257
S100A8; S100A9;	GO:0001816~cytokine production	2	22	9.090909	0.0022423	0.030104369
EREG; WNT3A;	GO:0001819~positive regulation of cytokine production	2	23	8.695652	0.0024326	0.03149312
EREG; AR;	GO:0042327~positive regulation of phosphorylation	2	23	8.695652	0.0024326	0.03149312
PALM; EHD3;	GO:0072661~protein targeting to plasma membrane	2	24	8.333333	0.0026302	0.033454875
ANXA9; NLGN2; CRNN;	GO:0016337~single organismal cell-cell adhesion	3	95	3.157895	0.0030343	0.03744796
WNT3A; GPRC5B;	GO:0061098~positive regulation of protein tyrosine kinase activity	2	26	7.692308	0.0030475	0.03744796
C4B; C6; SUSD4;	GO:0006958~complement activation, classical pathway	3	96	3.125	0.0031225	0.037730198
GCNT3;	GO:0002426~immunoglobulin production in mucosal tissue	1	1	100	0.0058316	0.041990889
SPINK5;	GO:0002787~negative regulation of antibacterial peptide production	1	1	100	0.0058316	0.041990889

ECM1;	GO:0002828~regulation of type 2 immune response	1	1	100	0.0058316	0.041990889
HMGA2;	GO:0003131~mesodermal- endodermal cell signaling	1	1	100	0.0058316	0.041990889
WNT3A;	GO:0003136~negative regulation of heart induction by canonical Wnt signaling pathway	1	1	100	0.0058316	0.041990889
ASPG;	GO:0006530~asparagine catabolic process	1	1	100	0.0058316	0.041990889
SLC7A5; SLC7A11;	GO:0006865~amino acid transport	2	34	5.882353	0.0050021	0.041990889
CHRNA7; HTR3A;	GO:0007271~synaptic transmission, cholinergic	2	37	5.405405	0.0058498	0.041990889
KLK8; EMP1;	GO:0008219~cell death	2	36	5.555556	0.0055604	0.041990889
EREG; GJB6; AR; NDN; WNK2;	GO:0008285~negative regulation of cell proliferation	5	377	1.32626	0.0054627	0.041990889
B3GNT6;	GO:0016269~O-glycan processing, core 3	1	1	100	0.0058316	0.041990889
AR;	GO:0019102~male somatic sex determination	1	1	100	0.0058316	0.041990889
WNT3A;	GO:0021874~Wnt signaling pathway involved in forebrain neuroblast division	1	1	100	0.0058316	0.041990889
CRYAB;	GO:0031109~microtubule polymerization or depolymerization	1	1	100	0.0058316	0.041990889
CHRNA7; SLC7A11;	GO:0035094~response to nicotine	2	34	5.882353	0.0050021	0.041990889
ABCA12;	GO:0035627~ceramide transport	1	1	100	0.0058316	0.041990889
HMGA2;	GO:0035978~histone H2A-S139 phosphorylation	1	1	100	0.0058316	0.041990889
EREG;	GO:0042108~positive regulation of cytokine biosynthetic process	1	1	100	0.0058316	0.041990889
SPINK5;	GO:0042640~anagen	1	1	100	0.0058316	0.041990889
KIAA1324;	GO:0044090~positive regulation of vacuole organization	1	1	100	0.0058316	0.041990889
S100A9;	GO:0045113~regulation of integrin biosynthetic process	1	1	100	0.0058316	0.041990889
RUNX3; KLK6;	GO:0045595~regulation of cell differentiation	2	31	6.451613	0.0042163	0.041990889
BMPR1B; AR;	GO:0045597~positive regulation of cell differentiation	2	35	5.714286	0.0052778	0.041990889
C6; CHRNA7; ECM1;	GO:0045766~positive regulation of angiogenesis	3	109	2.752294	0.0044138	0.041990889
SPNS2;	GO:0048073~regulation of eye pigmentation	1	1	100	0.0058316	0.041990889
EREG;	GO:0048160~primary follicle stage	1	1	100	0.0058316	0.041990889
FLT4; ABCA12;	GO:0048286~lung alveolus development	2	31	6.451613	0.0042163	0.041990889
WNT3A;	GO:0048337~positive regulation of mesodermal cell fate specification	1	1	100	0.0058316	0.041990889
KLK8; NLGN2;	GO:0050808~synapse organization	2	32	6.25	0.0044713	0.041990889

SCPEP1; CTSF;	GO:0051603~proteolysis involved in cellular protein catabolic process	2	31	6.451613	0.0042163	0.041990889
AR;	GO:0060520~activation of prostate induction by androgen receptor signaling pathway	1	1	100	0.0058316	0.041990889
AREG;	GO:0060598~dichotomous subdivision of terminal units involved in mammary gland duct morphogenesis	1	1	100	0.0058316	0.041990889
CNTN2;	GO:0071206~establishment of protein localization to juxtaparanode region of axon	1	1	100	0.0058316	0.041990889
WNT3A;	GO:0090676~calcium ion transmembrane transport via low voltage-gated calcium channel	1	1	100	0.0058316	0.041990889
CNTN2;	GO:0097090~presynaptic membrane organization	1	1	100	0.0058316	0.041990889
BDKRB2;	GO:1902239~negative regulation of intrinsic apoptotic signaling pathway in response to osmotic stress by p53 class mediator	1	1	100	0.0058316	0.041990889
WNT3A;	GO:2000081~positive regulation of canonical Wnt signaling pathway involved in controlling type B pancreatic cell proliferation	1	1	100	0.0058316	0.041990889
XDH; ACE2;	GO:2000379~positive regulation of reactive oxygen species metabolic process	2	29	6.896552	0.0037274	0.041990889
HMGA2;	GO:2000685~positive regulation of cellular response to X-ray	1	1	100	0.0058316	0.041990889
XDH;	GO:2001213~negative regulation of vasculogenesis	1	1	100	0.0058316	0.041990889
S100A8; S100A9;	GO:2001244~positive regulation of intrinsic apoptotic signaling pathway	2	30	6.666667	0.0039683	0.041990889
HMGA2; RUNX3;	GO:0002062~chondrocyte differentiation	2	39	5.128205	0.0064488	0.045391794
CHRNA7; TMPRSS11E;	GO:0050890~cognition	2	39	5.128205	0.0064488	0.045391794
EREG; AREG;	GO:0043434~response to peptide hormone	2	40	5	0.0067583	0.046664445
EREG; AREG;	GO:0045740~positive regulation of DNA replication	2	40	5	0.0067583	0.046664445
C6;	GO:0001970~positive regulation of activation of membrane attack complex	1	2	50	0.0087347	0.047258423
SPNS2;	GO:0002920~regulation of humoral immune response	1	2	50	0.0087347	0.047258423
HMGA2; PADI1;	GO:0006325~chromatin organization	2	41	4.878049	0.0070745	0.047258423
TSPAN8; BDKRB2; LIFR; DOK1;	GO:0007166~cell surface receptor signaling pathway	4	269	1.486989	0.008648	0.047258423
PI3;	GO:0007620~copulation	1	2	50	0.0087347	0.047258423

XDH;	GO:0009115~xanthine catabolic process	1	2	50	0.0087347	0.047258423
CLEC7A;	GO:0009756~carbohydrate mediated signaling	1	2	50	0.0087347	0.047258423
PTPRG; WNT3A;	GO:0010977~negative regulation of neuron projection development	2	41	4.878049	0.0070745	0.047258423
C4B;	GO:0032490~detection of molecule of bacterial origin	1	2	50	0.0087347	0.047258423
S100A9;	GO:0035606~peptidyl-cysteine S-trans-nitrosylation	1	2	50	0.0087347	0.047258423
CRYAB; AREG;	GO:0042542~response to hydrogen peroxide	2	45	4.44444	0.0084047	0.047258423
AR;	GO:0045720~negative regulation of integrin biosynthetic process	1	2	50	0.0087347	0.047258423
BMPR1B; ABLIM3; AR; HMGA2; WNT3A; GRHL3; NDN; BARX2;	GO:0045944~positive regulation of transcription from RNA polymerase II promoter	8	962	0.831601	0.0079646	0.047258423
WNT3A;	GO:0048343~paraxial mesodermal cell fate commitment	1	2	50	0.0087347	0.047258423
AR;	GO:0048638~regulation of developmental growth	1	2	50	0.0087347	0.047258423
WNT3A;	GO:0048697~positive regulation of collateral sprouting in absence of injury	1	2	50	0.0087347	0.047258423
CNTN2;	GO:0048710~regulation of astrocyte differentiation	1	2	50	0.0087347	0.047258423
CNTN2;	GO:0060168~positive regulation of adenosine receptor signaling pathway	1	2	50	0.0087347	0.047258423
AR;	GO:0060599~lateral sprouting involved in mammary gland duct morphogenesis	1	2	50	0.0087347	0.047258423
AR;	GO:0060748~tertiary branching involved in mammary gland duct morphogenesis	1	2	50	0.0087347	0.047258423
WNT3A;	GO:0061317~canonical Wnt signaling pathway involved in cardiac muscle cell fate commitment	1	2	50	0.0087347	0.047258423
WNT3A; SLC7A11;	GO:0070527~platelet aggregation	2	42	4.761905	0.0073972	0.047258423
SERPINB7;	GO:0090362~positive regulation of platelet-derived growth factor production	1	2	50	0.0087347	0.047258423
HMGA2;	GO:0090402~oncogene-induced cell senescence	1	2	50	0.0087347	0.047258423
DMKN;	GO:1903575~cornified envelope assembly	1	2	50	0.0087347	0.047258423
MGLL;	GO:2000124~regulation of endocannabinoid signaling pathway	1	2	50	0.0087347	0.047258423
ECM1;	GO:2000404~regulation of T cell migration	1	2	50	0.0087347	0.047258423

HMGA2;	GO:2001033~negative regulation of double-strand break repair via nonhomologous end joining	1	2	50	0.0087347	0.047258423
HMGA2;	GO:2001038~regulation of cellular response to drug	1	2	50	0.0087347	0.047258423
FMO6P; XDH; CYP2A13; SCD5; SDR9C7; RDH12;	GO:0055114~oxidation- reduction process	6	599	1.001669	0.0089981	0.048322925
ACE2;	GO:0002005~angiotensin catabolic process in blood	1	3	33.33333	0.0116293	0.049611962
CLEC7A;	GO:0002366~leukocyte activation involved in immune response	1	3	33.33333	0.0116293	0.049611962
KLK7;	GO:0002803~positive regulation of antibacterial peptide production	1	3	33.33333	0.0116293	0.049611962
ACE2;	GO:0003051~angiotensin- mediated drinking behavior	1	3	33.33333	0.0116293	0.049611962
ITLN1;	GO:0009624~response to nematode	1	3	33.33333	0.0116293	0.049611962
ACE2;	GO:0015827~tryptophan transport	1	3	33.33333	0.0116293	0.049611962
AR; EMP1;	GO:0016049~cell growth	2	54	3.703704	0.01177	0.049611962
NLGN2; NDN;	GO:0019233~sensory perception of pain	2	52	3.846154	0.0109786	0.049611962
WNT3A; RUNX3;	GO:0030097~hemopoiesis	2	54	3.703704	0.01177	0.049611962
CRYAB;	GO:0032387~negative regulation of intracellular transport	1	3	33.33333	0.0116293	0.049611962
ACE2;	GO:0032800~receptor biosynthetic process	1	3	33.33333	0.0116293	0.049611962
HMGA2;	GO:0035986~senescence- associated heterochromatin focus assembly	1	3	33.33333	0.0116293	0.049611962
HMGA2; NDN;	GO:0040008~regulation of growth	2	51	3.921569	0.0105921	0.049611962
EREG;	GO:0042700~luteinizing hormone signaling pathway	1	3	33.33333	0.0116293	0.049611962
CRYAB; SERPINB2; CEACAM5; FLT4; HMGA2;	GO:0043066~negative regulation of apoptotic process	5	445	1.123596	0.0106378	0.049611962
S100A12; ECM1; GPRC5B;	GO:0043123~positive regulation of I-kappaB kinase/NF-kappaB signaling	3	157	1.910828	0.0117217	0.049611962
TGM1;	GO:0043163~cell envelope organization	1	3	33.33333	0.0116293	0.049611962
CNTN2;	GO:0045163~clustering of voltage-gated potassium channels	1	3	33.33333	0.0116293	0.049611962
AR;	GO:0045726~positive regulation of integrin biosynthetic process	1	3	33.33333	0.0116293	0.049611962
GCNT3;	GO:0048729~tissue morphogenesis	1	3	33.33333	0.0116293	0.049611962
NDN;	GO:0048871~multicellular organismal homeostasis	1	3	33.33333	0.0116293	0.049611962

PALM;	GO:0060160~negative regulation of dopamine receptor signaling pathway	1	3	33.33333	0.0116293	0.049611962
FLT4;	GO:0060312~regulation of blood vessel remodeling	1	3	33.33333	0.0116293	0.049611962
BMPR1B;	GO:0060350~endochondral bone morphogenesis	1	3	33.33333	0.0116293	0.049611962
AR;	GO:0060769~positive regulation of epithelial cell proliferation involved in prostate gland development	1	3	33.33333	0.0116293	0.049611962
WNT3A;	GO:0061184~positive regulation of dermatome development	1	3	33.33333	0.0116293	0.049611962
RHCG;	GO:0070634~transepithelial ammonium transport	1	3	33.33333	0.0116293	0.049611962
CLEC7A;	GO:0071226~cellular response to molecule of fungal origin	1	3	33.33333	0.0116293	0.049611962
AR;	GO:0090003~regulation of establishment of protein localization to plasma membrane	1	3	33.33333	0.0116293	0.049611962
WNT3A;	GO:0090245~axis elongation involved in somitogenesis	1	3	33.33333	0.0116293	0.049611962
NLGN2;	GO:0097116~gephyrin clustering involved in postsynaptic density assembly	1	3	33.33333	0.0116293	0.049611962
BMPR1B;	GO:1902731~negative regulation of chondrocyte proliferation	1	3	33.33333	0.0116293	0.049611962
PTPRG;	GO:1903385~regulation of homophilic cell adhesion	1	3	33.33333	0.0116293	0.049611962
ACE2;	GO:1903598~positive regulation of gap junction assembly	1	3	33.33333	0.0116293	0.049611962
WNT3A;	GO:1904339~negative regulation of dopaminergic neuron differentiation	1	3	33.33333	0.0116293	0.049611962
WNT3A;	GO:1904798~positive regulation of core promoter binding	1	3	33.33333	0.0116293	0.049611962
NLGN2;	GO:1904862~inhibitory synapse assembly	1	3	33.33333	0.0116293	0.049611962

Supplemental Table 3.2 GO enrichment analysis

 ${f GO}$ terms with a padj value ${<}0.05$

3.6 Acknowledgements

We thank Michael Kulik and Ted Ross from the University of Georgia for assistance in the BSL-3 facility. This project was supported by R01-AA025854 (MK, CAE), F31-AA029000 (KFE) and the Indo-U.S. Science & Technology Forum (IUSSTF) Virtual Networks for COVID-19 (Ref: IUSSTF/VN-COVID/107/2020), India (MK, JDS).

3.7 Author Contributions

CAE, MK, KFE, RCE, CAJ, SKJ, EKL, MJL and AGBB designed and executed experiments. BSS and AJM provided airway cell brushings. KFE, RCR and RCE cultured cells, performed imaging and cytokine analysis. CAE, RCE, CAJ, SKJ, AGBB and SMT performed all BSL-3 experiments. IKC assisted with RNA-seq analysis. RCE, MK, CAE, and KFE analyzed the data, compiled the figures, and wrote the first draft of manuscript. MK, JDS, JML and CAE provided feedback and interpreted results. All of the co-authors edited and approved the manuscript.

References

- Bailey KL, Romberger DJ, Katafiasz DM, Heires AJ, Sisson JH, Wyatt TA, and Burnham EL. TLR2 and TLR4 Expression and Inflammatory Cytokines are Altered in the Airway Epithelium of Those with Alcohol Use Disorders. *Alcohol Clin Exp Res* 39: 1691-1697, 2015.
- 2. Bailey KL, Samuelson DR, and Wyatt TA. Alcohol use disorder: A pre-existing condition for COVID-19? *Alcohol* 90: 11-17, 2021.
- 3. Bailey KL, Sayles H, Campbell J, Khalid N, Anglim M, Ponce J, Wyatt TA, McClay JC, Burnham EL, Anzalone A, and Hanson C. COVID-19 patients with documented alcohol use disorder or alcohol-related complications are more likely to be hospitalized and have higher all-cause mortality. *Alcohol Clin Exp Res* 46: 1023-1035, 2022.
- 4. Berkel TD, and Pandey SC. Emerging Role of Epigenetic Mechanisms in Alcohol Addiction. *Alcohol Clin Exp Res* 41: 666-680, 2017.
- 5. Berkowitz DM, Danai PA, Eaton S, Moss M, and Martin GS. Alcohol abuse enhances pulmonary edema in acute respiratory distress syndrome. *Alcohol Clin Exp Res* 33: 1690-1696, 2009.
- 6. Bhattacharya P, Budnick I, Singh M, Thiruppathi M, Alharshawi K, Elshabrawy H, Holterman MJ, and Prabhakar BS. Dual Role of GM-CSF as a Pro-Inflammatory and a Regulatory Cytokine: Implications for Immune Therapy. *J Interferon Cytokine Res* 35: 585-599, 2015.
- 7. Bigdelou B, Sepand MR, Najafikhoshnoo S, Negrete JAT, Sharaf M, Ho JQ, Sullivan I, Chauhan P, Etter M, Shekarian T, Liang O, Hutter G, Esfandiarpour R, and Zanganeh S.

- COVID-19 and Preexisting Comorbidities: Risks, Synergies, and Clinical Outcomes. *Front Immunol* 13: 890517, 2022.
- 8. Blanco-Melo D, Nilsson-Payant BE, Liu WC, Uhl S, Hoagland D, Moller R, Jordan TX, Oishi K, Panis M, Sachs D, Wang TT, Schwartz RE, Lim JK, Albrecht RA, and tenOever BR. Imbalanced Host Response to SARS-CoV-2 Drives Development of COVID-19. *Cell* 181: 1036-1045 e1039, 2020.
- 9. Blazquez-Prieto J, Lopez-Alonso I, Amado-Rodriguez L, Batalla-Solis E, Gonzalez-Lopez A, and Albaiceta GM. Exposure to mechanical ventilation promotes tolerance to ventilator-induced lung injury by Ccl3 downregulation. *Am J Physiol Lung Cell Mol Physiol* 309: L847-856, 2015.
- 10. Bornstein SR, Rubino F, Khunti K, Mingrone G, Hopkins D, Birkenfeld AL, Boehm B, Amiel S, Holt RI, Skyler JS, DeVries JH, Renard E, Eckel RH, Zimmet P, Alberti KG, Vidal J, Geloneze B, Chan JC, Ji L, and Ludwig B. Practical recommendations for the management of diabetes in patients with COVID-19. *Lancet Diabetes Endocrinol* 8: 546-550, 2020.
- 11. Burnham EL, Halkar R, Burks M, and Moss M. The effects of alcohol abuse on pulmonary alveolar-capillary barrier function in humans. *Alcohol Alcohol* 44: 8-12, 2009.
- 12. Caillet-Saguy C, Durbesson F, Rezelj VV, Gogl G, Tran QD, Twizere JC, Vignuzzi M, Vincentelli R, and Wolff N. Host PDZ-containing proteins targeted by SARS-CoV-2. *FEBS J* 288: 5148-5162, 2021.

- 13. Calina D, Hartung T, Mardare I, Mitroi M, Poulas K, Tsatsakis A, Rogoveanu I, and Docea AO. COVID-19 pandemic and alcohol consumption: Impacts and interconnections.

 *Toxicol Rep 8: 529-535, 2021.
- 14. Camargo Moreno M, Lewis JB, Kovacs EJ, and Lowery EM. Lung allograft donors with excessive alcohol use have increased levels of human antimicrobial peptide LL-37. *Alcohol* 80: 109-117, 2019.
- 15. Chen G, Wu D, Guo W, Cao Y, Huang D, Wang H, Wang T, Zhang X, Chen H, Yu H, Zhang X, Zhang M, Wu S, Song J, Chen T, Han M, Li S, Luo X, Zhao J, and Ning Q. Clinical and immunological features of severe and moderate coronavirus disease 2019. *J Clin Invest* 130: 2620-2629, 2020.
- 16. Chen SP, Zhou B, Willis BC, Sandoval AJ, Liebler JM, Kim KJ, Ann DK, Crandall ED, and Borok Z. Effects of transdifferentiation and EGF on claudin isoform expression in alveolar epithelial cells. *J Appl Physiol* (1985) 98: 322-328, 2005.
- 17. Coyne CB, Vanhook MK, Gambling TM, Carson JL, Boucher RC, and Johnson LG. Regulation of airway tight junctions by proinflammatory cytokines. *Mol Biol Cell* 13: 3218-3234, 2002.
- 18. De Maio F, Lo Cascio E, Babini G, Sali M, Della Longa S, Tilocca B, Roncada P, Arcovito A, Sanguinetti M, Scambia G, and Urbani A. Improved binding of SARS-CoV-2 Envelope protein to tight junction-associated PALS1 could play a key role in COVID-19 pathogenesis. *Microbes Infect* 22: 592-597, 2020.

- 19. de Roux A, Cavalcanti M, Marcos MA, Garcia E, Ewig S, Mensa J, and Torres A. Impact of alcohol abuse in the etiology and severity of community-acquired pneumonia. *Chest* 129: 1219-1225, 2006.
- 20. Dranoff G, Crawford AD, Sadelain M, Ream B, Rashid A, Bronson RT, Dickersin GR, Bachurski CJ, Mark EL, Whitsett JA, and et al. Involvement of granulocyte-macrophage colony-stimulating factor in pulmonary homeostasis. *Science* 264: 713-716, 1994.
- 21. Fernandez AL, Koval M, Fan X, and Guidot DM. Chronic alcohol ingestion alters claudin expression in the alveolar epithelium of rats. *Alcohol* 41: 371-379, 2007.
- 22. Greenbaum A, Chaves SS, Perez A, Aragon D, Bandyopadhyay A, Bennett N, Fowler B, Hancock E, Lynfield R, McDonald-Hamm C, Reingold A, Ryan P, Schaffner W, Sharangpani R, Spencer M, Thomas A, Yousey-Hindes K, Zansky S, and Finelli L. Heavy alcohol use as a risk factor for severe outcomes among adults hospitalized with laboratory-confirmed influenza, 2005-2012. *Infection* 42: 165-170, 2014.
- 23. Hao S, Ning K, Kuz CA, Vorhies K, Yan Z, and Qiu J. Long-Term Modeling of SARS-CoV-2 Infection of In Vitro Cultured Polarized Human Airway Epithelium. *mBio* 11: 2020.
- 24. Hashimoto R, Takahashi J, Shirakura K, Funatsu R, Kosugi K, Deguchi S, Yamamoto M, Tsunoda Y, Morita M, Muraoka K, Tanaka M, Kanbara T, Tanaka S, Tamiya S, Tokunoh N, Kawai A, Ikawa M, Ono C, Tachibana K, Kondoh M, Obana M, Matsuura Y, Ohsumi A, Noda T, Yamamoto T, Yoshioka Y, Torisawa YS, Date H, Fujio Y, Nagao M, Takayama K, and Okada Y. SARS-CoV-2 disrupts respiratory vascular barriers by suppressing Claudin-5 expression. *Sci Adv* 8: eabo6783, 2022.

- 25. Hou YJ, Okuda K, Edwards CE, Martinez DR, Asakura T, Dinnon KH, 3rd, Kato T, Lee RE, Yount BL, Mascenik TM, Chen G, Olivier KN, Ghio A, Tse LV, Leist SR, Gralinski LE, Schafer A, Dang H, Gilmore R, Nakano S, Sun L, Fulcher ML, Livraghi-Butrico A, Nicely NI, Cameron M, Cameron C, Kelvin DJ, de Silva A, Margolis DM, Markmann A, Bartelt L, Zumwalt R, Martinez FJ, Salvatore SP, Borczuk A, Tata PR, Sontake V, Kimple A, Jaspers I, O'Neal WK, Randell SH, Boucher RC, and Baric RS. SARS-CoV-2 Reverse Genetics Reveals a Variable Infection Gradient in the Respiratory Tract. *Cell* 182: 429-446 e414, 2020.
- 26. Huang C, Wang Y, Li X, Ren L, Zhao J, Hu Y, Zhang L, Fan G, Xu J, Gu X, Cheng Z, Yu T, Xia J, Wei Y, Wu W, Xie X, Yin W, Li H, Liu M, Xiao Y, Gao H, Guo L, Xie J, Wang G, Jiang R, Gao Z, Jin Q, Wang J, and Cao B. Clinical features of patients infected with 2019 novel coronavirus in Wuhan, China. *Lancet* 395: 497-506, 2020.
- 27. Joshi PC, Applewhite L, Mitchell PO, Fernainy K, Roman J, Eaton DC, and Guidot DM.
 GM-CSF receptor expression and signaling is decreased in lungs of ethanol-fed rats. Am J
 Physiol Lung Cell Mol Physiol 291: L1150-1158, 2006.
- 28. Kalinina O, Golovkin A, Zaikova E, Aquino A, Bezrukikh V, Melnik O, Vasilieva E, Karonova T, Kudryavtsev I, and Shlyakhto E. Cytokine Storm Signature in Patients with Moderate and Severe COVID-19. *Int J Mol Sci* 23: 2022.
- 29. Katsura H, Sontake V, Tata A, Kobayashi Y, Edwards CE, Heaton BE, Konkimalla A, Asakura T, Mikami Y, Fritch EJ, Lee PJ, Heaton NS, Boucher RC, Randell SH, Baric RS, and Tata PR. Human Lung Stem Cell-Based Alveolospheres Provide Insights into SARS-CoV-2-Mediated Interferon Responses and Pneumocyte Dysfunction. *Cell Stem Cell* 27: 890-904 e898, 2020.

- 30. Kelly A, and McCarthy C. Pulmonary Alveolar Proteinosis Syndrome. *Semin Respir Crit Care Med* 41: 288-298, 2020.
- 31. Klingensmith NJ, Yoseph BP, Liang Z, Lyons JD, Burd EM, Margoles LM, Koval M, Ford ML, and Coopersmith CM. Epidermal Growth Factor Improves Intestinal Integrity and Survival in Murine Sepsis Following Chronic Alcohol Ingestion. *Shock* 47: 184-192, 2017.
- 32. Koval M. Junctional Interplay in Lung Epithelial Barrier Function. In: *Lung Epithelial Biology in the Pathogenesis of Pulmonary Disease*, edited by Sidhaye VK, and Koval M. Oxford: Academic Press, 2017, p. 1-20.
- 33. Lamers MM, and Haagmans BL. SARS-CoV-2 pathogenesis. *Nat Rev Microbiol* 20: 270-284, 2022.
- 34. Lamers MM, van der Vaart J, Knoops K, Riesebosch S, Breugem TI, Mykytyn AZ, Beumer J, Schipper D, Bezstarosti K, Koopman CD, Groen N, Ravelli RBG, Duimel HQ, Demmers JAA, Verjans G, Koopmans MPG, Muraro MJ, Peters PJ, Clevers H, and Haagmans BL. An organoid-derived bronchioalveolar model for SARS-CoV-2 infection of human alveolar type II-like cells. *EMBO J* 40: e105912, 2021.
- 35. Lang FM, Lee KM, Teijaro JR, Becher B, and Hamilton JA. GM-CSF-based treatments in COVID-19: reconciling opposing therapeutic approaches. *Nat Rev Immunol* 20: 507-514, 2020.
- 36. Lim ZJ, Subramaniam A, Ponnapa Reddy M, Blecher G, Kadam U, Afroz A, Billah B, Ashwin S, Kubicki M, Bilotta F, Curtis JR, and Rubulotta F. Case Fatality Rates for Patients with COVID-19 Requiring Invasive Mechanical Ventilation. A Meta-analysis. *Am J Respir Crit Care Med* 203: 54-66, 2021.

- 37. Linfield DT, Raduka A, Aghapour M, and Rezaee F. Airway tight junctions as targets of viral infections. *Tissue Barriers* 9: 1883965, 2021.
- 38. Lu Z, Kim DH, Fan J, Lu Q, Verbanac K, Ding L, Renegar R, and Chen YH. A non-tight junction function of claudin-7-Interaction with integrin signaling in suppressing lung cancer cell proliferation and detachment. *Mol Cancer* 14: 120, 2015.
- 39. Lynn KS, Easley KF, Martinez FJ, Reed RC, Schlingmann B, and Koval M. Asymmetric distribution of dynamin-2 and beta-catenin relative to tight junction spikes in alveolar epithelial cells. *Tissue Barriers* 9: 1929786, 2021.
- 40. Matute-Bello G, Liles WC, Radella F, 2nd, Steinberg KP, Ruzinski JT, Hudson LD, and Martin TR. Modulation of neutrophil apoptosis by granulocyte colony-stimulating factor and granulocyte/macrophage colony-stimulating factor during the course of acute respiratory distress syndrome. *Crit Care Med* 28: 1-7, 2000.
- 41. McCormick TS, Hejal RB, Leal LO, and Ghannoum MA. GM-CSF: Orchestrating the Pulmonary Response to Infection. *Front Pharmacol* 12: 735443, 2021.
- 42. Mehta AJ, and Guidot DM. Alcohol and the Lung. *Alcohol Res* 38: 243-254, 2017.
- 43. Mehta AJ, Yeligar SM, Elon L, Brown LA, and Guidot DM. Alcoholism causes alveolar macrophage zinc deficiency and immune dysfunction. *Am J Respir Crit Care Med* 188: 716-723, 2013.
- 44. Mitchell PO, Jensen JS, Ritzenthaler JD, Roman J, Pelaez A, and Guidot DM. Alcohol primes the airway for increased interleukin-13 signaling. *Alcohol Clin Exp Res* 33: 505-513, 2009.

- 45. Molina SA, Stauffer B, Moriarty HK, Kim AH, McCarty NA, and Koval M. Junctional abnormalities in human airway epithelial cells expressing F508del CFTR. *Am J Physiol Lung Cell Mol Physiol* 309: L475-487, 2015.
- 46. Morgan R, Manfredi C, Easley KF, Watkins LD, Hunt WR, Goudy SL, Sorscher EJ, Koval M, and Molina SA. A medium composition containing normal resting glucose that supports differentiation of primary human airway cells. *Sci Rep* 12: 1540, 2022.
- 47. Moss M, Bucher B, Moore FA, Moore EE, and Parsons PE. The role of chronic alcohol abuse in the development of acute respiratory distress syndrome in adults. *JAMA* 275: 50-54, 1996.
- 48. Mulay A, Konda B, Garcia G, Jr., Yao C, Beil S, Villalba JM, Koziol C, Sen C, Purkayastha A, Kolls JK, Pociask DA, Pessina P, de Aja JS, Garcia-de-Alba C, Kim CF, Gomperts B, Arumugaswami V, and Stripp BR. SARS-CoV-2 infection of primary human lung epithelium for COVID-19 modeling and drug discovery. *Cell Rep* 35: 109055, 2021.
- 49. Neveu WA, Mills ST, Staitieh BS, and Sueblinvong V. TGF-beta1 epigenetically modifies Thy-1 expression in primary lung fibroblasts. *Am J Physiol Cell Physiol* 309: C616-626, 2015.
- 50. Neveu WA, Staitieh BS, Mills ST, Guidot DM, and Sueblinvong V. Alcohol-Induced Interleukin-17 Expression Causes Murine Lung Fibroblast-to-Myofibroblast Transdifferentiation via Thy-1 Down-Regulation. *Alcohol Clin Exp Res* 43: 1427-1438, 2019.
- 51. Overgaard CE, Schlingmann B, Dorsainvil White S, Ward C, Fan X, Swarnakar S, Brown LA, Guidot DM, and Koval M. The relative balance of GM-CSF and TGF-beta1 regulates

- lung epithelial barrier function. Am J Physiol Lung Cell Mol Physiol 308: L1212-1223, 2015.
- 52. Paine R, 3rd, Standiford TJ, Dechert RE, Moss M, Martin GS, Rosenberg AL, Thannickal VJ, Burnham EL, Brown MB, and Hyzy RC. A randomized trial of recombinant human granulocyte-macrophage colony stimulating factor for patients with acute lung injury. *Crit Care Med* 40: 90-97, 2012.
- 53. Presneill JJ, Harris T, Stewart AG, Cade JF, and Wilson JW. A randomized phase II trial of granulocyte-macrophage colony-stimulating factor therapy in severe sepsis with respiratory dysfunction. *Am J Respir Crit Care Med* 166: 138-143, 2002.
- 54. Rauti R, Shahoha M, Leichtmann-Bardoogo Y, Nasser R, Paz E, Tamir R, Miller V, Babich T, Shaked K, Ehrlich A, Ioannidis K, Nahmias Y, Sharan R, Ashery U, and Maoz BM. Effect of SARS-CoV-2 proteins on vascular permeability. *Elife* 10: 2021.
- 55. Ravindra NG, Alfajaro MM, Gasque V, Huston NC, Wan H, Szigeti-Buck K, Yasumoto Y, Greaney AM, Habet V, Chow RD, Chen JS, Wei J, Filler RB, Wang B, Wang G, Niklason LE, Montgomery RR, Eisenbarth SC, Chen S, Williams A, Iwasaki A, Horvath TL, Foxman EF, Pierce RW, Pyle AM, van Dijk D, and Wilen CB. Single-cell longitudinal analysis of SARS-CoV-2 infection in human airway epithelium identifies target cells, alterations in gene expression, and cell state changes. *PLoS Biol* 19: e3001143, 2021.
- 56. Remap-Cap Investigators, Gordon AC, Mouncey PR, Al-Beidh F, Rowan KM, Nichol AD, Arabi YM, Annane D, Beane A, van Bentum-Puijk W, Berry LR, Bhimani Z, Bonten MJM, Bradbury CA, Brunkhorst FM, Buzgau A, Cheng AC, Detry MA, Duffy EJ, Estcourt LJ, Fitzgerald M, Goossens H, Haniffa R, Higgins AM, Hills TE, Horvat CM, Lamontagne F,

Lawler PR, Leavis HL, Linstrum KM, Litton E, Lorenzi E, Marshall JC, Mayr FB, McAuley DF, McGlothlin A, McGuinness SP, McVerry BJ, Montgomery SK, Morpeth SC, Murthy S, Orr K, Parke RL, Parker JC, Patanwala AE, Pettila V, Rademaker E, Santos MS, Saunders CT, Seymour CW, Shankar-Hari M, Sligl WI, Turgeon AF, Turner AM, van de Veerdonk FL, Zarychanski R, Green C, Lewis RJ, Angus DC, McArthur CJ, Berry S, Webb SA, and Derde LPG. Interleukin-6 Receptor Antagonists in Critically Ill Patients with Covid-19. *N Engl J Med* 384: 1491-1502, 2021.

- 57. Robinot R, Hubert M, de Melo GD, Lazarini F, Bruel T, Smith N, Levallois S, Larrous F, Fernandes J, Gellenoncourt S, Rigaud S, Gorgette O, Thouvenot C, Trebeau C, Mallet A, Dumenil G, Gobaa S, Etournay R, Lledo PM, Lecuit M, Bourhy H, Duffy D, Michel V, Schwartz O, and Chakrabarti LA. SARS-CoV-2 infection induces the dedifferentiation of multiciliated cells and impairs mucociliary clearance. *Nat Commun* 12: 4354, 2021.
- 58. Saitz R, Ghali WA, and Moskowitz MA. The impact of alcohol-related diagnoses on pneumonia outcomes. *Arch Intern Med* 157: 1446-1452, 1997.
- 59. Samuelson DR, Burnham EL, Maffei VJ, Vandivier RW, Blanchard EE, Shellito JE, Luo M, Taylor CM, and Welsh DA. The respiratory tract microbial biogeography in alcohol use disorder. *Am J Physiol Lung Cell Mol Physiol* 314: L107-L117, 2018.
- 60. Saunders JB, Aasland OG, Babor TF, de la Fuente JR, and Grant M. Development of the Alcohol Use Disorders Identification Test (AUDIT): WHO Collaborative Project on Early Detection of Persons with Harmful Alcohol Consumption--II. *Addiction* 88: 791-804, 1993.

- 61. Schlingmann B, Overgaard CE, Molina SA, Lynn KS, Mitchell LA, Dorsainvil White S, Mattheyses AL, Guidot DM, Capaldo CT, and Koval M. Regulation of claudin/zonula occludens-1 complexes by hetero-claudin interactions. *Nat Commun* 7: 12276, 2016.
- 62. Selickman J, Vrettou CS, Mentzelopoulos SD, and Marini JJ. COVID-19-Related ARDS: Key Mechanistic Features and Treatments. *J Clin Med* 11: 2022.
- 63. Selzer ML, Vinokur A, and van Rooijen L. A self-administered Short Michigan Alcoholism Screening Test (SMAST). *J Stud Alcohol* 36: 117-126, 1975.
- 64. Shepley-McTaggart A, Sagum CA, Oliva I, Rybakovsky E, DiGuilio K, Liang J, Bedford MT, Cassel J, Sudol M, Mullin JM, and Harty RN. SARS-CoV-2 Envelope (E) protein interacts with PDZ-domain-2 of host tight junction protein ZO1. *PLoS One* 16: e0251955, 2021.
- 65. Simet SM, Wyatt TA, DeVasure J, Yanov D, Allen-Gipson D, and Sisson JH. Alcohol increases the permeability of airway epithelial tight junctions in Beas-2B and NHBE cells.

 *Alcohol Clin Exp Res 36: 432-442, 2012.
- 66. Smith P, Jeffers LA, and Koval M. Effects of different routes of endotoxin injury on barrier function in alcoholic lung syndrome. *Alcohol* 80: 81-89, 2019.
- 67. Staitieh BS, Egea EE, Fan X, Amah A, and Guidot DM. Chronic Alcohol Ingestion Impairs
 Rat Alveolar Macrophage Phagocytosis via Disruption of RAGE Signaling. *Am J Med Sci*355: 497-505, 2018.
- 68. Sugarman DE, and Greenfield SF. Alcohol and COVID-19: How Do We Respond to This Growing Public Health Crisis? *J Gen Intern Med* 36: 214-215, 2021.

- 69. Teoh KT, Siu YL, Chan WL, Schluter MA, Liu CJ, Peiris JS, Bruzzone R, Margolis B, and Nal B. The SARS coronavirus E protein interacts with PALS1 and alters tight junction formation and epithelial morphogenesis. *Mol Biol Cell* 21: 3838-3852, 2010.
- 70. Terakado M, Gon Y, Sekiyama A, Takeshita I, Kozu Y, Matsumoto K, Takahashi N, and Hashimoto S. The Rac1/JNK pathway is critical for EGFR-dependent barrier formation in human airway epithelial cells. *Am J Physiol Lung Cell Mol Physiol* 300: L56-63, 2011.
- 71. Thacker VV, Sharma K, Dhar N, Mancini GF, Sordet-Dessimoz J, and McKinney JD. Rapid endotheliitis and vascular damage characterize SARS-CoV-2 infection in a human lung-on-chip model. *EMBO Rep* 22: e52744, 2021.
- 72. Toto A, Ma S, Malagrino F, Visconti L, Pagano L, Stromgaard K, and Gianni S. Comparing the binding properties of peptides mimicking the Envelope protein of SARS-CoV and SARS-CoV-2 to the PDZ domain of the tight junction-associated PALS1 protein. *Protein Sci* 29: 2038-2042, 2020.
- van Zuylen WJ, Rawlinson WD, and Ford CE. The Wnt pathway: a key network in cell signalling dysregulated by viruses. *Rev Med Virol* 26: 340-355, 2016.
- 74. Vanderheiden A, Ralfs P, Chirkova T, Upadhyay AA, Zimmerman MG, Bedoya S, Aoued H, Tharp GM, Pellegrini KL, Manfredi C, Sorscher E, Mainou B, Lobby JL, Kohlmeier JE, Lowen AC, Shi PY, Menachery VD, Anderson LJ, Grakoui A, Bosinger SE, and Suthar MS. Type I and Type III Interferons Restrict SARS-CoV-2 Infection of Human Airway Epithelial Cultures. *J Virol* 94: 2020.
- 75. Voelkel NF, Bogaard HJ, and Kuebler WM. ARDS in the time of corona: context and perspective. *Am J Physiol Lung Cell Mol Physiol* 323: L431-L437, 2022.

- 76. Wang R, Hume AJ, Beermann ML, Simone-Roach C, Lindstrom-Vautrin J, Le Suer J, Huang J, Olejnik J, Villacorta-Martin C, Bullitt E, Hinds A, Ghaedi M, Rollins S, Werder RB, Abo KM, Wilson AA, Muhlberger E, Kotton DN, and Hawkins FJ. Human airway lineages derived from pluripotent stem cells reveal the epithelial responses to SARS-CoV-2 infection. *Am J Physiol Lung Cell Mol Physiol* 322: L462-L478, 2022.
- 77. Wittekindt OH. Tight junctions in pulmonary epithelia during lung inflammation. *Pflugers Arch* 469: 135-147, 2017.
- 78. Wolters PJ, Wray C, Sutherland RE, Kim SS, Koff J, Mao Y, and Frank JA. Neutrophilderived IL-6 limits alveolar barrier disruption in experimental ventilator-induced lung injury. *J Immunol* 182: 8056-8062, 2009.
- 79. Wyatt TA, Bailey KL, Simet SM, Warren KJ, Sweeter JM, DeVasure JM, Pavlik JA, and Sisson JH. Alcohol potentiates RSV-mediated injury to ciliated airway epithelium. *Alcohol* 80: 17-24, 2019.
- 80. Yang J, Ran M, Li H, Lin Y, Ma K, Yang Y, Fu X, and Yang S. New insight into neurological degeneration: Inflammatory cytokines and blood-brain barrier. *Front Mol Neurosci* 15: 000, 2022.
- 81. Yeligar SM, Mehta AJ, Harris FL, Brown LAS, and Hart CM. Pioglitazone Reverses Alcohol-Induced Alveolar Macrophage Phagocytic Dysfunction. *J Immunol* 207: 483-492, 2021.
- 82. Yeligar SM, and Wyatt TA. Alcohol and lung derangements: An overview. *Alcohol* 80: 1-3, 2019.

- 83. Zhu N, Wang W, Liu Z, Liang C, Wang W, Ye F, Huang B, Zhao L, Wang H, Zhou W, Deng Y, Mao L, Su C, Qiang G, Jiang T, Zhao J, Wu G, Song J, and Tan W. Morphogenesis and cytopathic effect of SARS-CoV-2 infection in human airway epithelial cells. *Nat Commun* 11: 3910, 2020.
- 84. Ou X, Liu Y, Lei X, Li P, Mi D, Ren L, Guo L, Guo R, Chen T, Hu J, Xiang Z, Mu Z, Chen X, Chen J, Hu K, Jin Q, Wang J, Qian Z. Characterization of spike glycoprotein of SARS-CoV-2 on virus entry and its mmune cross-reactivity with SARS-CoV. *Nat Commun.* 11(1):1620, 2020.
- 85. Mannervik B, Awasthi YC, Board PG, Hayes JD, Di Ilio C, Ketterer B, Listowsky I, Morgenstern R, Muramatsu M, Pearson WR, et al. Nomenclature for human glutathione transferases. *Biochem J.* 282 (Pt 1)(Pt 1):305-6, 1992.
- Roy MG, Livraghi-Butrico A, Fletcher AA, McElwee MM, Evans SE, Boerner RM, Alexander SN, Bellinghausen LK, Song AS, Petrova YM, Tuvim MJ, Adachi R, Romo I, Bordt AS, Bowden MG, Sisson JH, Woodruff PG, Thornton DJ, Rousseau K, De la Garza MM, Moghaddam SJ, Karmouty-Quintana H, Blackburn MR, Drouin SM, Davis CW, Terrell KA, Grubb BR, O'Neal WK, Flores SC, Cota-Gomez A, Lozupone CA, Donnelly JM, Watson AM, Hennessy CE, Keith RC, Yang IV, Barthel L, Henson PM, Janssen WJ, Schwartz DA, Boucher RC, Dickey BF, Evans CM. Muc5b is required for airway defence. *Nature*. 505(7483):412-6, 2014.
- 87. Zhang C, Hu Z, Lone AG, Artami M, Edwards M, Zouboulis CC, Stein M, Harris-Tryon TA. Small proline-rich proteins (SPRRs) are epidermally produced antimicrobial proteins that defend the cutaneous barrier by direct bacterial membrane disruption. *Elife*.11:e76729, 2022.

- 88. Foell D, Wittkowski H, Vogl T, Roth J. S100 proteins expressed in phagocytes: a novel group of damage-associated molecular pattern molecules. J Leukoc Biol. 81:28–37. 2007.
- 89. Aoki T, Matsumoto Y, Hirata K, Ochiai K, Okada M, Ichikawa K, Shibasaki M, Arinami T, Sumazaki R, Noguchi E. Expression profiling of genes related to asthma exacerbations. *Clin Exp Allergy*. 39(2):213-21. 2009.
- 90. Lee TH, Jang AS, Park JS, Kim TH, Choi YS, Shin HR, Park SW, Uh ST, Choi JS, Kim YH, Kim Y, Kim S, Chung IY, Jeong SH, Park CS. Elevation of S100 calcium binding protein A9 in sputum of neutrophilic inflammation in severe uncontrolled asthma. *Ann Allergy Asthma Immunol*. 111(4):268-275. 2013.
- 91. Mumby S, Kermani NZ, Garnett JP, Pavlidis S, Wilson SJ, Howarth PJ, Thomas MJ, Adcock IM, López-García C. CEACAM5 is an IL-13-regulated epithelial gene that mediates transcription in type-2 (T2) high severe asthma. *Allergy*. 77(11):3463-3466. 2022.
- 92. Montazersaheb S, Hosseiniyan Khatibi SM, Hejazi MS, Tarhriz V, Farjami A, Ghasemian Sorbeni F, Farahzadi R, Ghasemnejad T. COVID-19 infection: an overview on cytokine storm and related interventions. *Virol J.* 19(1):92. 2022.
- 93. Ng CT, Fong LY, Abdullah MNH. Interferon-gamma (IFN-γ): Reviewing its mechanisms and signaling pathways on the regulation of endothelial barrier function. *Cytokine*. 166:156208. 2023.
- 94. Shibabaw T. Inflammatory Cytokine: IL-17A Signaling Pathway in Patients Present with COVID-19 and Current Treatment Strategy. *J Inflamm Res*. 13:673-680. 2020.
- 95. National Institute on Alcohol Abuse and Alcoholism (NIAAA). Alcohol and Tobacco. *Alcohol Alert (No. 39)*. Rockville, MD: NIAAA, 1998.
- 96. Bailey KL, Smith H, Mathai SK, Huber J, Yacoub M, Yang IV, Wyatt TA, Kechris K,

- Burnham EL. Alcohol Use Disorders Are Associated With a Unique Impact on Airway Epithelial Cell Gene Expression. *Alcohol Clin Exp Res.* 44(8):1571-1584. 2020.
- 97. Mackey K, Ayers CK, Kondo KK, Saha S, Advani SM, Young S, Spencer H, Rusek M, Anderson J, Veazie S, Smith M, Kansagara D. Racial and Ethnic Disparities in COVID-19-Related Infections, Hospitalizations, and Deaths: A Systematic Review. Ann Intern Med. 174(3):362-373. 2021.
- 98. Price-Haywood EG, Burton J, Fort D, Seoane L. Hospitalization and Mortality among Black Patients and White Patients with Covid-19. *N Engl J Med*. 382(26):2534-2543. 2020.

Chapter 4: Characterization of alcohol-exposed airway cells

Kristen F. Easley, Ryan Reed, and Michael Koval

This work is in the preliminary phase of data analysis and has not been published.

4.1 Abstract

Chronic alcohol use significantly increases people's risk of developing lung infections and acute respiratory distress syndrome (ARDS). This increased sensitivity to injury is caused in part by dysfunction of the alveolar epithelial barrier. However, little is known about how alcohol impacts epithelial cells in the conducting airway, i.e. the trachea and bronchi, which are the first line of defense against infectious pathogens in the lungs. I treated healthy human bronchial epithelial cells with 10mM, 60mM and 100mM ethanol and found that ethanol-treated airway cells had a decrease in barrier function during differentiation but had similar barrier function to untreated cells once differentiation into a mucociliary monolayer was complete. Additionally, primary airway epithelial cells isolated from healthy (non-AUD) and alcoholic (AUD) patients had a similar barrier function result and most samples from chronic alcohol users remained migratory and in an "unjammed" state, since areas of stretched cells and swirls of cells were present after differentiation. Rat tracheal cells were more susceptible to in vitro ethanol exposure since barrier function was significantly lower than untreated cells once differentiation was complete. The protein junctional adhesion molecule A (JAM-A) regulates barrier function and epithelial cell migration and may play a role in causing the sustained unjammed phenotype, although in vitro exposure did not decrease JAM-A expression. I also discovered that unjamming may be an age-dependent phenotype, though further analysis must be done to confirm this.

4.2 Introduction

Since 1785, chronic alcohol use has been linked to an increase in the risk of developing pulmonary infections (1). Chronic alcohol use also increases the incidence of acute respiratory distress syndrome (ARDS) by 3-4 fold (2). ARDS is due to alveolar flooding, with sepsis from bacterial pneumonia being one of the most common causes. Further, the mortality rate of ARDS is unacceptably high at 35 to 55%. The increase in risk of infection and ARDS due to chronic alcohol use is due to multiple factors: oxidative stress, lung immune system dysfunction, and alveolar barrier dysfunction (3, 4, 5). However, we have yet to understand how the conducting airway epithelial barrier, the first line of defense against pathogens in the lung, is impacted by chronic alcohol use.

Little is known about how chronic alcohol use impacts the conducting airway epithelial cell barrier other than that it causes improper beating of cilia on ciliated cells (6, 7). Acute alcohol exposure studies *in vitro* show a decrease in tight junction protein expression and barrier function of airway cells; but acute vs chronic exposure can have drastically different effects (8). Airway epithelial cells contain cell adhesion complexes, including tight junctions, that regulate the permeability of ions and small molecules between cells and into the sterile interstitium of the lung. Tight junctions consist of transmembrane proteins that directly control paracellular permeability connected to the actin cytoskeleton by cytosolic scaffold proteins such as ZO-1 and ZO-2 (9). The transmembrane protein Junctional Adhesion Molecule A (JAM-A) regulates paracellular permeability of small molecules (~3-4 kDa) and coordinates with other transmembrane proteins to regulate overall tight junction integrity and barrier function (10, 11). In addition, there is evidence that JAM-A inhibits migration of epithelial cells; for instance, breast cancer cells with low levels of JAM-A are more migratory and invasive than cells highly expressing JAM-A (12, 13).

To elucidate how chronic alcohol exposure impacts conducting airway epithelial cells, we treated healthy human and rat airway cells with ethanol in vitro and measured barrier function by transepithelial electrical resistance (TER). Additionally, we examined cultured bronchial brushings from chronic alcoholic patients. In vitro ethanol exposure caused a decrease in transepithelial electrical resistance (TER) during differentiation in human airway cells, but this result was not sustained upon the completion of differentiation (day 14). Rat airway cells have increased sensitivity to ethanol exposure since barrier function was lower in treated cells on day 14 of differentiation. Airway epithelial cells isolated from healthy (non-AUD) and alcoholic (AUD) patients had similar barrier function responses to in vitro treated cells, in that TER was similar on day 14, but the non-AUD sample had increased TER during differentiation compared to the AUD sample. Additionally, we found that most of the AUD samples exhibited an exaggerated "unjammed" morphology, characterized by areas of stretched cells and swirls of cells across the monolayer. As a recent example of unjamming in airway epithelial disease, airway cells from asthma patients cultured in vitro exhibit the sustained unjammed phenotype (18-19). Upon examination however, we found that unjamming positively correlates with patient age. Some AUD patient samples showed diminished JAM-A although healthy cells treated with ethanol do not show a decrease in JAM-A expression. Taken together, these data reveal that alcohol exposure may affect barrier function of airway cells at sites of active differentiation or repair. More experiments need to be performed to determine if JAM-A plays a role in unjamming and whether this is caused by chronic alcohol exposure.

4.3 Material and Methods

4.3.1 Donor Consent

Research involving human research participants was performed in accordance with the Declaration of Helsinki guidelines. All human subject protocols were reviewed and approved by the Emory University Institutional Review Board and the Atlanta Veterans Affairs Health Care System Research and Development Committee. Potential subjects for study enrollment were screened using the Short Michigan Alcohol Screening Test and AUD Identification Test (16, 17). Individuals with a history of AUD were recruited from the Substance Abuse Treatment Program at the Atlanta Veterans Affairs Health Care System, and otherwise healthy control subjects were recruited from general Veterans Affairs medical clinics (14). Additional subject inclusion criteria included active alcohol abuse, in which the last alcoholic drink was <8d prior to bronchoscopy. Subjects were excluded if they primarily abused substances other than alcohol, were HIV positive, or had abnormal chest radiographs.

4.3.2 Airway epithelial cell culture and EtOH treatment

Cells from bronchial brushings were expanded in co-culture with irradiated 3T3 fibroblast feeder cells in F+Y reprogramming media (FYRM) as previously described (15). FYRM was changed every other day until the cells were ~70-90% confluent and then the cells were isolated by first removing the 3T3 feeder layer using calcium/magnesium-free phosphate buffered saline supplemented with 1 mM EDTA (PBS/EDTA), followed by detaching epithelial cells by incubating with Accutase (Sigma-Aldrich #A6964) at RT for 10 minutes. For experiments, cells were thawed, expanded using FYRM and then seeded on Transwell permeable supports pre-coated with type IV collagen (Sigma-Aldrich #C7521) at a density of 150,000 cells per 6.5 mm Transwell (Costar #3450, 24 well) or 350,000 cells per 12 mm Transwell (Costar # 3460, 12 well) in E-ALI medium (15). E-ALI medium was based on previous formulations with modifications to glucose

(150 mg/dl; 8.3 mM), CaCl₂ (1 mM), heparin (2 μ g/ml), L-glutamine (2.5 mM), hydrocortisone (960 mg/ml), bovine pituitary extract (20 μ g/ml), and Mg²⁺ (0.5 μ M). E-ALI medium is changed every other day with washing of the apical surface (15). Using this protocol, monolayers were fully differentiated 14 days after transitioning to ALI.

Human airway cells were treated with ethanol for 10 days at the basal cell stage and continued treatment during differentiation at a low, medium and high concentrations as previously described (20, 21). Rat airway cells were not dosed at the basal cell stage. Ethanol treated cells were grown and differentiated in a separate incubator from no treatment control to avoid ethanol vapor effects.

4.3.3 Rat airway epithelial cell isolation and culture

Rat lungs were removed from animal and tracheas and bronchi were isolated. They were sliced into small rings and washed with HBSS containing antibiotics and digested in 1% protease solution consisting of Ham's F-12 medium (Hyclone #SH30026.FS) supplemented with 1.0% w/v Protease XIV (Sigma-Aldrich #P5147), 0.1% w/v DNAse I (Sigma-Aldrich #DN25), for 16 hours at 4 degrees. Large pieces of tissue were removed and remaining cells were collected and mixed with 1mL FBS. Cells were centrifuged at 500xg for 10 minutes. Cells were resuspended in 10mL F12 containing 5mg DNAse and 100mg BSA to disrupt cell clumps. Cells were incubated on ice for 5 minutes followed by filtration through a 100um filter. Cells were centrifuged again and resuspended in medium for plating on 6 well dishes with 3t3 fibroblasts and rat F+Y medium. Once cells were confluent, they were similarly passaged and seeded on Transwell permeable supports coated with type I rat tail collagen (Roche #45-11179179001). FYRM and E-ALI reagent concentrations were altered for rat cells from media formulations previously used in our lab (15,

22). Same products were used unless otherwise indicated. For 500mL FYRM: 112.5mL DMEM (4.5g/L glucose) (Sigma-Aldrich #D6429), 362.5mL F12 Hams, 25mL FBS, 5ug/mL Insulin (Sigma-Aldrich #I1882), 24ug/mL Adenine, 8.33ng/mL Cholera Toxin, 10ng/mL epidermal growth factor (Sigma, #E4127), 480 ng/mL hydrocortisone, 200ng/mL Voriconazole, 0.2% Primocin, 0.1% Plasmocin. For 500mL E-ALI: 235mL DMEM (4.5g/L glucose) (Sigma-Aldrich #D6429), 235mL F12 Hams, 50ug/mL Penicillin/Streptomycin (Gibco, #15070063), 5ug/mL Insulin (Sigma-Aldrich #I1882), 0.1ug/mL Hydrocortisone, 0.1ug/mL Cholera Toxin, 5ug/mL Transferrin, 500nM Phospohethanolamine, 500nM Ethanolamine, 25ng/mL epidermal growth factor (Sigma-Aldrich, #E4127), 0.5% bovine pituitary extract, 30mM HEPES, 1.5mg BSA, 5x10-8M Retinoic Acid.

4.3.4 Transepithelial Resistance (TER)

TER was measured using an EVOM Voltohmmeter (World Precision Instruments, #EVOM2). Before measuring, cells were washed with Dulbecco's Phosphate Buffered Saline containing Ca⁺² and Mg⁺² (DPBS, Corning # 21-030-CV) followed by a 15-minute incubation at 37°C in Ringer's solution (140 mM NaCl, 5 mM KCl, 0.36 mM K₂HPO₄, 0.44mM KH₂PO₄, 1.3 mM CaCl₂ • 2 H₂O, 0.5 mM MgCl₂ • 6 H₂O, 4.2 mM NaHCO₃, 10 mM Na HEPES, 10 mM glucose).

4.3.5 Immunofluorescence Microscopy

Cells on Transwell permeable supports were rinsed with DPBS then fixed with 4% paraformaldehyde (PFA) for 10 minutes at RT in the dark. This was followed by a DPBS rinse and 2 minutes of fixation in 1:1 methanol/acetone at RT. Cells were then washed 3x with DPBS.

Cells were permeabilized in 0.5% Triton X-100/DPBS++ for 5 minutes, followed by two 5-minute incubations in blocking solution (0.5% Triton X-100 and 5% Goat serum in DPBS). Primary antibodies were added (diluted in 3% BSA in DPBS) and incubated overnight at 4°C. The cells were washed 3x with DPBS and then incubated for 1h at RT with fluorescent secondary antibodies diluted in 3% BSA. The secondary antibodies were removed and the cells were further incubated for 10 minutes in Hoechst 33342 (ThermoFisher # 62249) diluted 1:1000 in DPBS to stain nuclei. Cells were washed 3x with DPBS, and Transwells were mounted on slides using Vectashield mounting solution (Vector Labs #H-1000-10).

Primary antibodies used for immunofluorescence: rabbit anti-ZO-1 (Invitrogen 402200, 1:100 dilution) and Mouse anti JAM-A (abcam #ab267407, 1:100 dilution). Secondary antibodies used for immunofluorescence: Alexa fluor 568 goat anti-mouse (Invitrogen A11031, 1:1500 dilution) Alexa fluor 488 goat anti-rabbit (Invitrogen #A11034, 1:1500 dilution). Images were taken using either a Nikon Ti Eclipse with epifluorescence and processed using 3D deconvolution and FIJI.

4.3.6 Statistics

Statistics were calculated using Graphpad Prism 8.0 and significance was determined using ordinary two-way ANOVA with Sidak's multiple comparison test (ethanol-treated non-AUD and AUD cells) or two-way ANOVA with Tukey's multiple comparisons test (ethanol-treated human and rat cells).

4.4 Results

4.4.1 Ethanol treatment in vitro decreases barrier function only during differentiation

To determine if ethanol treatment in vitro decreases barrier function, healthy bronchial cells were expanded and differentiated in the presence or absence of either 10mM, 60mM and 100mM ethanol. These concentrations represent blood alcohol concentrations (BAC) of low intake of alcohol, average BAC of someone with alcohol poisoning, and average BAC of chronic alcohol users, respectively (Overgaard, Szabo). Expansion occurs for approximately 10 days and air-liquid interface (ALI) differentiation from basal cells to a mucocilliary monolayer containing ciliated cells, secretory cells and basal cells is complete in 14 days. Ethanol treatment in vitro decreases the transepithelial electrical resistance (TER) in three independent samples (Figures 4.1A, 4.1B and 4.1C) but only during differentiation in most samples (day 3, day 8, day 10). Depending on the sample and day of TER measurement, this response occurs in a dose dependent manner. By day 14, two samples have similar TER values between control and ethanol treated cells. This result is similar to baseline TER measurements in Chapter 3 comparing non-AUD and AUD TER on Day 14 (Figure 3.2G). In many cases, untreated cells have a higher TER during differentiation (day 3, day 8 or day 10) compared to once differentiation is complete (day 14). For ethanol treated cells, this is mostly not the case.

In addition to our *in vitro* bronchial cell culture system, our lab frequently utilizes rodent models to study alcohol use disorder on lung function. I adapted our human airway cell isolation protocol, F+Y media and E-ALI media for rat cells (22) to eventually combine our alcohol-fed rat model with *in vitro* studies. The rat cells did not passage well past p1, and, therefore, I did not expose them to ethanol during this comparatively short basal-cell stage. I found that the rat airway cells are more sensitized to 60mM ethanol treatment (Figure 4.1D) compared to the human airway cells. For untreated cells, TER was higher on day 14 compared to day 3. On day 14, TER was significantly lower in ethanol-treated cells compared to untreated cells. This highly sensitized

model system may be useful to identify potential changes in tight junction protein levels and regulation due to ethanol exposure.

In addition to culturing healthy bronchial cells from human patients (non-AUD), we also cultured bronchial cells isolated from patients with AUD. Since AUD cells were only exposed to alcohol and its metabolites in vivo, I wanted to determine if barrier function would change due to 60mM and 100mM ethanol treatment. In Figure 4.1E, I show that ethanol treatment in vitro decreases TER in the non-AUD cells only during differentiation (day 6 and day 9), which is a similar result to the healthy samples in Figures 4.1A, 4.1B and 4.1C. Interestingly, the TER of the AUD sample does not change when exposed to ethanol. In addition, the TER of the non-AUD sample is significantly higher during differentiation compared to the AUD sample, and I observed no difference in TER on Day 14 between the non-AUD cells and AUD cells, similar to the results in Figures 4.1A, 4.1B, 4.1C. On day 3 of differentiation, the cultures are mostly basal cells with varying degrees of differentiation and cell-type ratios on days 6, 8, 9 and 10. These timepoints could represent localized spots of monolayer repair in vivo. Taken together, these data suggest that airway cells increase barrier function during repair to protect against flux of macromolecules and microbes into the interstitial space. Ethanol exposure may negate this phenotype and render airway cells more susceptible to infection.

4.4.2 Most AUD patient samples are unjammed

To determine if chronic ethanol use alters bronchial cell shape, we cultured and differentiated non-AUD and AUD cells and stained for the tight junction protein ZO-1. Staining for ZO-1 easily reveals the shape of airway cells. Cells from two non-AUD patients exhibit a normal, cobblestone-like pattern (Figure 4.2A) revealing cells of different sizes. Most AUD patient

samples (Figure 4.2B) exhibit an interesting pattern where cells appear stretched and, in some cases, are larger than non-AUD cells (AUD2). This phenotype is known as unjamming and indicates that cells are undergoing collective cell migration across the monolayer, which is not a typical function of differentiated airway cells. It is important to note that AUD5 does not seem to exhibit the unjammed phenotype. While different exposures to and diseases of the airway can cause unjamming *in vitro* (18, 19), chronic alcohol use is potentially a previously unknown cause.

4.4.3 Some AUD patient samples show diminished JAM-A

Loss of the tight junction protein JAM-A has been implicated in collective cell migration (12, 13). I stained for JAM-A and observed that AUD2, AUD4 and AUD5 have low expression of JAM-A (Figure 4.3B) compared to non-AUD samples (Figure4.3A). Differences in cell size between non-AUD and AUD cells makes this result difficult to measure but can be observed qualitatively. It is important to note that AUD samples with higher JAM-A expression, such as AUD1, still exhibit the unjammed phenotype. More patient isolates would be needed to correlate chronic alcohol use *in vivo* differential levels of JAM-A expression.

4.4.4 Ethanol treatment *in vitro* does not decrease JAM-A expression and may cause unjamming.

To determine if ethanol exposure decreases JAM-A expression, and therefore, causes unjamming, we stained the bronchial cells dosed with three concentrations of ethanol for JAM-A (Figure 4.4). We found that dosing cells with ethanol *in vitro* does not decrease JAM-A expression nor alter JAM-A localization. The control cells show unjamming to a low degree, while the 10mM and 60mM ethanol treated cells exhibit the unjammed phenotype. Interestingly, the 100mM

ethanol treated cells did not show unjamming, which indicates that this phenotype may depend on the ethanol dosage. It is possible that 24 days of ethanol exposure is not enough to generate the severe unjammed phenotype or decrease in JAM-A levels that we see in some AUD patient samples. This experiment would need to be repeated with additional bronchial cell isolates as well as for a longer incubation time to determine if chronic ethanol exposure causes unjamming.

4.4.5 Unjamming correlates with patient age

To further determine if AUD or additional variables correlate with unjamming, we created a table of patient samples and observed smoking status, gender and age (Table 4.1). The samples collected from patients aged 43 and older all exhibit unjamming, while samples from patients aged 29 and younger do not have the unjammed phenotype. There does not appear to be any correlation of unjamming with between AUD and smoking status or sex, although more samples are needed to determine this. The ability for lung cells to properly repair and regenerate in response to insults decreases as we age (23). We can potentially use our model system to capture this correlation and study how aging, in addition to alcohol use disorder, causes unjamming in airway epithelial cells.

4.5 Discussion

Alcohol Use Disorder (AUD) significantly increases the risk of patients developing ARDS due to a respiratory infection or ventilator use (27). The mechanisms behind this increased risk include increased oxidative stress (lack of antioxidant activity), lung immune system dysfunction, and alveolar barrier dysfunction (3, 4, 5). The airway epithelium is the first line of defense against pathogens in the lung, and we have yet to understand how chronic alcohol use impairs the function of these cells or their ability to repair and regenerate. In this study, we investigate how *in vitro* and

in vivo alcohol exposure impact barrier function of differentiating and fully differentiated cells, tight junction proteins and collective cell migration.

Epithelial cell barrier function is important for proper flux of ions, fluids and macromolecules across the cell barrier and keeping pathogens and toxins from entering the sterile environment of the lung (24, 25, 26). In rodent models, chronic alcohol exposure has been shown to negatively impact endothelial and alveolar barrier function (27, 28). To study how chronic ethanol use effects the barrier of airway cells, we utilized our physiologically improved *in vitro* culture system introduced in Chapter 2 to derive and culture airway cells from patients with and without AUD. We took a subset of healthy human and rat cells and treated them with 10mM, 60mM and 100mM ethanol for up to 24 days and compared the effects to AUD cells.

We found that in three separate patient samples, ethanol treatment *in vitro* decreases the transepithelial electrical resistance (TER) but only during differentiation in most samples (Figures 4.1A-4.1C) For most samples, especially on day 8 and day 10 of differentiation, we see that untreated cells have higher barrier function compared to day 14. A similar result is seen when we treat non-AUD cells with 60mM and 100mM ethanol (Figure 4.1E). Early days of differentiation in our model system could potentially represent localized spots of repair and regeneration since the cultures contain mostly basal cells. The TER for 60mM and 100mM ethanol treatment compared to control on day 3 is quite striking. To our knowledge, the effects of chronic alcohol exposure on basal cells in the lung have not been studied, although many groups have observed detrimental responses to stem cells pools in other organ systems (29). Reduced proliferation and promotion of epithelial to mesenchymal transition (EMT) are observed changes when hepatic stem cells are exposed to alcohol (30). In intestinal stem cells, alcohol exposure decreases the expression of stem cell markers (31). Because basal cells differentiate into cell types found in the airway

epithelium, any alterations in basal cell function and differentiation potential due to chronic ethanol exposure would be detrimental to airway function.

Interestingly, we found that rat airway cells did not respond to *in vitro* ethanol exposure in a similar fashion to human airway cells, although it is important to note that the basal cells were not exposed to ethanol during the expansion stage. In control cells, barrier function increased from day 3 to day 14 of differentiation (Figure 4.1D). We observed a significant decrease in 60mM ethanol treated cells on day 14 compared to control. This result is similar to what we observe when we isolate and culture alveolar epithelial cells from alcohol- and control-fed rats (28). It is certainly possible that rat airway cells respond differentially and are more susceptible to ethanol exposure than human airway cells. Because bronchial brushings from AUD patients are not readily available, we aim to combine the alcohol-fed rat model and *in vitro* culture system in the future to study how long-term ethanol exposure impacts airway cells.

Additionally, we found that 4 out of 5 AUD patient samples exhibit unjamming, while non-AUD cells exhibit normal morphologies (Figure 4.2). Ethanol exposure in vitro may cause unjamming, although this experiment will need to be repeated with additional primary cell isolates (Figure 4.4). Unjamming is a form of collective cell migration and is distinct from EMT (32). Collective cell migration is a necessary cellular mechanism that occurs during development and repair. However, there are many cases where unjamming of the airway epithelium is a response to mechanical stress, irradiation, and pro-inflammatory cytokines (19, 33). Additionally, airway cells cultured from asthmatic patients exhibit a prolonged unjammed phenotype (19).

In Figures 4.2 and 4.3, we observed areas of the monolayer where AUD cells appear larger in size. This result may be due to bunching of the Transwell due to unjamming rather than actual change in cell size. Future directions include using confocal tile imaging and generating 3D

renderings of the entire monolayer to accurately determine if AUD cells are larger in size.

Because the tight junction protein JAM-A has been linked to collective cell migration, we stained for JAM-A in differentiated non-AUD and AUD cells and observed any changes in intensity and/or localization. We found that AUD2, AUD4 and AUD5 have decreased JAM-A intensity compared to non-AUD cells (Figure 4.3). However, the differences in cell size between samples make this difficult to quantify. Future directions for this experiment include using image processing to develop an accurate way to measure and compare JAM-A intensity in cells of different sizes. We can correlate this with qRT-PCR and immunoblot probing for JAM-A. It is important to note that AUD cells that have higher JAM-A expression may also exhibit the unjammed phenotype (AUD1) so there is no correlation between these two outcome variables.

To test whether a decrease in JAM-A correlates with or causes unjamming, we performed immunofluorescence in differentiated cells exposed to 3 concentrations of ethanol for 24 days. We found that JAM-A does not decrease with ethanol treatment *in vitro* and that unjamming may occur depending on the ethanol dose (Figure 4.4). The control cells are slightly unjammed, while the 10mM and 60mM ethanol treated cells do exhibit unjamming. Surprisingly, the 100mM ethanol treated cells are completely jammed. Only one primary cell line was used for this experiment, and we would benefit from repeating this experiment with more cell isolates. An additional future direction would include knocking down JAM-A in basal cells, differentiating them into a mucocilliary monolayer and measuring unjamming. We should also measure TGF-beta levels in both *in vivo* and *in vitro* ethanol-exposed cells, since TGF-beta increases with chronic alcohol use and is known to cause unjamming (33).

In Table 1, we determined that unjamming status most closely correlated with age, and was irrespective of AUD status, smoking status and sex. Differentiated cells from patients aged 43 and

older all exhibit the unjammed phenotype while cells from patients aged 29 and younger did not exhibit the unjammed phenotype. Aging is a complex phenomenon; but in this case, aging could refer to diminished capacity of repair, leading to unwarranted collective cell migration potentially at the expense of differentiation. For example, cells expressing senescence markers such as GDF15 might be prone to unjamming (34). Future work would help determine whether this is the case.

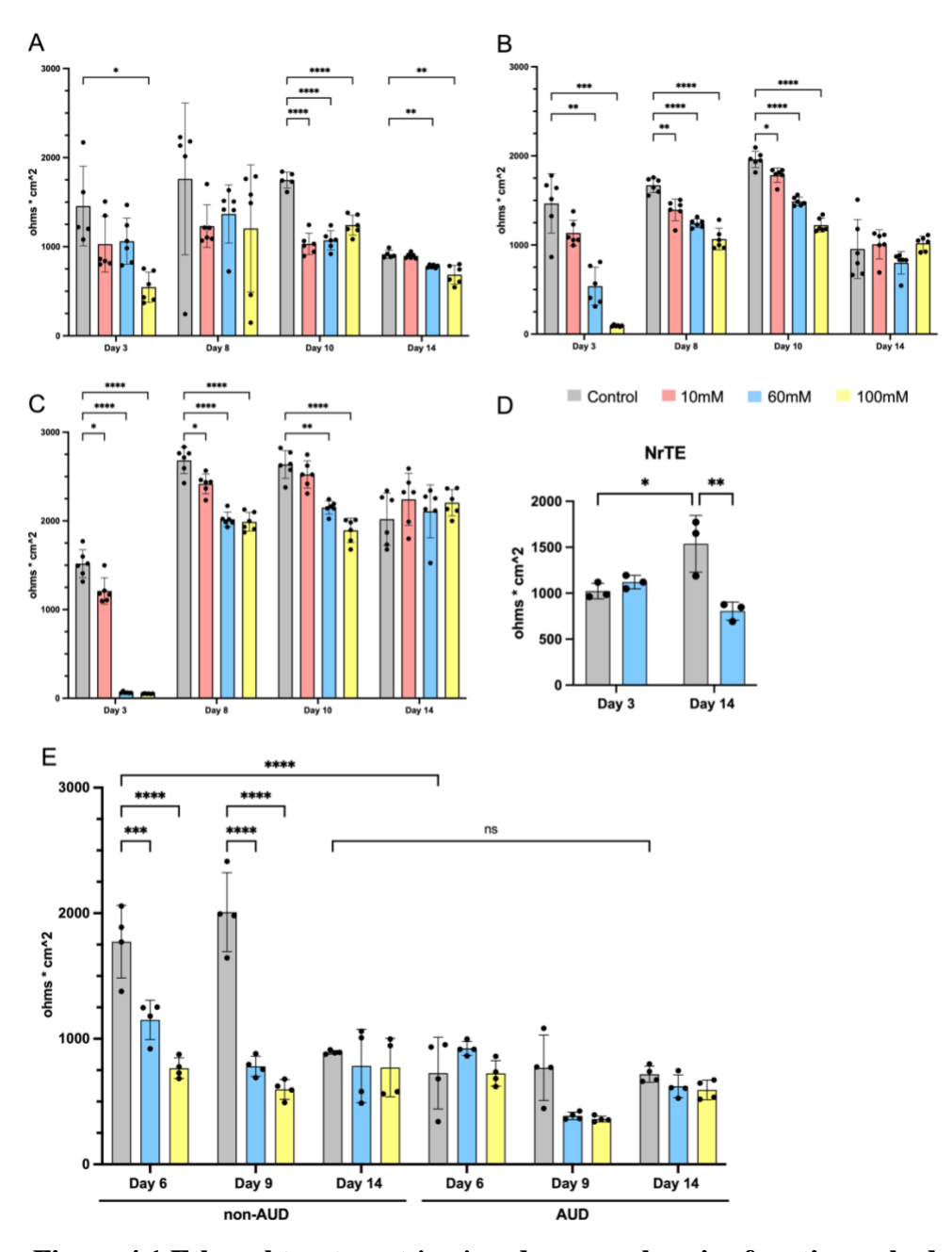


Figure 4.1 Ethanol treatment *in vitro* decreases barrier function only during differentiation.

(**A-C**) Non-diseased bronchial cells from three different patients were dosed with no treatment (grey) 10 (salmon), 60 (blue) and 100mM (yellow) ethanol at the basal cell stage for 10 days and during differentiation for 14 days. TER (ohms x cm²) was measured on day 3, day 8, day 10 and day 14 of differentiation. N=5-6 Transwells per sample, per treatment. (**D**) NrTE= normal rat

tracheal cells. Isolation and culture of NrTEs are described in Methods. N=3 Transwells per sample, per treatment. (**E**) AUD=Alcohol Use Disorder. Cells from one non-AUD patient and one AUD patient were used. TER was measured on day 6, day 9 and day 14. Cells were dosed with ethanol for 10 days at the basal cell stage and during differentiation for 14 days. N= 4 Transwells per sample, per treatment. *= $p \le 0.05$, **= $p \le 0.01$, ***= $p \le 0.001$ and ****= $p \le 0.0001$.

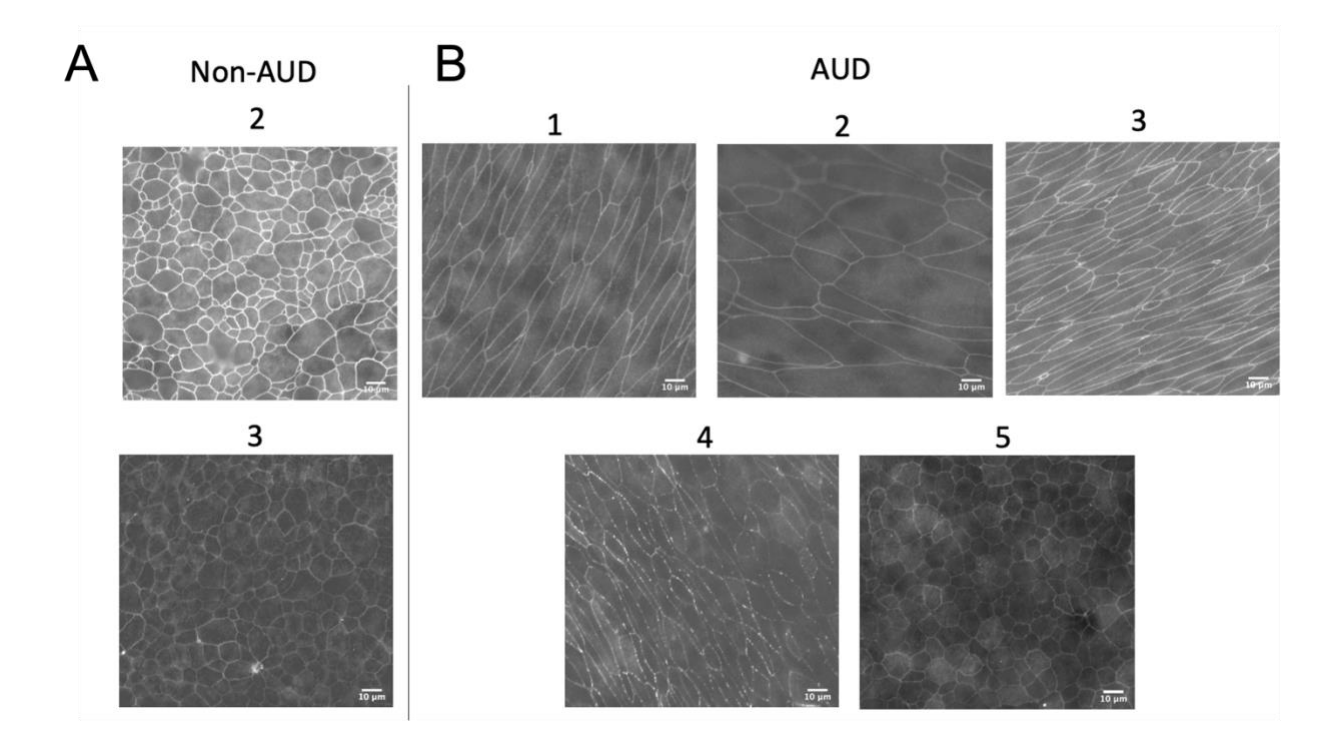


Figure 4.2 Most AUD cells are unjammed.

AUD= Alcohol Use Disorder. Non-diseased bronchial cells (**A**) and bronchial cells form AUD patients (**B**) were differentiated, processed for immunofluorescence, and stained for the tight junction protein ZO-1. Number above image is the sample identifier. All samples were imaged at 40x magnification.

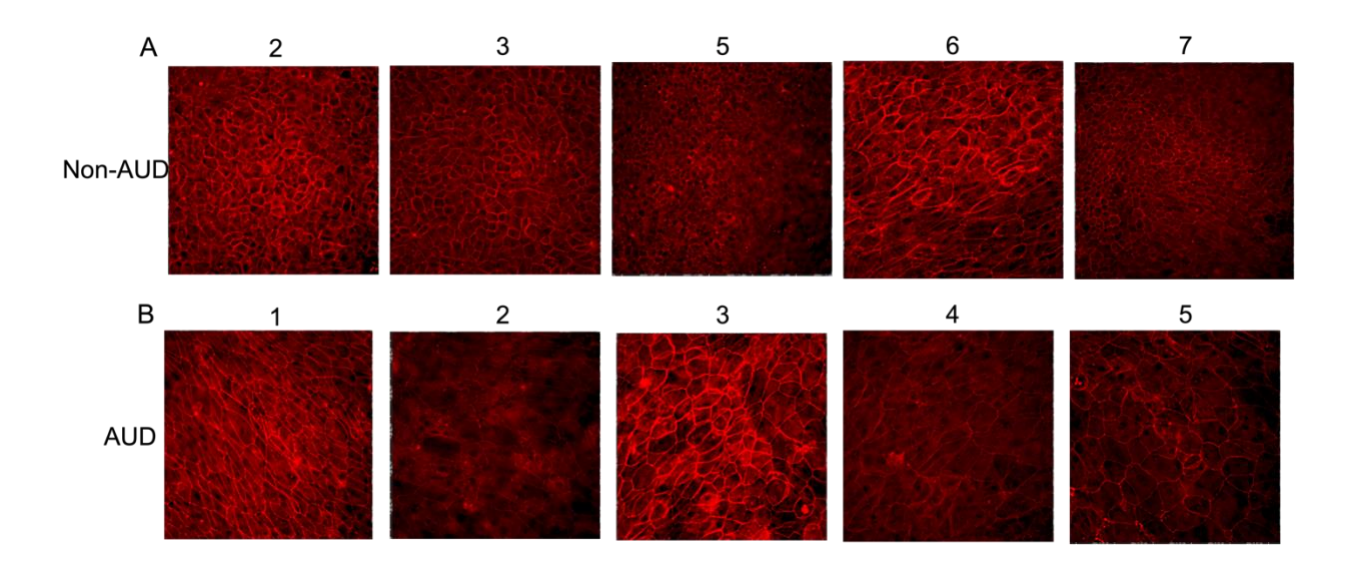


Figure 4.3 Some AUD patient samples show diminished JAM-A.

AUD= Alcohol Use Disorder. Non-diseased bronchial cells (**A**) and bronchial cells form AUD patients (**B**) were differentiated, processed for immunofluorescence, and stained for the tight junction protein JAM-A. Number above image is the sample identifier. All samples were imaged at 40x magnification.

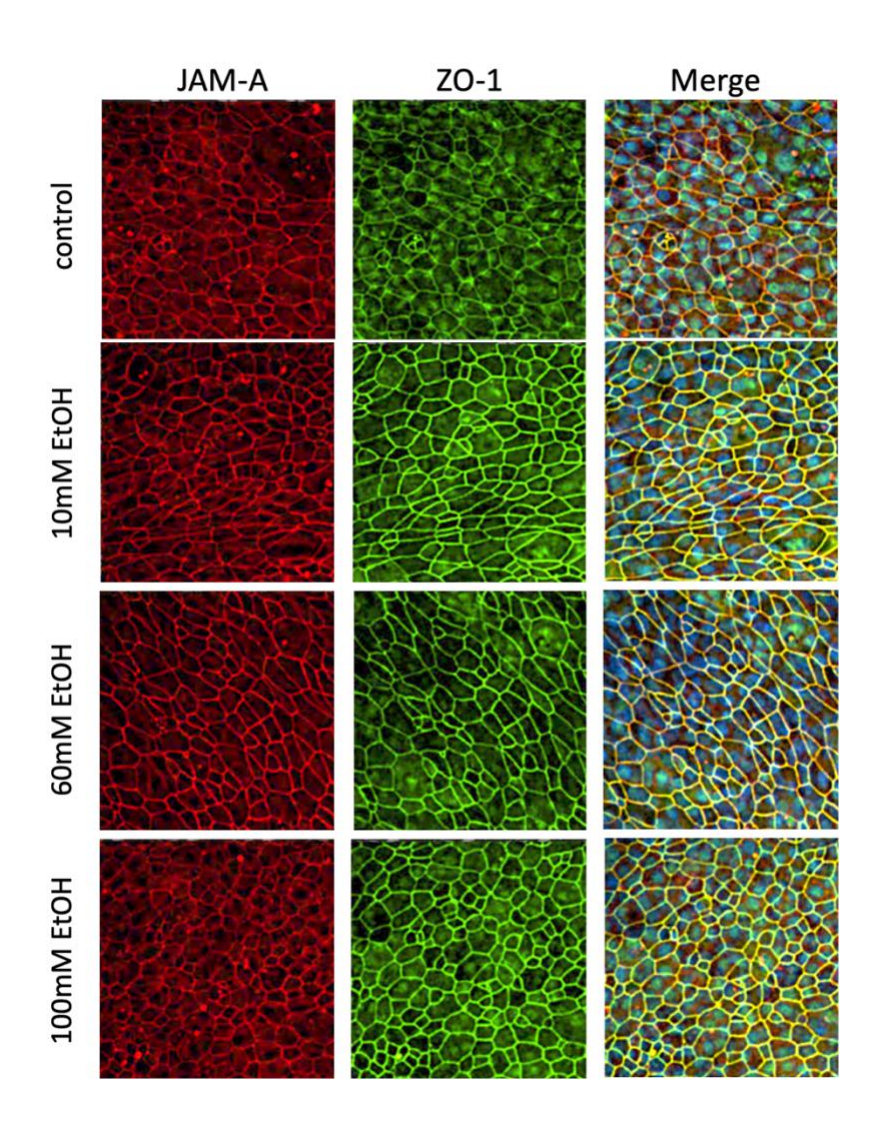


Figure 4.4 Ethanol treatment *in vitro* does not decrease JAM-A expression and may cause unjamming.

Non-diseased bronchial cells were dosed with 10mM, 60mM and 100mM ethanol or without ethanol (control) at the basal cell stage for 10 days and during differentiation for 14 days. Cells were differentiated, processed for immunofluorescence, and stained for the tight junction proteins JAM-A (red) ZO-1 (green). Third column indicates merge of red and green channels with Hoechst 33342 dye staining nuclei (blue). N=1 Transwell with 5 fields per view captured for each condition. All samples were imaged at 40x magnification.

Identifier	AUD?	Age	Unjammed?	Smoker?	Sex
1	No	~2	no	No	Male
2	No	3	no	No	Male
3	No	20	no	No	Male
4	No	56	yes	No	Male
5	No	29	no	Yes	Male
6	No	58	yes	Yes	Male
1	Yes	43	yes	No	Female
2	Yes	50	yes	Yes	Male
3	Yes	52	yes	Yes	Male
4	Yes	51	yes	No	Male
5	Yes	27	no	No	Female

Table 4.1. Unjamming correlates with patient age.

Patient sample identifiers match identifiers in Figures 4.2 and 4.3 above immunofluorescence images. Orange shading represents the correlation between age and unjamming status. Older patient samples exhibit the unjammed phenotype, regardless of AUD status, smoking status and sex.

References

- 1. Zhang, P., Bagby, G. J., Happel, K. I., Raasch, C. E. & Nelson, S. Alcohol abuse, immunosuppression, and pulmonary infection. Curr Drug Abuse Rev 1. (2008).
- Kershaw, C. D. & Guidot, D. M. Alcoholic lung disease. Alcohol Res Health 31, 66-75 (2008).
- 3. D'Souza, N. B., Mandujano, J. F., Nelson, S., Summer, W. R. & Shellito, J. E. Alcohol ingestion impairs host defenses predisposing otherwise healthy mice to Pneumocystis carinii infection. Alcohol Clin Exp Res. (1995).
- 4. Holguin, F., Moss, I., Brown, L. A. & Guidot, D. M. Chronic ethanol ingestion impairs alveolar type II cell glutathione homeostasis and function and predisposes to endotoxin-mediated acute edematous lung injury in rats. J Clin Invest. (1998).
- 5. Jurkovich, G. J. et al. The effect of acute alcohol intoxication and chronic alcohol abuse on outcome from trauma. JAMA 270, 51-56 (1993).
- 6. Maurer, D., & Liebman, J. Effects of ethanol on in vitro ciliary motility. Journal of Applied Physiology. (1988).
- 7. Wyatt, T. A. & Sisson, J. H. Chronic ethanol downregulates PKA activation and ciliary beating in bovine bronchial epithelial cells. Am J Physiol Lung Cell Mol Physiol. (2001).
- 8. Xu, M. et al. Chronic ethanol exposure enhances the aggressiveness of breast cancer: the role of p38gamma. Oncotarget. (2016).
- 9. Molina SA, Stauffer B, Moriarty HK, Kim AH, McCarty NA, Koval M. Junctional abnormalities in human airway epithelial cells expressing F508del CFTR. Am J Physiol Lung Cell Mol Physiol. (2015).
- 10. Mitchell, L. A. et al. Junctional adhesion molecule A promotes epithelial tight junction

- assembly to augment lung barrier function. Am J Pathol. (2015).
- 11. Otani, T. et al. Claudins and JAM-A coordinately regulate tight junction formation and epithelial polarity. J Cell Biol. (2019).
- 12. Naik, M. U., Naik, T. U., Suckow, A. T., Duncan, M. K. & Naik, U. P. Attenuation of junctional adhesion molecule-A is a contributing factor for breast cancer cell invasion. Cancer Res. (2008).
- 13. Wang, Y. & Lui, W. Y. Transforming growth factor-beta1 attenuates junctional adhesion molecule-A and contributes to breast cancer cell invasion. Eur J Cancer. (2012).
- 14. Mehta AJ, Yeligar SM, Elon L, Brown LA, and Guidot DM. Alcoholism causes alveolar macrophage zinc deficiency and immune dysfunction. *Am J Respir Crit Care Med.* 2013.
- 15. Morgan R, Manfredi C, Easley KF, Watkins LD, Hunt WR, Goudy SL, Sorscher EJ, Koval M, and Molina SA. A medium composition containing normal resting glucose that supports differentiation of primary human airway cells. *Sci Rep* 12: 1540, 2022.
- 16. Saunders JB, Aasland OG, Babor TF, de la Fuente JR, and Grant M. Development of the Alcohol Use Disorders Identification Test (AUDIT): WHO Collaborative Project on Early Detection of Persons with Harmful Alcohol Consumption--II. *Addiction*. 1993.
- 17. Selzer ML, Vinokur A, and van Rooijen L. A self-administered Short Michigan Alcoholism Screening Test (SMAST). *J Stud Alcohol*. 1975.
- 18. Park, J. A. & Fredberg, J. J. Cell Jamming in the Airway Epithelium. Ann Am Thorac Soc. (2016).
- 19. Park, J. A. et al. Unjamming and cell shape in the asthmatic airway epithelium. Nat Mater. (2015).
- 20. Overgaard CE, Schlingmann B, Dorsainvil White S, Ward C, Fan X, Swarnakar S, Brown

- LA, Guidot DM, Koval M. The relative balance of GM-CSF and TGF-β1 regulates lung epithelial barrier function. Am J Physiol Lung Cell Mol Physiol. 2015
- 21. Szabo G, Mandrekar P, Dolganiuc A, Catalano D, Kodys K. Reduced alloreactive T-cell activation after alcohol intake is due to impaired monocyte accessory cell function and correlates with elevated IL-10, IL-13, and decreased IFNgamma levels. Alcohol Clin Exp Res. 2001.
- 22. Kaartinen L, Nettesheim P, Adler KB, Randell SH. Rat tracheal epithelial cell differentiation in vitro. In Vitro Cell Dev Biol Anim. 1993 Jun;29(6):481-92. doi: 10.1007/BF02639383. PMID: 27519750.
- 23. Navarro S, Driscoll B. Regeneration of the Aging Lung: A Mini-Review. Gerontology. 2016.
- 24. Hellings PW, Steelant B. Epithelial barriers in allergy and asthma. J Allergy Clin Immunol. 2020.
- 25. Brune K, Frank J, Schwingshackl A, Finigan J, Sidhaye VK. Pulmonary epithelial barrier function: some new players and mechanisms. Am J Physiol Lung Cell Mol Physiol. 2015.
- 26. Yuksel H, Turkeli A. Airway epithelial barrier dysfunction in the pathogenesis and prognosis of respiratory tract diseases in childhood and adulthood. Tissue Barriers. 2017.
- 27. Moss M, Bucher B, Moore FA, Moore EE, Parsons PE. The role of chronic alcohol abuse in the development of acute respiratory distress syndrome in adults. JAMA. 1996.
- 28. Schlingmann B, Overgaard CE, Molina SA, Lynn KS, Mitchell LA, Dorsainvil White S, Mattheyses AL, Guidot DM, Capaldo CT, Koval M. Regulation of claudin/zonula occludens-1 complexes by hetero-claudin interactions. Nat Commun. 2016.
- 29. Di Rocco G, Baldari S, Pani G, Toietta G. Stem cells under the influence of alcohol: effects

- of ethanol consumption on stem/progenitor cells. Cell Mol Life Sci. 2019.
- 30. Shi X, Chang CC, Basson MD, Upham BL, Wei L, Zhang P. Alcohol disrupts human liver stem/progenitor cell proliferation and differentiation. J Stem Cell Res Ther. 2014.
- 31. Lu R, Voigt RM, Zhang Y, Kato I, Xia Y, Forsyth CB, Keshavarzian A, Sun J. Alcohol injury damages intestinal stem cells. Alcohol Clin Exp Res. 2017.
- 32. Mitchel JA, Das A, O'Sullivan MJ, Stancil IT, DeCamp SJ, Koehler S, Ocaña OH, Butler JP, Fredberg JJ, Nieto MA, Bi D, Park JA. In primary airway epithelial cells, the unjamming transition is distinct from the epithelial-to-mesenchymal transition. Nat Commun. 2020.
- 33. O'Sullivan MJ, Mitchel JA, Das A, Koehler S, Levine H, Bi D, Nagel ZD, Park JA. Irradiation Induces Epithelial Cell Unjamming. Front Cell Dev Biol. 2020.
- 34. Wan Y, Fu J. GDF15 as a key disease target and biomarker: linking chronic lung diseases and ageing. Mol Cell Biochem. 2023 Apr 24:1–14. doi: 10.1007/s11010-023-04743-x. Epub ahead of print. PMID: 37093513; PMCID: PMC10123484.

Chapter 5: Conclusions and Future Directions

5.1 Overview of findings and significance

Understanding how the airway epithelium responds to insults is key for developing and improving therapies for diseases that affect the airway. The airway epithelium is the first line of defense against inhaled pollutants and pathogens, and diseases that directly and indirectly impact the airway can alter the cellular response to these insults. In an effort to mimic the *in vivo* microenvironment of the airway, we created E-ALI medium with physiologic glucose levels that supports differentiation of primary bronchial epithelial cells in culture (Chapter 2) and provides a platform for studying airway epithelial cell function. We found that bronchial epithelial cells differentiated in E-ALI medium showed insulin-stimulated glucose uptake and increased barrier function, which were both inhibited by high glucose concentrations. This medium also supported primary nasal CF airway epithelia as demonstrated by immunofluorescence of airway cell markers and electrophysiological analysis. These results have implications for how hyperglycemia may impact airway cell metabolism and function, in addition to overall lung health.

We leveraged this physiologically improved *in vitro* model to study how chronic alcohol use and SARS-CoV-2 infection impact bronchial epithelial cell function (Chapter 3). Bulk RNA sequencing analysis of bronchial cells from non-AUD and AUD patients revealed 117 upregulated differentially expressed (DE) genes and 47 downregulated DE genes in AUD cells compared to non-AUD cells. In AUD cells, SARS-CoV-2 receptors ACE2 and two TMPRESS isoforms were upregulated while genes related to antioxidant defenses, cell repair and innate immune function were downregulated. GO enrichment analysis indicated that AUD cells adapted an inflammatory, epidermal profile that indicates that AUD cells may be primed for a more severe infection. We

infected the non-AUD cells and AUD cells with SARS-CoV-2 for 72 hours and found that the barrier function of AUD cells did not recover after 72 hours, while the barrier function of non-AUD cells recovered above baseline. SARS-CoV-2 infection of both AUD and non-AUD cells displayed a decrease in β catenin expression, an adherens junction protein important for maintaining cell-cell contacts. Lastly, multiplex analysis of cytokine secretion by SARS-CoV-2 infected cells revealed that many pro-inflammatory cytokines, including IL-1β and IFNγ, showed higher levels of secretion by AUD cells during the 72h period post-infection as compared to non-AUD cells. Taken together, our data suggests that AUD may prime airway cells for a worse outcome in SARS-CoV-2 infection. AUD cells are not cultured in the presence of alcohol, but our results indicate that chronic alcohol use has lasting effects. How chronic alcohol exposure alters the epigenome of airway epithelial cells should be examined.

To further understand the molecular mechanisms underlying alcohol's detrimental impacts on airway epithelial cell barrier function, we dosed basal stem cells with a low, medium and high concentration of ethanol during expansion and differentiation (Chapter 4). I found that ethanol-treated bronchial cells had a decrease in transepithelial electrical resistance (TER) during differentiation but had similar barrier function to untreated cells once differentiation into a mucociliary monolayer was complete. Additionally, primary airway epithelial cells isolated from healthy (non-AUD) and alcoholic (AUD) patients had a similar barrier function result. I found that rat tracheal cells were more susceptible to *in vitro* ethanol exposure since barrier function was significantly lower than untreated cells once differentiation was complete. When examining non-AUD and AUD cells by immunofluorescence, I found that some samples exhibited aberrant collective cell migration, a phenotype known as unjamming. The protein junctional adhesion molecule A (JAM-A) regulates barrier function and epithelial cell migration and may play a role

in causing the sustained unjammed phenotype, although *in vitro* exposure did not decrease JAM-A expression. Lastly, I discovered that unjamming may be an age-dependent phenotype, though further analysis must be done to determine this. Taken together, these data suggest that prolonged ethanol exposure may have detrimental effects on basal cell barrier function and implies that differentiation potential could be negatively affected. Further, this work suggests ageing airway epithelial cells have upregulated cellular repair mechanism, although how this contributes to airway epithelial dysfunction in the context of aberrant collective cell migration is unknown at present.

5.2 Future Directions

5.2.1 Implications of hyperglycemia on airway cell function

Our work suggests that glucose levels can affect metabolism and barrier function, and other work implies this this might be the case with CF, given that CF-related diabetes is a common comorbidity. In parallel with the work produced in Chapter 2, our lab investigated how glucose availability is regulated in the healthy and CF airway. In healthy airway cells, insulin stimulated glucose uptake and temporarily increased barrier function assessed by TER and dye flux analysis. CF cells with the F508del mutation did not increase glucose uptake in the presence of insulin and exhibited a selective increase in paracellular permeability to calcein (0.63 kDa). Further, this insulin-stimulated barrier tightening in healthy cells occurs via the phosphatidylinositol 3-kinase (PI3K)/protein kinase B (Akt) pathway and requires functional CFTR. This work highlights crosstalk between glucose metabolism and tight junctions (1).

Because the insulin-stimulated barrier tightening occurs quickly, it would be interesting to observe changes in tight junction protein turnover. Endocytosis and recycling of tight junction

proteins can be measured utilizing a cell-surface biotinylation assay (2). It is important to note that healthy and CF airway cells express similar levels of ZO-1, ZO-2, F11R, claudin-1, claudin-3, claudin-4, claudin-5 and claudin-7, at least at the RNA level (3).

5.2.2 Investigating alcohol-induced modifications to the epigenome and transcriptome

RNA-seq analysis of cultured bronchial cells from patients with AUD indicates that AUD cells adapted an inflamed, epidermal gene expression profile compared to non-AUD cells. These cells are not cultured in the presence of ethanol, hinting at widespread epigenetic alterations due to chronic ethanol consumption. Additionally, my work in Chapter 4 using AUD cells and in vitro ethanol exposed cells indicates that basal cells are especially impacted by prolonged ethanol exposure. We could employ one or more epigenetic analyses to determine how chronic alcohol use permanently alters the epigenome: methyl-seq to detect changes in DNA methylation, ChIP-seq to detect differences in histone modification and transcription factor binding, or ATAC-seq to determine regions of chromatin accessibility in addition to identifying active promoters, enhancers, and cis-regulatory elements.

Further, we can couple epigenetic analyses with single-cell RNA-seq to understand how chronic alcohol exposure impacts the differentiation potential of basal cells. Single-cell RNA-seq will not only enable us to tease apart cell-type specific changes in gene expression, but also can elucidate if cell-type percentages are altered. It is currently unknown if chronic alcohol use impacts cell-type percentages. However, smoking is known to increase goblet cell numbers and decrease club and ciliated cell numbers in the small airway (4). It is conceivable that chronic alcohol use could have the same effect.

In addition to the AUD cells, we see a similar persistent phenotype when alveolar type II

cells are isolated from alcohol-fed rats and differentiated into alveolar type I cell within the span of one week. The type I cells display decreased barrier function in the presence of no ethanol (5). Interestingly, human bronchial cells from AUD patients showed no difference in barrier function after differentiation was complete, indicating that the airway epithelium compensated for any alcohol-induced changes in barrier permeability. However, our work in Chapter 3 indicates that the second-hit hypothesis of alcohol-induced lung injury holds true. As stated in chapter 4, one explanation could be that rat cells are more sensitive to *in vivo* and *in vitro* alcohol exposure, indicating species differences in response to chronic alcohol. This is important to note when using our model systems, but illustrates that the rat model, one in which we can decrease genetic and environmental variability, is useful for mechanistic studies.

5.2.3 Improvements to our *in vitro* ethanol exposure model

In the liver, alcohol is broken down by the alcohol dehydrogenase (ADH) enzyme into acetaldehyde, a short-lived, yet dangerous byproduct. Acetaldehyde is further broken down to acetate by aldehyde dehydrogenase (ALDH) (6). In the lung, acetaldehyde circulation contributes to oxidative stress by depleting available glutathione levels. (7). In addition, lung epithelial cells are constantly exposed to alcohol vapor since alcohol readily diffuses from the airway blood supply into the airway (8). However, the lung has low ADH activity compared to the liver, indicating that lung cells do not contain the machinery to metabolize alcohol (9). While our *in vitro* ethanol exposure model exposes airway epithelial cells to alcohol vapors, it is likely that very little acetaldehyde is being produced.

To better mimic the effects of alcohol exposure and its dangerous metabolite, we could utilize an extracellular Ach-generating system (AGS) developed by Ganesan et al. (10). The AGS

includes yeast ADH, nicotinamide adenine dinucleotide (NAD⁺) and 50mM ethanol and medium changes or treatment can occur at 48 hours of exposure. Using this system with bronchial epithelial cells at the expansion and differentiation stages would better mimic chronic alcohol exposure and enable us to parse out specific TJ barrier changes to ethanol and acetaldehyde.

5.2.4 Linking aging-related effects to unjamming in airway epithelial cells

Most of the studies related to unjamming and airway epithelial cells focus on unjamming in the context of asthma (11, 12, 13). In order to determine if unjamming occurs as a consequence of aging, we can first examine studies that elucidated age-related differences in gene expression in airway epithelial cells. One study used tracheobronchial epithelial biopsies and generated three different bulk transcriptomic experiments: homeostatic laser capture-micro dissected whole epithelium, homeostatic fluorescence-activated cell-sorted basal cells and proliferating cultured basal cells (14). Overall, the investigators found age-related differences in gene expression, but found no gross anatomical differences or differences in cell type proportions in whole tissue. However, pathway analysis indicates that the UV response and TGF beta signaling pathways were upregulated. Interestingly, irradiation of differentiated airway epithelial cells causes unjamming in a TGF-β receptor-dependent manner. (12). Speculation of whether airway epithelial cell unjamming occurs *in vivo* and is biologically relevant is ongoing. However, unjamming is essentially collective cell migration and may be the result of upregulated repair mechanisms due to airway insults.

A second study examined age in the context of airway epithelial cell barrier function. They identified 55 genes related to epithelial barrier function to be significantly associated with age (15). While they focused specifically on genes related to barrier function, we can examine their list of

differentially expressed genes, identify genes of interest, perform knockdown experiments in cells from young patients, and observe for unjamming. In parallel, we can use qRT-PCR and immunoblot to probe candidate genes in non-AUD cells from patients of various ages that do and do not exhibit the unjammed phenotype. Together, these experiments can elucidate mechanisms that link age to unjamming/ collective cell migration in airway epithelial cells.

References

- Molina SA, Moriarty HK, Infield DT, Imhoff BR, Vance RJ, Kim AH, Hansen JM, Hunt WR, Koval M, McCarty NA. Insulin signaling via the PI3-kinase/Akt pathway regulates airway glucose uptake and barrier function in a CFTR-dependent manner. Am J Physiol Lung Cell Mol Physiol. 2017 May 1;312(5):L688-L702. doi: 10.1152/ajplung.00364.2016.
 Epub 2017 Feb 17. PMID: 28213469; PMCID: PMC5451595.
- Nishimura N, Sasaki T. Cell-surface biotinylation to study endocytosis and recycling of occludin. Methods Mol Biol. 2008;440:89-96. doi: 10.1007/978-1-59745-178-9_7. PMID: 18369939.
- Molina SA, Stauffer B, Moriarty HK, Kim AH, McCarty NA, Koval M. Junctional abnormalities in human airway epithelial cells expressing F508del CFTR. Am J Physiol Lung Cell Mol Physiol. 2015 Sep 1;309(5):L475-87. doi: 10.1152/ajplung.00060.2015.
 Epub 2015 Jun 26. PMID: 26115671; PMCID: PMC4556929.
- 4. Rostami MR, LeBlanc MG, Strulovici-Barel Y, Zuo W, Mezey JG, O'Beirne SL, Kaner RJ, Leopold PL, Crystal RG. Smoking shifts human small airway epithelium club cells toward a lesser differentiated population. NPJ Genom Med. 2021 Sep 8;6(1):73. doi: 10.1038/s41525-021-00237-1. PMID: 34497273; PMCID: PMC8426481.
- Guidot DM, Modelska K, Lois M, Jain L, Moss IM, Pittet J-F, Brown LAS. Ethanol ingestion via glutathione depletion impairs alveolar epithelial barrier function in rats. Am J Physiol Lung Cell Mol Physiol. 2000;279:L127–L135.
- 6. Zakhari S. Overview: how is alcohol metabolized by the body? Alcohol Res Health. 2006;29(4):245-54. PMID: 17718403; PMCID: PMC6527027.

- Moss M, Guidot DM, Wong-Lambertina M, Ten Hoor T, Perez RL, Brown LA. The effects
 of chronic alcohol abuse on pulmonary glutathione homeostasis. Am J Respir Crit Care
 Med. 2000 Feb;161(2 Pt 1):414-9. doi: 10.1164/ajrccm.161.2.9905002. PMID: 10673179.
- 8. George SC, Hlastala MP, Souders JE, Babb AL. Gas exchange in the airways. J Aerosol Med. 1996 Spring;9(1):25-33. doi: 10.1089/jam.1996.9.25. PMID: 10172721.
- Manautou JE, Carlson GP. Comparison of rat pulmonary and hepatic cytosolic alcohol dehydrogenase activities. J Toxicol Environ Health. 1992 Jan;35(1):7-18. doi: 10.1080/15287399209531589. PMID: 1728667.
- 10. Ganesan M, Zhang J, Bronich T, Poluektova LI, Donohue TM Jr, Tuma DJ, Kharbanda KK, Osna NA. Acetaldehyde accelerates HCV-induced impairment of innate immunity by suppressing methylation reactions in liver cells. Am J Physiol Gastrointest Liver Physiol. 2015 Oct 1;309(7):G566-77. doi: 10.1152/ajpgi.00183.2015. Epub 2015 Aug 6. PMID: 26251470; PMCID: PMC6842870.
- 11. Park JA, Kim JH, Bi D, Mitchel JA, Qazvini NT, Tantisira K, Park CY, McGill M, Kim SH, Gweon B, Notbohm J, Steward R Jr, Burger S, Randell SH, Kho AT, Tambe DT, Hardin C, Shore SA, Israel E, Weitz DA, Tschumperlin DJ, Henske EP, Weiss ST, Manning ML, Butler JP, Drazen JM, Fredberg JJ. Unjamming and cell shape in the asthmatic airway epithelium. Nat Mater. 2015 Oct;14(10):1040-8. doi: 10.1038/nmat4357. Epub 2015 Aug 3. PMID: 26237129; PMCID: PMC4666305.
- 12. O'Sullivan MJ, Mitchel JA, Das A, Koehler S, Levine H, Bi D, Nagel ZD, Park JA. Irradiation Induces Epithelial Cell Unjamming. Front Cell Dev Biol. 2020 Feb 11;8:21. doi: 10.3389/fcell.2020.00021. PMID: 32117962; PMCID: PMC7026004.

- 13. Park JA, Mitchel JA, Qazvini NT, Kim JH, Park CY, Butler JP, Israel E, Randell SH, Shore SA, Drazen JM, Fredberg JJ. Compressive Stress Causes an Unjamming Transition and an Epithelial-Mesenchymal Transition in the Airway Epithelium in Asthma. Ann Am Thorac Soc. 2016 Mar;13 Suppl 1(Suppl 1):S102. doi: 10.1513/AnnalsATS.201506-382MG. PMID: 27027941; PMCID: PMC5015726.
- 14. Maughan EF, Hynds RE, Pennycuick A, Nigro E, Gowers KHC, Denais C, Gómez-López S, Lazarus KA, Orr JC, Pearce DR, Clarke SE, Lee DDH, Woodall MNJ, Masonou T, Case KM, Teixeira VH, Hartley BE, Hewitt RJ, Al Yaghchi C, Sandhu GS, Birchall MA, O'Callaghan C, Smith CM, De Coppi P, Butler CR, Janes SM. Cell-intrinsic differences between human airway epithelial cells from children and adults. iScience. 2022 Oct 20;25(11):105409. doi: 10.1016/j.isci.2022.105409. PMID: 36388965; PMCID: PMC9664344.
- 15. de Vries M, Nwozor KO, Muizer K, Wisman M, Timens W, van den Berge M, Faiz A, Hackett TL, Heijink IH, Brandsma CA. The relation between age and airway epithelial barrier function. Respir Res. 2022 Mar 3;23(1):43. doi: 10.1186/s12931-022-01961-7. PMID: 35241091; PMCID: PMC8892715.